Synthesis and Characterization of Organic Conjugated Polymer/ ZnO Nano-particle Films for Solar Cell Application

A THESIS SUBMITTED IN FULFILMENT OF THE REQUIREMENTS FOR

THE DEGREE OF MASTER OF SCIENCE

Ali Azarifar

B. SCI. (Phys.)

M.Sc (Phys.)

Applied Chemistry

School of applied Sciences

Science, Engineering and Technology Portfolio

RMIT University

March 2013

Declaration of the Candidate

I certify that except where due acknowledgement has been made, the work is that of the author alone; the work has not been submitted previously, in whole or in part, to qualify for any other academic award; the content of the thesis is the result of work which has been carried out since the official commencement date of the approved research program; and, any editorial work, paid or unpaid, carried out by a third party is acknowledged.

Ali Azarifar
15 March 2013

Abstract

Hybrid thin films show great promise as a novel material for solar energy conversion devices. Using present knowledge from polymer bulk hetero-junction solar cells, the design of a simple, and potentially low cost, hybrid solar cell based on metal oxides and conjugated polymers is presented. The hybrid material properties are often superior to the sum of the intrinsic properties of the components and often have a functionality that is not present in either of the individual materials [1].

In this research, hybridization of organic conducting polymer and metal oxide semiconductor on nanometer scale in fabricating of a bulk hetero-junction solar cell will be investigated. ZnO nanoparticles were chosen as nanoparticle semiconductors and Poly(3-hexylthiophene-2,5-diyl) (P3HT) is used as a conductive polymer. ZnO and P3HT are individually very important functional materials. Additionally, ZnO nanoparticles have transparency over the whole visible region and have good electron mobility compared to other wide band gap materials such as TiO_2 [61,62]. The P3HT semiconductor polymer is important because of its high absorption coefficient in the visible region. In addition to the aforementioned intrinsic properties of these functional materials, in the hybrid of ZnO/P3HT energy levels of ZnO nanoparticles and P3HT polymer are matching and the hybrid layer can act as an active layer to absorb the visible solar light and release the electric charges.

Uniform ZnO nanoparticles with small particle size distribution were synthesized. High resolution TEM imaging was performed to study the size and shape of the ZnO nanoparticles. The synthesized particles mainly range between 5-7 nm. To prepare the ZnO/P3HT hybrid solution we optimized the dispersion of the ZnO nanoparticles in the methanol/chloroform mixture solution (avoiding ZnO agglomeration). We obtained good dispersion of ZnO nanoparticles in a mixed solution of 4.5% methanol and 95.5% chloroform. Glass coated with ITO was used as a substrate followed by a poly (3,4ethylenedioxythiophene) poly (styrene sulfonate) (PEDOT:PSS) layer, spin coated on the ITO substrate. Above the PEDOT:PSS layer we spin coated a hybrid (ZnO/P3HT) layer followed by

depositing aluminium electrodes using the metal evaporation technique. We studied the quality of the film formation and the aluminium electrodes using optical and scanning electron microscopies. Also we studied the absorption and emission hybrid films using UV-Visible and florescent spectroscopies. By changing the blend (ZnO/P3HT) concentration and the ratio of ZnO and P3HT as the initial parameters we could optimise the optical properties. 5 mg/mL ZnO nanoparticles and 10 mg/mL P3HT concentrations with 50% ZnO and 50% P3HT ratio resulted in the best optical characteristics in the hybrid films. The concentration of the PEDOT:PSS was also optimised. We found that 0.65% PEDOT:PSS concentration results the highest electrical measurements of the prepared Bulk heterojunction solar cell. Using the optimised parameters we prepared the bulk hetero-junction solar cells and conducted the electrical tests including incident photon to electron conversion efficiency IPCE and J-V characterization. We found that optimized parameters resulted in 19% IPCE and 1.13 $mA.Cm^{-2}$ I_{SC} and 0.23 V_{OC}. We chose three prepared solar cells; 1. best performing with 50% -50% ZnO/P3HT ratio , 2.worst performing with 50% -50% ZnO/P3HT ratio 3. solar cell with 30%-70% ZnO/P3HT ratio) to study the morphology of their hybrid layer using AFM and surface profiler. Up to some extend we could understand and relate the hybrid film morphologies to the obtained electrical performance of these three bulk hetero-junction solar cells. In compar to other lab-prepared bulk hetero-junction solar cells the best performing bulk hetero-junction solar cell has a better hybrid film uniformity. Also in the best performing bulk hetero-junction solar cell the roughnesses and mean granular sizes of the film over the surface were very similar. We used AFM to correlate the quality of the film surface with the electrical performance and found that uniform and continuous films are very important in the performance of the solar cell device.

Table of Contents

Chapter 1 1
1. Introduction 1
1.2 Thesis outline 2
Chapter 2 4
2. History and literature review 4
2.1 Three generations of Photovoltaic development 4
2.2 Research options for the present study 21
2.3 Project objectives 22
Chapter 3 25
3. Fabrication 25
3.1 Synthesis of ZnO nanoparticles 25
3.2 Structural characterization of ZnO nanoparticles 29
3.3 Bulk hetero-junction solar Cell Fabrication 36
3.4 Aluminium Electrodes, desighn and structure investigation of Bulk heterojunction solar 41
Chapter 4 50
4. Optical Study 50
4.1 Optical spectroscopy analysis 50
4.2 Aging effect study on the prepared Hybrid film 57
Chapter 5 61
5. Electrical measurements 61
5.1 photovoltaic characterization 61
5.2 Solar cell characterization 61
5.3 Studying the effect of few important parameters in the Solar cell performance 65
Chapter 6 72
6. Surface morphology of Hybrid film investigation using AFM 72
6.1 Highest performing solar cell 73
6.2 The lowest performing solar cell (made of agglomerated solution) 78
6.3 30%-70% (mass ratio) ZnO/P3HT solar cell 85
6.4 Step height of the aluminium electrode and the thickness study of the best performing solar cell films 91
Chapter 7 95

Conclusions and Future work 95
References 100

Acknowledgements

I would like to express my appreciation to everyone who has helped me during the different stages of this Master Thesis. Many people have contributed, however certain individuals deserve special recognition. Dr Jared Cole, my supervisor, who has provided me with great deal of valuable input and insight throughout my research. I appre

ciate his encouragement, thought-provoking conversations and guidance.
Dr. Andrew Greentree, who helped me to shape my thesis and came with lots of valuable suggestions and corrections, I really appreciate his sincere helps. Andrew I am always thankful to you!

I should thank Professor Andrew Smith, dean of school of applied sciences, RMIT, for his grate support and positive attitude. He is the person who I will never forget and always will remember him with grate respect.

I am very thankful to Mr. Phil Francis, manager of RMIT electron microscopy, for his always assistance and important instructions in well performing the electron microscopy of the samples. Dr. Jim Partridge, who have assisted me in performing AFM related measurements, I am thankful to him. I would like to thank Dr. Colin Rix also for editing my thesis and his helpful suggestions.

My kind father and mother, without you and your prayers I have nothing. I only can thank you for your sincere and continuous supports, you are always in my heart. My kind and beloved wife, I am always grateful to you for your tremendous helps and heartedly supports. Without your supports and devotions it would be impossible to accomplish this thesis. I am always thankful for God’s mercy and grace.

Abbreviations

P3HT	Poly(3-hexylthiophene-2,5-diyl)
PEDOT:PSS	poly(3,4ethylenedioxythiophene)poly(styrene sulfonate)
UV-Vis Spectroscopy	Ultra violet-visible Spectroscopy
HRTEM	High Resolution Transmission Electron Microscopy
TEM	Transmission Electron Microscopy
SEM	Scanning Electron Microscopy
AFM	Atomic Force Microscopy
IPCE	Incident Photon to Electron Conversion Efficiency
HOMO	Highest Occupied Molecular Orbital
LUMO	Lowest Unoccupied Molecular Orbital

List of Figures

Figure 2.1: Bulk hetero-junction blend in a hybrid solar cell.....11

Figure2.2: Photovoltaic process in organic solar cells. 12

Figure 2.3: Mechanism of charge development in a bulk hetero-junction solar cell. ……..……14

Figure2.4: Progress of research-scale photovoltaic device efficiencies, under simulated terrestrial radiation conditions.....15

Figure 3.1: UV–Visible absorption spectrum of ZnO nanoparticles dispersed in the chloroform/methanol mixture (94-6 Volume ratio): (1) is the freshly prepared ZnO solution, and (2) is the ZnO nanoparticle solution after three months. ……27

Figure 3.2: UV–Visible absorption spectrum of highly agglomerated ZnO nanoparticles dispersed in the chloroform/methanol mixture (94-6 Volume ratio) after four month. ……..…..28

Figure 3.4: (a) Transmission electron micrograph (TEM) of ZnO nanoparticle.....32

Figure 3.4: (b) Particle size distribution obtained from TEM micrograph.....33

Figure 3.5: The Energy- dispersive X-ray (EDAX) spectrum of the purified ZnO nanoparticles.....34

Figure 3.6: Preparation of hetero-junction solar cell.....35

Figure 3.7: Bulk hetero-junction solar cell fabricated in laboratory. It consists of the ITO layer on the glassier substrate. The PEDOT:PSS layer spin casted on top of ITO layer and the Hybrid layer (Pink –redish color) spin casted on the PEEDOT:PSS layer and finally Aluminium electrodes deposited on the hybrid layer using metal evaporation technique (in maximum 1.8 x 10^{-3} pa chamber pressure).....36

Figure 3.8: Well dispersed and agglomerated ZnO nanoparticles in solution.....39

Figure 3.9: Schematic diagram of the Bulk hetero-junction solar cell structure. The best and the worst electrodes(in terms of IPCE and J-V characters) a,b,c points (Top, middle, bottom) adjacent to the best aluminum electrode and d, e, f points (Top, middle, bottom) adjacent to the worst electrode.....42

Figure 3.10: Aluminium electrodes without silver paste (at left) and with silver paste (at right)……..43

Figure 3.11: Optical imaging of a) hybride layer (mixture of P3HT and ZnO nanoparticles) b) Aluminium deposited electrode on the Hybrid.....44

Figure 3.12: SEM images of the surface of bulk hetero-junction solar cell. a) surface of cell 100x magnifications b) Surface of the aluminium electrode with 13000x magnifications. c)

Surface of aluminium electrode with 40000x magnifications……47

Figure 4.1: UV-Visible spectrum of the Pure P3HT and 50% -50% ZnO/P3HT hybrid films on the glass substrate after spin coating with 1500 rpm speed.....51

Figure 4.2: Emission spectrum of the Pure P3HT and 50% -50% ZnO/P3HT hybrid films on the glass substrate after spin coating with 1500 rpm speed.

.....52

Figure 4.3: Emission spectra of the annealed and not annealed hybrid films on the glass.....53

Figure 4.4: Absorption spectra of the hybrid film with different ZnO and P3HT ratio.....54

Figure 4.5: Emission spectra of different ratios of Hybrid film drop-casted on glass.....55

Figure 4.6: Absorption spectrum of a set of different ZnO/P3HT ratio hybrid films on glass substrates after nine month.....58

Figure 4.7: Emission spectrum of a set of different ZnO/P3HT ratio hybrid films on glass substrates after nine month.....59

Figure 5.1: Solar cell measurements of best performing solar cell a) IPCE measurement b) J-V measurements.....62

Figure 5.2: Solar cell measurements of lowest performing solar cell a) IPCE measurement b) J-V measurements.....63

Figure 5.3: Solar cell measurements of 30-70% lab- made bulk hetero-junction solar sell a) IPCE measurement b) J-V measurements……64

Figure 5.4: a) PEDOT:PSS concentration of 0.65 Wt% and blend layer thickness reduction. b) PEDOT:PSS concentration of 1.3 Wt%. c) PEDOT:PSS concentration of 0.65 Wt% (diluted to half concentration). In all a, b, c the ZnO/P3HT mass ratio is 50%-50%. A) IPCE characteristic B) J-V characteristic.....69

Figure 6.1: 3D AFM images of the Best sample. The best and the worst electrodes (in terms of IPCE and J-V characters) a,b,c points (Top, middle, bottom) adjacent to the best aluminium electrode and d, e, f points (Top, middle, bottom) adjacent to the worst electrode. The scanned area is 3µm x 3µm.....71

Figure 6.2: Plane AFM images and roughness measurements The best and the worst electrodes (in terms of IPCE and J-V characters) a,b,c points (Top, middle, bottom) adjacent to the best aluminium electrode and d, e, f points (Top, middle, bottom) adjacent to the worst electrode.....73

Figure 6.3: Mean grian size measurements. The best and the worst electrodes (in terms of IPCE and J-V characters) a,b,c points (Top, middle, bottom) adjacent to the best

aluminium electrode and d, e, f points (Top, middle, bottom) adjacent to the worst electrode.....75

Figure 6.4: 3D AFM images of the lowest performing solar cell. The best and the worst electrodes (in terms of IPCE and J-V characters) a,b,c points (Top, middle, bottom) adjacent to the best aluminium electrode and d, e, f points (Top, middle, bottom) adjacent to the worst electrode. The scanned area is 3µm x 3µm.....77

Figure 6.5: Plane AFM images and roughness measurements of the lowest performing solar cell. The best and the worst electrodes (in terms of IPCE and J-V characters) a,b,c points (Top, middle, bottom) adjacent to the best aluminium electrode and d, e, f points (Top, middle, bottom) adjacent to the worst electrode. ……..……...79

Figure 6.6: Mean grain size measurement of the lowest performing solar cell. The best and the worst electrodes (in terms of IPCE and J-V characters) a,b,c points (Top, middle, bottom) adjacent to the best aluminium electrode and d, e, f points (Top, middle, bottom) adjacent to the worst electrode.....81

Figure 6.7: 3D AFM images of 30-70% (mass ratio) ZnO/P3HT solar cell. The best and the worst electrodes (in terms of IPCE and J-V characters) a,b,c points (Top, middle, bottom) adjacent to the best aluminium electrode and d, e, f points (Top, middle, bottom) adjacent to the worst electrode. The scanned area is 3µm x 3µm. ……83

Figure 6.8: Plane AFM images and roughness measurements of 30-70% (mass ratio) ZnO/P3HT solar cell. The best and the worst electrodes (in terms of IPCE and J-V characters) a,b,c points (Top, middle, bottom) adjacent to the best aluminium electrode and d, e, f points (Top, middle, bottom) adjacent to the worst electrode. ……..…86

Figure 6.9: Mean grain size measurement of 30-70% (mass ratio) ZnO/P3HT solar cell. The best and the worst electrodes (in terms of IPCE and J-V characters) a,b,c points (Top, middle, bottom) adjacent to the best aluminium electrode and d, e, f points (Top, middle, bottom) adjacent to the worst electrode. ……..……..87

Figure 6.10: Thickness measurements of Hybrid layer and aluminium electrode using surface profiler. a) Thickness of the only 50-50% (mass ratio) ZnO/P3HT hybrid film on the glass. b) Step height of the only aluminium electrode on the ITO coated glass. c) Step height of aluminium electrode deposited on the hybrid layer in the bulk hetero-junction solar cell……..…91

List of Tables

Table 3.1: Required information for particle size measurement using Scherrer's formula. These are extracted from the X-ray diffraction pattern depicted in figure 3.3. ……34

Table 3.2: The ITO glass specification and patterning process (Luminescence Technology Corp.).....40

Table 5.1: The tested cell parameters. The bold numbers are the optimum chosen parameters for the highest cell performance.....71

Table 6.1: The Best performing lab- made bulk hetero-junction solar sell. Roughness and granular size of the points a,b,c,d,e,f. ……....78

Table 6.2: The lowest performing lab- made bulk hetero-junction solar sell. Roughness and granular size of the points a,b,c,d,e,f. ……..…….....84

Table 6.3: The 30-70% lab- made bulk hetero-junction solar sell. Roughness and granular size of the points a,b,c,d,e,f.....91

Chapter 1

1. Introduction

1.1 Background to the study

Energy is one of the main concerns of today's world and will remain as one of the top 10 problems for the next 50 years. With regards to the growth of world population from 7.075 billion in 2013 to 8-10 billion people in 2015, global energy demand is estimated to increase from ~12 TW to ~20 TW in 2050. Therefore it is evident that the biggest challenge for the next decades is to produce approximately 10 TW energy more. Indeed, for the sake of peace and prosperity it should be cheap and environmental friendly [2].

Among the available sources of energy solar energy is the best option which is cheaper, easy to access and environmental friendly. To date, different types of solar energy to electricity conversion systems have been developed. The solar cells can be divided into three generations; first-generation; Silicon based solar cells, Second-generation; thin film solar cells and third-generation which are organic solar cells. Current market is dominated by single-crystal and polycrystalline solar cells which is almost 94% of the market [3].

The non-economical costs of ~$4/W for crystal silicon solar cells was not significantly efficient to influence the energy production market. The best estimates was that the costs will reduce to $1/W-$1.5/W in the next 10 years. This cost is still much higher than the energy price expectation/goal by the U.S. Department of Energy for the next decay which should be ~$0.33/W [38,67]. Second generation of solar cells, which are based on thin film technologies, do not require silicon wafers and therefore can be manufactured with significantly lower cost. The current cost of this producing energy with this solar cell is ~ $1/W, which is a quarter of cost using silicon solar cells. These cells comprise 5.6% of the market [3]. Worldwide the prices are decreasing, for example in the German market a cost of $ 6.5/W in 2006 has come down to $ 2.6/W in 2011 (system price for roof

top installation) [80]. Back in 2009/20010, industry was aiming to $1/W C-Si solar cell cost as a medium term price but even cheaper prices at about $ 0.5/W are being offered by Chinese producers [81].

Expensive wafer-based silicon solar cells and thin film solar cells has prompted scientists to search for alternative material combinations for use in solar cell applications. This has engendered the third-generation concept of photo voltaic technologies. The goal is to achieve moderate efficiency of 15-20%, at a very low cost [4]. One approach that has the capacity to reach these levels is that of bulk hetero-junction solar cells.

A Bulk hetero-junction is based on the combination of organic and inorganic materials in a hybrid layer sandwiched between two electrodes. Although this will lead to low-cost and flexible (plastic) photovoltaics, the demonstrated hybrid solar cells have very low power conversion efficiencies (PCE).
There are several reasons for the low efficiency of bulk hetero-junction solar cells and in this project we are trying to optimize the performance of these cells by focussing on the following factors:

- The quality of the nanoparticles.
- The miscibility of the particles in the polymer solution.
- The nature of the nanoparticle / polymer interfacial region.
- The preparation of the electrode surfaces.
- The preparation of the ZnO/P3HT layer.

1.2 Thesis outline

Chapter 1 starts with a brief background to the study and introduces the objectives of the study. In chapter 2, the working principles of Bulk hetero-junction solar cell have been discussed and the related literatures have been reviewed. Chapter 3

describes the fabrication of bulk hetro-junction solar cell. Starting with describing the synthesis of ZnO nanoparticles and the characterization of the synthesized ZnO nanoparticles and finally hybridizing the ZnO nanoparticles with the conductive polymer and then fabricating the Bulk hetero-junction solar cell. Chapter 4 presents the optical studies performed on the hybrid films. Chapter 5 presents the results for the electrical measurements of the three selected solar cell devices prepared in laboratory. In chapter 6, we have studied the morphology of the hybrid films on the same three bulk hetro-junction were chosen to study in chapters 5 and tried to compare the morphologies of the hybrid surfaces and relate to their obtained electrical results. Conclusion of the thesis and the suggested future works will be presented in chapter 7.

Chapter 2

2. History and literature review

The idea of developing the technology to harvest solar light/energy started in 1839 with the discovery of the “photovoltaic effect” - the phenomenon by which the light absorbed by a material can induce charge separation to create free charges that lead to an electric current. The first solar cell was made by Charles Fritts in 1883 [60] who coated the semiconductor selenium with an extremely thin layer of gold to create electrically conducting junctions, and achieved a conversion efficiency of approximately 1%.

Solar cell technology has now become a major focus of energy research to improve the efficiency and functioning of solar cells, as it is now recognised that the reliance on fossil fuels cannot be sustained in the future due to their limited availability and the contribution of their combustion products to climate change.

The most common and successful photovoltaic solar cell is the silicon based system invented by Russel Ohl in 1941 [60] which, at that time, had a maximum efficiency of 6%. Currently, similar silicon based solar cells are being mass produced and sold commercially. Although they are relatively expensive, the single crystal silicon solar cell holds the highest conversion record in the current market by performing at 16-18% efficiency [36]. In 1991, Gratzel and O’Regan [65] created a breakthrough in the construction of solar cells. The key component in the operation of this solar cell was a dye which was used as a sensitizer to harvest additional solar energy and hence increase the efficiency of the cell. When compared to solid state devices, this is an unconventional solar cell since it does not use a p-n junction to generate the electricity.

2.1 Three generations of Photovoltaic development

Photovoltaic solar cells are divided into three categories; Crystalline silicon, Thin film, and hybrid solar cells. In this section we will discuss the differences in their efficiency and structure.

2.1.1 Crystalline silicon solar cell

In this type of solar cell, crystalline silicon is the main component which acts as the solar light absorber. The p-n junction is a large area of this device and is the region between the p-doped and n-doped part of the silicon crystal. The concept of p-n junction is very important to understand. This will help us to understand the solar cell function. A p-n junction is an interface between two different types of semiconductors. In crystalline silicon solar cells p-n junction is the intersect between the p-type and n-type silicon semiconductor. After attaching the n-type and p-type semiconductors Fermi levels of two semiconductors equilibrates and reach the same energy level. Therefore it creates a bending in the conducting and valence bands and causes a potential difference for the electrons and a potential difference for holes. This creates an electric field that both carriers experience. The p-n junction causes the excitons created by an incoming photon to disassociate to electrons and holes. Creating p-type and n-type semiconductors is possible by adding specific atomic impurities to the semiconductor via different techniques [5], [6]. The p-n junction acts as a diode and exhibits a diodic current-voltage characteristic. The efficiency in this solar cell device is very much dependent on the quality of the crystalline silicon. High purity crystals with low impurity levels result in higher conversion efficiencies of solar light to electricity. It is important to know that the extra photon energy above the band gap energy is converted to heat. This heat is one of the main limits in achieving high efficiency in converting solar radiation to electricity.

Almost 280 MW of solar electric power were sold worldwide in the year 2000 and more than 90% of this was generated from crystalline silicon based solar cell technology [7]. Indeed, this first generation photovoltaic solar cell is the leading technology in commercial production and has dominated the market. Crystalline solar cells and poly crystalline solar cells are the two most commonly used solar cells in the market. In terms of price, crystalline silicon solar cells are the most expensive.

2.1.2 Thin film technology solar cell

Thin film solar cell devices are based on the deposition of a thin-film functional semiconductor on a silicon substrate with the intention of achieving higher efficiency than crystalline silicon solar cells. These cells operate similar to the silicon solar cells except that the deposited layer is the sunlight absorber. This device does not contain a bulk crystalline layer.

The structure consists of several layers of p-n junction material. For example, Si, GaAs, CuS and etc. This helps to capture more of the solar energy and also absorbs a wider spectrum of solar radiation to be converted to electricity. Another important advantage of the thin film solar cells is that they require less material for fabrication [8]. Moreover, the use of different methods of film deposition provides the opportunity to choose the cheapest method, such as Chemical Vapour Deposition (CVD). Using this technique, very thin layers of silicon, of the order of 10 μm thick, have been deposited, which reduces cost. The best efficiency reported for a hetero-junction solar cell was 19.5% in December 2005, considering that this is a laboratory achieved data and has not been commercialized due to few problems mainly the durability [9]. Therefore still single crystal silicon solar cell holds the highest conversion record in the current market. To date, even though thin film photovoltaic cells are much cheaper to produce than bulk silicon solar cells (the so-called first generation solar photovoltaic) their application is limited by their lower efficiency.

2.1.3 Hybrid Solar Cells

Silicon-based solar cells and inorganic semiconductors can be considered to generate mobile charge carriers as they are photo-excited by sunlight. In order to harvest more energy two main points need to be considered. First, ultra-pure and highly crystalline silicon is required to achieve high efficiency and remove the impurities which act as charge traps in the crystal. This makes the fabrication of these solar panels very expensive. The second point is that these crystals and the assembled solar panels are very fragile. Therefore, a more robust arrangement is

desirable, and so the idea of printable hybrid solar cells is being considered as one of the most attractive options for organic solar cells [10].

Such hybrid devices generally consist of a polymer / inorganic nanoparticle combination fabricated as a film. This requires nanoparticles with high electron mobility and good physical and chemical stability (eg. ZnO, CdS, CdSe, TiO2, PbS) [26] admixed with a light-weight conductive polymer, which provides an ideal electron–transfer medium suitable for use in a solar cell device [27]. This is especially attractive if it allows for easy processibility and low cost.

Unfortunately, in spite of extensive investigations during recent years the conversion efficiencies of such hybrid devices are still comparatively low. Promising power conversion efficiencies have been achieved by optimizing the structure to give improved electron transfer between particles, especially those systems based on CdSe. However, cadmium, selenium and lead are quite toxic and damaging to the environment. This has led researchers to focus on the less-toxic materials, ZnO and TiO_2. Both these compounds are wide band gap semiconductors that are also non-toxic and low cost, which makes them ideal for use in hybrid solar cells [26].

There are two techniques currently used to create the hybrid layer in bulk hetero-junction solar cells. The preferred method, due to its simplicity, is the blend process in which an appropriate nanoparticle/quantum dot and a conductive polymer are simply mixed together. This is done in a proportional solvent which simultaneously dissolves the organic polymer and the inorganic nanoparticles. A non-proportional solvent will result in agglomeration of nanoparticles and/or suspension of the polymer in the solvent. The second method, termed the penetration process, is carried out by either growing the nanostructures or pasting the metal oxide nanoparticles on the substrate, and then a solution of the polymer is poured over them in a way that it penetrates into the pores of the prepared layer until the solvent completely evaporates. This method has the advantage of

providing better charge percolation pathways. This increases the probability of electrons and holes to reach to the cathode and anode. Electrons travel through the Nanoparticles network and holes through the polymeric media [27, 37].

The bulk hetero-junction approach was introduced to overcome the very small exciton diffusion length, which in conductive polymers is in the range 4-10 nm [39-43]. An exciton is the bound state between an electron and hole. The most important difference between organic and inorganic semiconductors as materials being implied in photovoltaic devices is that the resultant exciton in organic semiconductors is not easily split by the electric field [40]. In contrast to inorganic semiconductors in which only few meV energy is required to dissociate the electron and hole in organic semiconductors approximately 100-400 meV energy is required. In the case of inorganic semiconductors the ambient thermal energy kT is enough to dissociate the electron–hole bonds. Considering the exciton diffusion length in organic semiconductors which is in the range of 5-12 nm there should be a p-n junction in this range to cause the electron–hole dissociation. The best characterised organic semiconductor examples are poly-3-hexyl-thiophene (P3HT) with exciton diffusion length of 5.4 nm, and [6,6]-phenyl C61-butyric acid methyl ester (PCBM) which is around 10.5 nm [30,38]. The exciton diffusion length is an important character which needs to be kept in mind while forming the hybrid film because it is related to the rate of charge creation, and hence impacts directly on the efficiency of the solar energy capture process [38-41].

The hetero-junction design is based on the premise that the donor and acceptor centres should be in very close contact for efficient charge transfer, and this is achieved by intimate mixing of the donor and acceptor particles. To maximize exciton dissociation, the domain sizes should be comparable to the exciton diffusion length. Figure 2.1 presents a schematic cross-section through such a hybrid device illustrating the arrangement of the donor/acceptor blend.

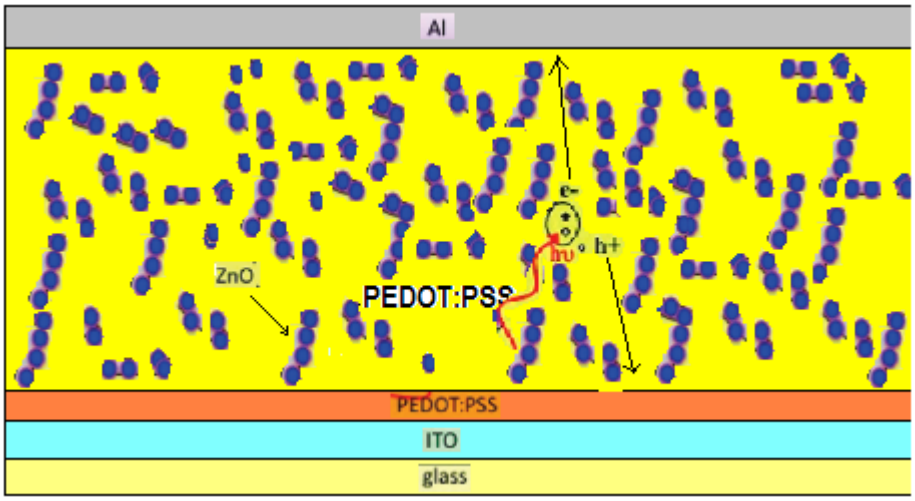

Figure 2.1 Bulk hetero-junction solar cell. Indium Tin Oxide (ITO) is the anode. and ZnO nanoparticles and P3HT are the components of the active layer which are the thickest layer approximately 30-200 nm, PEDOT:PSS is the electron blocking layer and Aluminium (Al) is the cathode.

The very low efficiency of the double layer p-n junction type solar cells can be improved using the bulk hetero-junction structure as it is depicted in Figure 2.1. This is an example of an ideal hetero-junction structure, with domains of a similar size to the exciton diffusion length, and continuous pathways to the electrodes to prevent losses through recombination at the electrodes and shunt pathways. Various types of bulk hetero-junction system have been developed, including polymer-fullerene blends, polymer- polymer blends, block copolymers, and organic-inorganic hybrid layers.

Figure 2.1 illustrates the basic structure of the bulk hero-junctionsolar cell.

In the operation of this hybrid cell, the P3HT polymer component absorbs photons and generates excitons, which, upon dissociation, donate electrons across the polymer/nanoparticle interface to the ZnO nanoparticles acting as the electron acceptor. The holes will remain in the polymer and travels to the anode. The schematic flow chart of photovoltaic organic solar cells is shown in Figure 2.2 below.

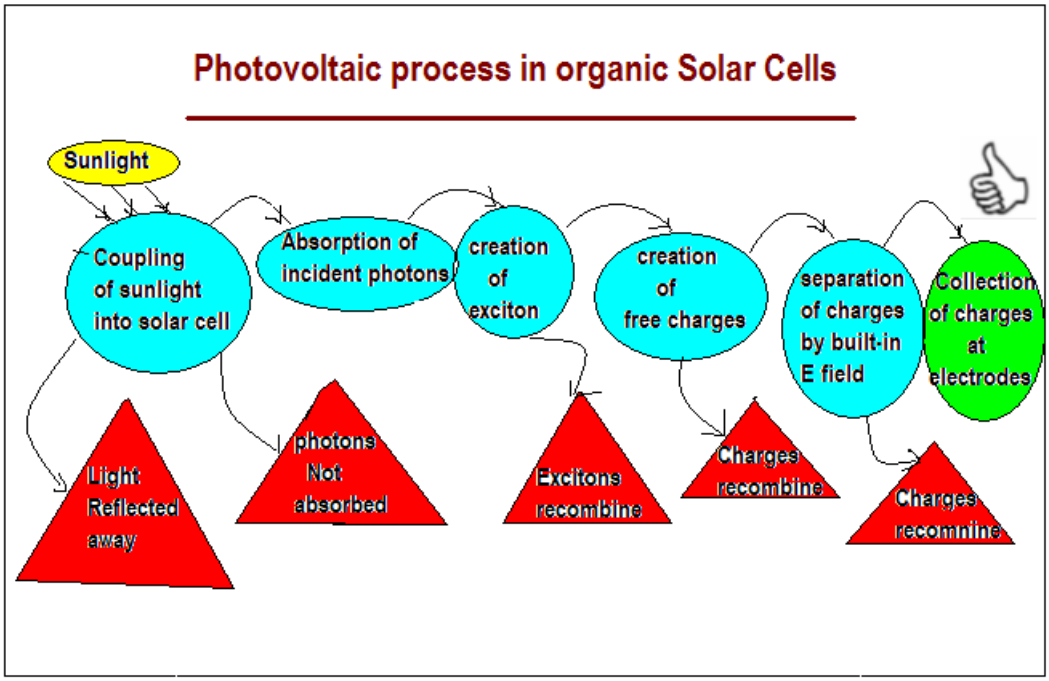

Figure 2.2 Photovoltaic process in organic solar cells [18]. The blue colour circles indicate the desirable process after sunlight incident on the solar cell. In this process after the absorption of light, exciton will be created followed by dissociation and separation of charges by the built-in electric field and finally collection of the charges at the electrodes. The red triangles indicate the probable, undesired process which may not end to the collection of the charges at electrodes. These can be; light reflection from the solar cell, not absorption of photons, exciton recombination and charges recombination.

Figure 2.2 shows the steps in the operation of an organic solar cell and includes the losses, which are represented by the red triangles. A fraction of light gets reflected and so the photons cannot be absorbed in the solar cell. In this project, light reflection could be mainly related to the morphology of the hybrid film surface. The photons absorbed in the P3HT region result in the creation of excitons, or bound electron-hole pairs, which are not free to move separately. The created excitons near the ZnO nanoparticles will have a higher chance to get dissociated. Excitons need to reach to the ZnO region before recombination during transport. The excitons then dissociate, to generating a free electron/hole pair charges, where the charges will be collected at the aluminium (electrons) and ITO (holes) electrodes. A potential difference is then created and an electric current can flow. To maximise the efficiency of the process, higher emission quenching is desirable. Emission or Photoluminescence quenching happens when the generated excitons dissociate at the donor-acceptor interface and do not recombine to result in

photoluminescence. Stronger quenching results in higher efficiency in a bulk heterojunction solar cell. The phenomenon of emission quenching can be investigated using fluorescent spectroscopy.

Figure 2.3 presents different stages that result in extraction of electrons from the cell. Here the mechanism of charge separation in a hetero-junction/hybrid solar cell is illustrated schematically. Step 1: Photo-excitation, which is the initial electronic excitation from the HOMO (highest occupied molecular orbital) energy level to the LUMO (Lowest unoccupied molecular orbital) level in the P3HT semiconductor. This happens after absorbing the light in a certain wavelength range which is a characteristic of the polymer semiconductor. The result of this excitation is the appearance of excitons in the polymer. Step 2: exciton dissociation; is the transfer of the electron from the P3HT LUMO to the ZnO LUMO. Step 3: transferring of electron from the LUMO of ZnO to cathode and hole from the HOMO of P3HT to ITO anode. Step 4, recombination of the separated electron and hole and returning back to its ground state in the P3HT semiconductor. 5: Recombination of electron already in the LUMO of ZnO with the hole in the P3HT semiconductor. [44,45].

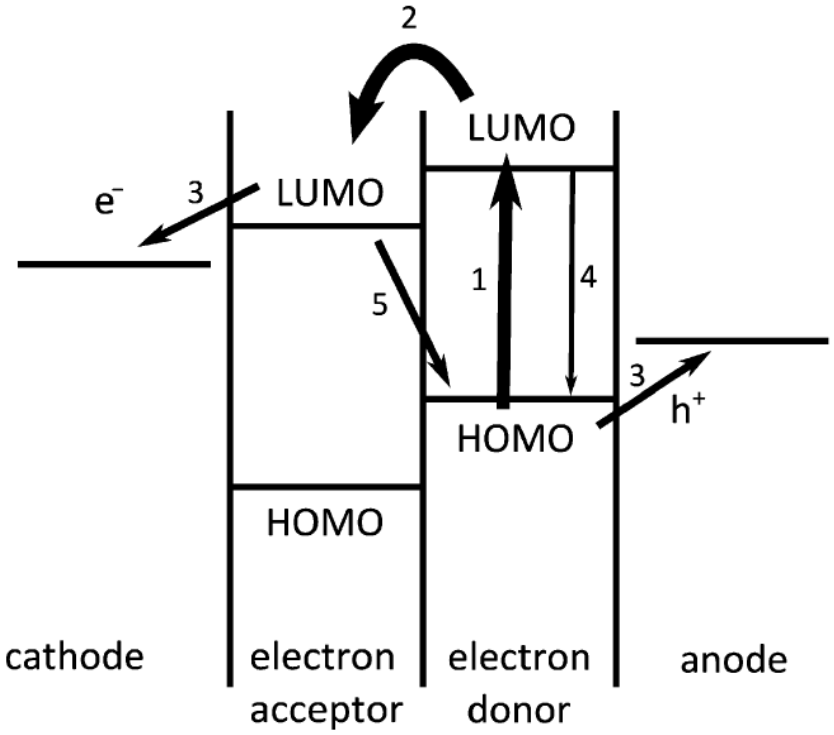

Figure 2.3 Mechanism of charge development in a bulk hetero-junction solar cell. HOMO is the highest occupied molecular orbital, LUMO is the lowest unoccupied molecular orbital, e- and h+ stand for electron and hole. Step1 is the photo excitation from the HOMO electronic level to LUMO, Step 2 is exciton dissociation, step 3 is the transferring of electron from the LUMO of ZnO to cathode and hole from the HOMO of P3HT to ITO, step 4 is the recombination of the separated electron and hole and returning back to its ground state, step 5 is the Recombination of electron already in the LUMO of ZnO with the hole in the P3HT semiconductor [17].

In comparison to bilayer solar cells, bulk hetero-junction solar cells possess a large interfacial surface area with much smaller domains of donor and acceptor which expedite the dissociation of excitons into electron and holes. That reduces the probability of electron/hole recombination and decay, and enhances the probability of exciton dissociation which allows the use of thicker films with increased light harvesting potential. However, the intermixing of the two phases into small domains tends to decrease the order in the molecular packing and means that continuous pathways are harder to produce, and isolated domains, which cause recombination losses, may exist. In addition, the larger interfacial area encourages recombination, and poor control of the phase morphology means that shunt pathways may exist. Balancing the increased photo generation yield against the increased recombination losses requires optimisation of the microstructure of the blend film [10].

The development of solar energy technology has been moving towards organic photovoltaic cells or, more specifically, flexible plastic solar cells. Based on statistics obtained by the National Renewable Energy Laboratory (NREL) in the United States, the efficiency of organic solar cells has been increasing by optimizing the processing conditions, especially by improving the quality of the active layer. Figure 2.4 shows the current trend in research solar-cell for light to electricity conversion efficiency, where it can be seen that efficiencies exceeding 4% had been achieved by 2005 and have almost doubled by 2011 [63].

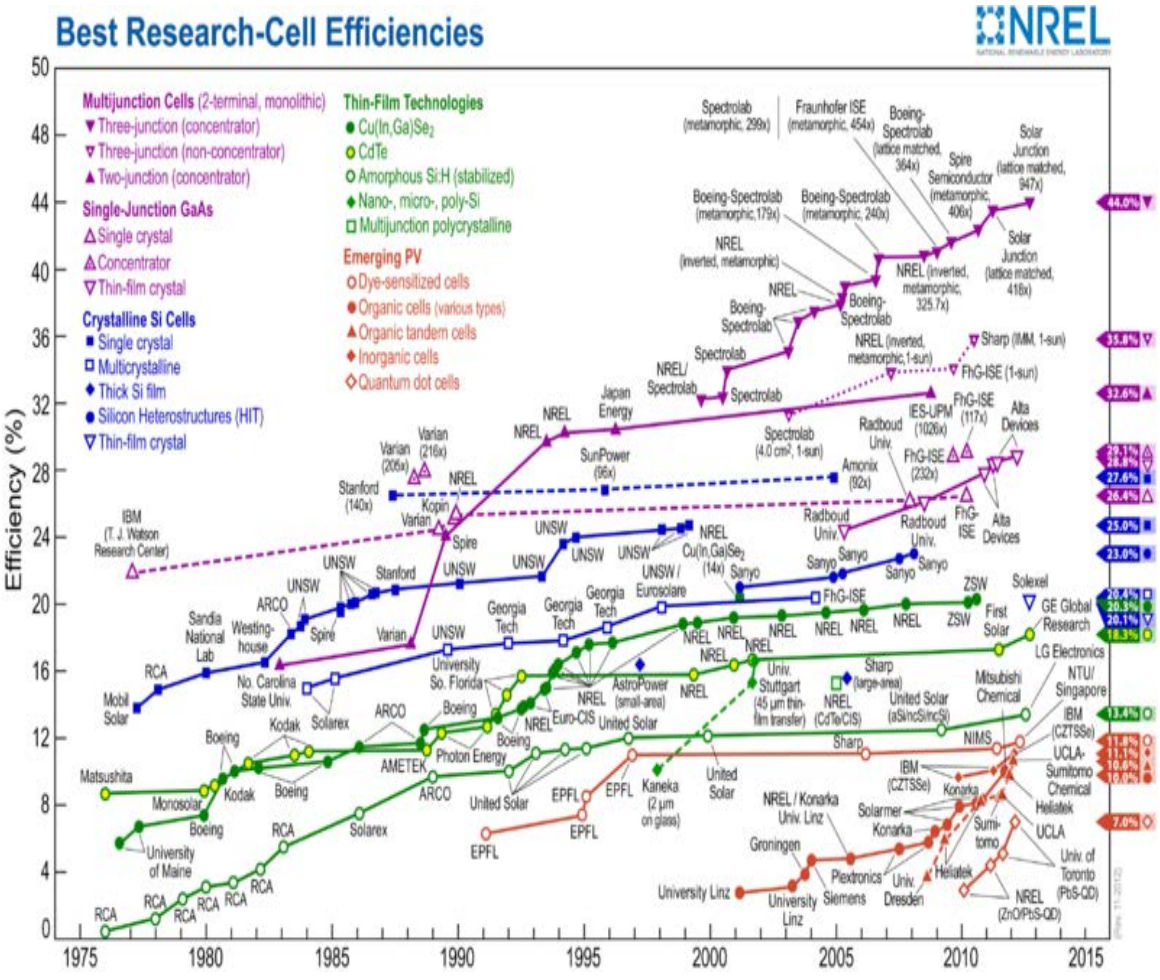

Figure 2.4. Progress of research-scale photovoltaic device efficiencies, under simulated terrestrial radiation conditions (AM 1.5M – see following text) [63].

In order to make meaningful comparisons of the performance of solar cells, the term ‘air mass’ (AM) is used as a value/coefficient that specifies the path length travelled by the solar radiation. This value is approximately equal to 1/cos(z)

where z is the Zenith angle in degrees. The Zenith angle is defined as the angle between a line perpendicular to the earth's surface and the sun. An AM value of 1.5 is conventionally used for testing photovoltaic devices exposed to terrestrial radiation, and this corresponds to a zenith angle of 48.2^0 [3].

In 1959, the first research investigation on an organic photo-voltaic (PV) cell was undertaken on an anthracene single crystal. The efficiency was extremely low and the maximum photo-voltage measured was 200 mV [60]. Since then, many years of research and investigation have demonstrated that the maximum efficiency obtainable from single (or homo-junction) organic materials is about 0.1%. Thus, with this efficiency limitation, solar cell devices of this type are quite impractical.

The mechanism of charge separation following the absorption of sunlight by a conjugated organic molecule results in the production of a mobile excitonic state. Simply speaking, an 'exciton' is an entity created by the columbic attraction between an electron and hole, after the electron has been displaced from its orbital by high energy photons (energies above the absorption edge). In this state, the electron is still associated with the excited atom, and it can either recombine with the atom or completely separate.

Now the force of attraction (F) between oppositely charged particles is given by:

$$F = k\, q_1\, q_2 / d^2$$

Equation 2.1 d is distance between charges, q_1 and q_2, k is Coulomb's constant

Equation 2.1 shows that the attractive force is inversely proportional to the dielectric constant. Hence, the low dielectric constant of an organic material (typically 2-4), compared to inorganic oxide nanoparticle semiconductors (or quantum dots),(11.9 in Si, 16 in Ge and 13.1 in GaAs). Therefore it is evident that the electron-hole combination is tightly bound in polymers, and this is the main reason that the excitons in organic semiconductors do not dissociate even at ambient thermal energies. In addition, the electric field resulting from the asymmetrical work functions of the electrodes is not strong enough to dissociate these photo-generated excitons [32,28] and so charge separation in organic materials is a major obstacle to the generation of an electric potential difference. It

is worthy to know that the dielectric property will reduce by reducing the particle size in inorganic nanoparticles [55]

In 1986 a major discovery by Tang paved the way to solve the problem of dissociating the exciton. He found that much higher efficiencies (about 1%) can be attained whenever an electron acceptor (A) and an electron donor (D) compound are brought together in one cell [33]. After this breakthrough, research in PV solar cells focused on the creation of a structure based on having a layer of a donor material adjacent to an acceptor material. This hetero-junction (p- and n-junction) concept is now the basis of all three common types of Photovoltaic Solar cells; (i) dye sensitized solar cells [34], (ii) planar organic semiconductor cells [33], and (iii) high surface area, or bulk, hetero-junction solar cells (BHJ) [12-15].

A revolutionary development occurred in the mid-1990's with the introduction of a blended structure or bulk hetero-junction, wherein the donor and acceptor were proportionally blended together. The important point which distinguishes this device from a bi-layer or homo-junction device is the huge interlayer contact area between the donor organic semiconductor and the acceptor inorganic nanoparticles. It has been found that the exciton created in the conjugated polymer has a very short lifetime, of the order of a nanosecond, and this result in a very short diffusion range, of the order of 5 to 10 nm [16]. Thus, since the overall thickness of the blended film is approximately 200-300nm, this provides a very high probability of the exciton interacting at a particle interface, resulting in electron-hole separation, so charge generation occurs throughout the active layer. However, to be effective, an appropriate charge transfer pathway must be present in each material to conduct the charge carriers (electrons and holes) to the respective electrodes.

One of the major obstacles in improving the efficiency is the control of the morphology of the organic polymer / inorganic nanoparticle blend so it can function efficiently, even when the diffusion length of the created exciton in the conjugated polymer is in the range of 5 to 10 nm [17]. Using ZnO nanoparticles/nanorods, in combination with poly 3-hexyl thiophene (P3HT), as acceptor and donor materials respectively, and optimizing the morphology of this active layer, has been one of the main concerns of many research groups [6,19,21].

Applying P3HT in bulk hetero-junction solar cell devices as a conductive conjugated polymer is advantageous due to its high light absorbance and superior charge carrier mobility when compared to other conjugated polymers, especially its high hole mobility [18]. ZnO nanoparticles possess suitable chemical and physical properties, the most important characteristic being its wide and direct band gap which is ideal for bulk hetero-junction devices. The band edges are from 4.4 ev to 7.6 ev. This means the compound does not absorb in the near-infra red and visible spectral regions, thus allowing the bulk of the sunlight to be absorbed by the conjugated polymer. Also, due to its high dielectric constant ZnO behaves as a good electron acceptor [31, 16, 19]. A further advantage is that the ZnO nanoparticles are easily synthesised, and there is no need for additional surface modification to make these particles soluble/compatible in organic solvents.

A major thrust to improve the performance of these hetero-junction organic solar cells concerns the enhancement of the interfacial contact between the conjugated organic polymer and the inorganic nanoparticle [6]. Chen *et.al* (2009) have studied the effect of interfacial linker molecules on ZnO nanorods by monitoring the changes/improvements in photovoltaic performance and resultant photo conversion efficiency. In a hetero-junction solar cell based on ZnO, P3HT and linker molecule, mercurochrome ($C_{20}H_8Br_2HgNa_2O_6$). This linker molecule increased the short-circuit current density (J_{sc}) from 1.96 to 2.45 mA/cm^2 , the open-circuit voltage from 0.38 to 0.46 V , and the fill factor from 40 to 46, which led to an overall increase in efficiency of the solar cell device from 0.3% to 0.5% [32]. The ZnO nanorods also improved the conduction pathway for the dissociated electrons and minimised the chance of them being trapped in discontinuous pathways. In addition, in Chen's design, the direction of the exciton incident to the aligned nanorods decreased the possibility of electron - hole recombination [6].

Further studies on the effect of spectral mismatch have also been done by modifying the absorption spectra of the absorbing /active layer, and a P3HT/ Methanofullerene mixed layer/film showed some improvement in the overall performance of the hybrid solar cell [6].The effect of annealing and changes in film thickness on the performance of solar cells also have been investigated. In these experiments they have taken advantage of regio-regular P3HT because it is an

ideal conductive/semi-conductive material due to its stability and spectral absorption in the red region of sunlight. In this instance, for devices with an active layer thickness of 43 nm, under an Air Mass of 1.5, and subject to 100 mW/cm^2 light illumination, they achieved a 3.2% power conversion efficiency (PCE) with fill factors up to 67%. After thermal annealing at the optimized temperature and active layer thickness, they achieved a PCE up to 4.0%, which is among the highest efficiencies reported in the year 2005 [20, 21].

Ackermann et.al (2010) also tried to modify the surface of ZnO nanorods using Tetra(4-carboxyphenyl) porphyrin (TCPP). He dye-sensitised the ZnO nanorods by grafting the TCPP molecules on the surface of ZnO nanorods. This direct grafting of TCPP molecules on the surface of ZnO nanorods resulted a very efficient electron injection process into the ZnO nanorods after the light absorption. Furthermore, by increasing the TCPP concentration aggregation of ZnO nanorods within the P3HT has been obsereved. Here they concluded that adition of TCPP results in increasing the Photo current generation in the P3HT/ZnO mixture considering a strong modification in the morphology [73].

Friend et.al (2010) also has done research on enhancing the efficiency of hybrid photovoltaic device. He used P3HT as the active material and ZnO solution-processed flat film modified by a self assembled monolayer of phenyl-C61-butyric acid (PCBA) as electron extracting electrode. Here the EQE of the self-assembled monolayer modified device reached 9% which greatly improved over the 3% of the unmodified device. Friend show that both the Short circuit current and open circuit voltage have significantly improved [75]. Yan et.al (2010), has used the combination of P3HT and nanofibrouse ZnO network to create the active layer and investigate the results. He has found out that by increasing the thickness of the active layer the lifetime of carriers will reduce. This was the first time using this structure of ZnO in P3HT and the resultant efficiency was 0.51% [73]. The year after in 2011 Janssen came up with the idea of creating more intimacy between P3HT and the ZnO nanoparticles. This was done by side chain functionalization of P3HT. Photoinduced absorption showed quantitavie charge generation for Poly(3-hexylthiophene-2,5-diyl) derivative (P3HT-E) and ZnO and not for P3HT: ZnO. This resulted a very good improvement in solar performance [69].

Reichman et.al (2012) and his group have followed the P3HT:ZnO hybrid by investigating the charge transport and charge transfer at the acceptor and donor interfacial. Here they have used a field effect transistor to study the photo current generation . There have been a comparison between Charge transfer at the heterojuctions of P3HT:ZnO and P3HT:Tiol-ZnO. Here the role of thiol modification of ZnO incharge transfer and charge transport within the bulk heterojunction interface was indicated through comparison of the threshold voltage and the FET mobility betweenP3HT/thiol-ZnO and P3HT/ZnO FETs. Of course role of thiol molecules as an ultrathin passivation layer for the ZnO surface in enhancing photoinduced charge separation at the interface has not been identified in Reichman's group investigations [71]. Cui et.al (2012) has continued the research on optimising ZnO nanorods and P3HT by enriching P3HT with Graphene and grafting porphyrin molecules on the surface of the ZnO nanorods. Adding graphene to P3HT has reduced the resistivity of the P3HT by two orders of magnitude and resulted in increasing the hole mobility. Also direct grafting of the porphyrin molecules to ZnO have resulted in a very efficient electron enjection into the ZnO nanorods. In overall these modifications has improved the solar cell efficiency [72].

Using Squarine dye and fullerene C60 Yang et.al (2012) has achieved more than 6% efficiency using. The results show that the heterojunction structure in tems of morphology and thickness are very crucial parameters. Here Yang group has optimized the thickness in order to achieve high efficiency, Their optimum thickness is between 50 to 90 nm. They also emphasis on using a dye with high absorption coefficient and a bandgap which covers near red region of sunlight spectrum [76]. This high efficiency dose not indicate that ZnO:P3HT hybrid is a no worthy combination because theoretically it has been calculated that a short circuit current of 5.2 mACm2 and a fill factor of 52% (under AM1.5 illumination) and with the calculated open circuit voltage of 2.07 V then the device efficiency would be 5.6%. This result makes ZnO:P3HT hybrid quite attractive for technological applications [78]. Chen et.al (2013), in his research on ZnO:P3HT has come with the idea of using poly(3-hexylthiophene)-b-poly(ethylene oxide) (P3HT-b-

PEO) well-defined P3HT-b-PEO diblock copolymer as an interfacial compatibilizer to control P3HT/ZnO hybrid system morphology and thereby improve the power-conversion efficiency. This interfacial compatibilizer helps the ZnO nanoparticles to well distribute in the P3HT polymer and also controls the phase separation and enhances the crystallinity of P3HT. In overall this modifications can represent a promising way to improve the photo voltaic properties of this solar cells. It is worthy to mention that the PCE is still low even after these improvements by utilizing compatibilizer. The reason mention for this by this research group is that the Polymer and ZnO nanoparticles used in this experiment they both have large band gaps, therefore they are not able to absorb a vast spectrum of the sunlight [74]. Recently, more research groups are focusing on donor-acceptor interfacial rectifications in order to improve the photovoltaic properties. Wu et.al (2013) investigated the effect of interfacial improvement of the ZnO nanorods and P3HT polymer. The modifications were done by epitaxial room temperature ZnO shell and also by D149 dye molecules before the P3HT was added. The J_{sc} of the modified ZnO nanorods decreased and V_{oc} and FF were considerably improved. In overall the modified and not modified ZnO surfaces in conjugation with the P3HT have almost showed the same efficiency of 1.16% [77].

Hayase et.al (2013) studied the charge separation and charge recombination dynamics in P3HT:ZnO and P3HT:dye:Zno bulk heterojunction hybrid solar cells using transient absorption spectroscopy. Here again the aim was to understand what changes can an interfacial modification bring to bulk heterojunction solar cell. The dye used in this experiment was SQ36 which has absorption in the near infrared region (NIR) of the sunlight spectrum. Studying the charge separation and recombination was done by using obtical absorption of P3HT in the region of visible and optical absorption of dye (SQ36) in the region of NIR. Hayase group found that in the case of P3HT:ZnO charge separation happened within 1ps and there was a significant charge recombination due ZnO surface states and the coulomb attraction between electrons in ZnO and holes in P3HT. But in dye treated ZnO charge separation occurred over 3-4 ps (for the visible light absorption) and 10ps (for the NIR light absorption). Here the charge recombination was largly reduced due to locating the dye at the interface [79].It is noteworthy that

the 4% efficiency achieved by Shrotriya's [20] group was the result of combining two very promising materials, P3HT and Phenyl-C61-butyric acid methyl ester (PCBM), and further work is continuing to substitute PCBM and fullerene derivatives with other inorganic nanoparticles to optimise performance. Nano-sized TiO_2, CdSe and ZnO are being used as highly functional materials in the area of optoelectronics.Janssen has also studied in detail the ZnO nanoparticles and P3HT hybrid films. He has brought into consideration the effect of the morphology and the thickness of the hybrid films [21]. In his research, Janssen has found out that thicker P3HT/ZnO cells outperform the thinner solar cells because of increasing current density, for constant fill factor. They also found that the internal quantum efficiency (IQE) increases significantly with layer thickness from 20% for 50 nm to up to 50% for cells with active layer thickness > 150 nm. Therefore, in thicker layers, not only the photon absorption increases but also this photons are more efficiently can be transferred into collected current.

McGehee and his group has used TiO_2 nanoparticles in a hybrid hetero-junction solar cell device [57,58]. The maximum external quantum efficiency observed was 10%, and the estimated PCE efficiency was 0.45% under AM 1.5 conditions. Several other groups have reported efficiencies for TiO_2 / conjugated polymer hybrids from 0.40 to 0.45% [58]. Replacing TiO_2 with ZnO nanoparticles led to a significant improvement in the performance of the hybrid device. Combining the external quantum efficiency of ZnO nanoparticles with the conjugated polymer Poly[2-methoxy-5-(3',7'-dimethyloctyoxy)-1,4-phenylenevinylene] (MDMO-PPV) gave an estimated short-circuit current density of 3.9 mA/cm^2 at AM.1.5 ($100mW/cm^2$) and a final PCE efficiency of 1.6%.

McGehee demonstrated a fourfold improvement for the ZnO:MDMO-PPV solar cell[59]. However, the efficiency is less than that of the best CdSe:polymer bulk hetero-junction solar cell. For example, a device based on CdSe nanoparticles and the conjugated polymer mix MDMO-PPV in a stratified layer design, exhibited a short-circuit current (Jsc) of 6.42 mA/cm^2, an open circuit voltage of 760 mV, a fill factor of 0.44 (89.9 mA/cm^2 under AM.1.5) and an external quantum efficiency of 52% with 2.4% PCE efficiency. It is notable that, compared to a CdSe based

hybrid cell, a ZnO based device performs at a higher Voc (open-circuit voltage) and FF (fill factor) but a lower Jsc (short-circuit current) [59].

The external quantum efficiencies and final power conversion of the ZnO/conjugated polymer based devices show a significant improvement when compared to the reported hybrid polymer solar cells based on TiO_2 and similar CdSe polymer cells. This highlights the attractiveness of ZnO nanoparticles as an important material for application in bulk hetero-junction solar cells. The higher Jsc for ZnO in comparison to CdSe can be attributed to the absence of light absorption in the visible region of ZnO. CdSe contributes to the cell current by hole transfer in the visible region up to 675 nm which is beyond the absorption region of the polymer [16].

The Janssen group conducted a study of the performance of a bulk hetero-junction solar cell consisting of ZnO nanoparticles and poly 3-hexyl thiophene [16]. This article detailed the fabrication of the solar cell and listed its optimized parameters [35]. A comparison between devices using P3HT and MDMO-PPV as electron donors and using ZnO nanoparticles as the common acceptor material found that the external quantum efficiency of ZnO: P3HT is 27% versus 40% for the ZnO:MDMO-PPV cell, with the IPCE efficiency also much lower, 0.9% ZnO: P3HT versus 1.6% for the ZnO : MDMO-PPV based device.

2.2 Research options for the present study

On the basis of the preceding discussion, it is concluded that further improvements to the ZnO : P3HT based bulk hetero-junction solar cell are feasible, especially with regard to optimising the interaction between the nanoparticles and the conjugated polymers. The effect of annealing is another variable that can be investigated, since it has a significant effect on device efficiency. Jansen and his group have also studied the effect of the three–dimensional shape and morphology of the hybrid layer on the efficiency of the bulk hetero-junction solar cell [21]. They imaged the cross-section of a typical P3HT/ZnO photo-voltaic cell using transmission electron microscopy, and also reconstructed the volumes of P3HT/ZnO layers using electron tomography. On the basis of this study they concluded that by increasing the thickness of the ZnO/P3HT active layer the

charge generation becomes much more efficient, but the internal quantum efficiency cannot exceed 50% because of difficulty in collecting the generated charges. Hence, improved control over the morphology of the photo-active layer can result in enhanced performance and efficiency of the device, and this is a major purpose of the present study.

2.3 Project objectives

The aim of this study is to understand the effect of several parameters on the efficiency of bulk hetero-junction solar cells. Hybrid solar cells are chosen for this study due to their simplicity of production (solution-based processibility) and comparative cheapness and their flexibility. Other advantages include their wide range of applicability due to their processibility on very thin substrates, and the low preparation temperature in comparison to silicon-based solar photovoltaic cells. The purpose of the project is two-fold; first, to create clear, proper hybrid films for implying in bulk hetero-junction solar cells, and second, to investigate the optical and electrical characteristics of the hybrid films.

To achieve these objectives, the project was subdivided into four phases: a) synthesis of the semiconductor metal oxide (ZnO) followed by purification and characterisation, and its phase transfer into a stable solution; b) blending of the ZnO and P3HT and then spin-coating the hybrid solution on the prepared ITO glass substrate; c) investigation of the optical and electrical characteristics of the hybrid film; and, d) Surface study of the hybrid films.

The initial step was to reproduce the bulk hetero-junction ZnO/P3HT solar cell as a bench mark to provide a set of reference performance characteristics. On the basis of an analysis of the data, the following parameters can be optimised; (i) Active layer condition, (ii) Hole conducting layer, and, (iii) Surface morphology. Which should result in improvement of the functionality of the solar cell and its solar light-to-electron conversion efficiency.

The solar cell chosen for study is based on a hybrid layer made of ZnO nanoparticles and regio-regular poly 3-hexyl thiophen (P3HT). The ZnO nanoparticles were used to take advantage of their high dielectric constant and wide electronic band gap, which enables them to act as a good electron acceptor. The regio-regular P3HT was utilised due to its excellent hole mobility and photosensitivity [34, 35].

Here, in the proposed method of synthesis of ZnO nanoparticles the effort is to avoid using water in the reaction. The reason is that water in the final mixed solution is an unwanted material which reduces the solubility of P3HT in the chloroform and helps to increase the agglomeration of ZnO nanoparticles in the mixture. The properties of ZnO nanoparticles is investigated and a set of complete characterization and imaging, including XRD and XPS are performed.

The miscibility of the particles in the polymer solution; The miscibility of ZnO nanoparticles in the P3HT polymer solution is a very critical part of the experiment, since an ideal blend of these two materials (i.e. the ratio of the donor and acceptor in the active layer) should provide a good pathway for charge carriers to reach the electrodes and achieve a high efficiency.

One of the main challenges is to optimise the stability of the ZnO nanoparticles in the P3HT chloroform solution, since they are likely to have a tendency to agglomerate due to their high surface charge.

The preparation and etching of the ITO substrate is also very important. Quality of the surface etching on the ITO is critical to ensure optimal electrical contact with the polymer hybrid to achieve maximum efficiency of the solar cell. A spectroscopic study of the layers/films in this solar cell, including the hole conducting (electron blocking) layer and the active layer, is an essential part of the project. Atomic force microscopy is used to study the surface morphology of electrodes.

After spin-coating of the hybrid layer on the ITO substrate an aluminium metal electrode/contact was deposited on the active layer, using a metal evaporator operating under a comparatively high vacuum. This is to prevent the deposition of aluminium oxide instead of pure aluminium. Aluminium oxide is an insulator and in an electrode with increasing the fraction of aluminium oxide instead of pure

aluminium the series resistance will increase which decreases the efficiency of the solar cell.

The preparation of the ZnO/P3HT layer achieved using a spin coater instrument, whereby the films were drop-cast on the substrate. Further processing, including vacuum annealing was also undertaken. Absorption spectroscopy was used to characterise the solution which is the solution containing the ZnO nanoparticles prepared before spin coating the layers and for the films formed after solvent evaporation. Fluorescence spectroscopy was also used to provide information regarding the functionality and quality of the active layer. Atomic force microscopy was used to study the surface morphology of the film including the active layer and electrodes.

Subsequently, the assembled hybrid hetero-junction solar cell was subjected to the required tests in the RMIT University solar cell laboratory. These tests and measurements included the incident photon to electron conversion efficiency (IPCE) and measurement of the I-V (current-voltage) behaviour of the fabricated device, which is used to calculate the total efficiency. In overall, these studies are expected to provide further knowledge about how hybrid solar cells function and a deeper understanding of their behavioural characteristics, specifically their optical properties, and how they are related to the overall performance of the solar cells.

Chapter 3

3. Fabrication

The experimental procedure is divided into three main stages, with the ultimate goal being to prepare a high performance bulk hetero-junction solar cell device. One of the most important components of the hybrid layer in this device is the ZnO nanoparticles. As explained in the Introduction (Chapter 1), ZnO nanoparticles act as electron acceptors in the hybrid film, and this critical property is highly dependent on the size and shape of the nanoparticles [24].

3.1 Synthesis of ZnO nanoparticles

The first step is to synthesise highly stable ZnO nanoparticles using Pacholski's method [23]. In this procedure, the ZnO nanoparticles were synthesized by alkaline hydrolysis of zinc acetate dihydrate, $(CH_3COO)_2Zn.2H_2O$, using the strong base potassium hydroxide (KOH) dissolved in methanol, according to the following chemical equation :

$$Zn^{2+} + 2OH^- \rightarrow Zn(OH)_2 \xrightarrow{\text{heat / methanol / } 60^oC} ZnO + H_2O$$

During the 2 Hours it took to complete this reaction, the temperature was held at 60^0C. As it is suggested [23], a mole ratio of 1.0 Zn^{2+} : 1.7 OH^- was used, indicating a slight molar deficiency of KOH from the theoretical 1.0 Zn^{2+} : 2.0 OH^- suggested by the balanced chemical equation, above.

It is worth noting that this synthesis of ZnO nanoparticles is achieved by hydrolysis of the precursor zinc acetate dihydrate salt in an alcoholic solution of the strong base, KOH, which leads to precipitation of the Zn^{2+} ions as ZnO nanoparticles. The precursor is removed by washing with methanol during the purification. The white ZnO nanoparticles absorb weakly in the visible region of the electromagnetic spectrum due to their wide band gap (3.2 eV), and this lack of absorption by the solution/dispersion can be taken as an indication that the synthesis has proceeded correctly and the solubility of the nanoparticles is satisfactory.

By preparing a zinc acetate solution in methanol having a concentration of 100 mm, and a potassium hydroxide solution in methanol having a concentration of 170 mm, equal volumes of the solutions could be mixed to provide the reaction mole ratio suggested by Weller [23]. The preparation began by heating the zinc acetate solution to 60^0C while stirring to produce a well agitated solution, then an equal volume of KOH solution with 27^0C temperature was added drop wise over a period of 10 minutes. The inaccuracy in the method of KOH addition to the solution results in non-uniform ZnO nanoparticles size. This means that if the KOH solution is added all at once or the rate of addition changes it will result in non-uniform ZnO nanoparticles solution. This has been experienced during several times of synthesis.The correct rate was found experimentally by systematically varying the rates and the resultant ZnO sizes were checked with HTEM to confirm the best result and optimal KOH rate. Having a constant speed of magnetic stirring (300 round per minute) and steady rate of KOH addition was found very important. During the KOH addition, the clear solution changed from transparent to milky, and then gradually changed back to transparent. After two hours heating and continuous stirring, the ZnO nanoparticles were isolated using a centrifuge (Eppendorf 5804) with the supernatant being removed as completely as possible. The ZnO nanoparticles were then purified by washing three times with room temperature methanol. This method has the advantages of not using any template or surface modifying molecules, and not using water in the reaction mixture.

The harvested ZnO nanoparticles were then dispersed in a mixture solvent having the optimized composition of 94-6 (Volume ratio) chloroform-methanol. The best mixture of Chloroform and methanol was determined by a series of trials at various mixture ratios. The presence of methanol in the chloroform is essential, because without it, the dispersibility of the ZnO in the solvent will dramatically get reduced and will result in agglomeration and precipitation.

removing the supernatant was calculated to be in the range of 100-180 mg/mL depending on variations in the performance of the experiment. This value was obtained by evaporating a sample of the ZnO/chloroform-methanol mixture to

dryness in an oven at 120 ^{o}C. The step to step method for the ZnO nanoparticle synthesis is listed below:

1. The mass of each precursor, zinc acetate dihydrate (($CH_3COO)_2Zn.2H_2O$) and potassium hydroxide (KOH), was calculated based on the concentrations needed in the experiment :
   Mass = (Concentration in mole/L) x (M.W. in g/mole) x (total Volume in L).
   The concentration of the KOH used in the reaction was 1.7 times the concentration of the zinc acetate dihydrate as mentioned above.

2. Both precursors were then dissolved in methanol in separate 50 mL volumetric flasks.

3. The zinc acetate–methanol solution was then placed into a 3-neck round bottom flask and heated to 60^{o}C using a heating mantle fitted with a thermostatic controller. The thermometer was placed to monitor and control the temperature. The solution container was very well sealed in order to prevent the methanol loss.Continuous stirring was performed using a magnetic stirrer.

4. The potassium hydroxide-methanol solution was then added drop wise into the zinc acetate solution over a period of 10 minutes (corresponding to approximately 5 mL per minute) using a dropping funnel for control. This rate have been determined experimentally through a systematic variation in the rate of KOH addition and imaging the resultant particles sizes and morphologies by transmission electron microscopy.

5. The progress of the synthesis can be divided into three stages based on the colour and appearance of the solution. At first, after about 20-30% of the potassium hydroxide has been added, the solution starts to become cloudy, and this milkiness increases throughout the addition; then, after a few minutes, the suspension starts to gradually become clear and transparent; finally, after another 20-30 minutes, the solution again becomes cloudy and

this persists till the end of the reaction. Absorbance spectra were taken at the end of each stage of the reaction to provide a basis for estimating particle size and distribution. Jasco V-670 absorbance spectrometer was used for the absorption spectroscopy.

6. At the end of the reaction, and after cooling the solution to room temperature, isolation and purification of the ZnO nanoparticles was achieved using an Eppendorf 5804 centrifuge, operating at 3000 rpm for 10 minutes. After removal of the supernatant reaction mixture, the ZnO nanoparticles were washed three times with 23 ^{0}C methanol.

7. The ZnO nanoparticles were then dispersed in the mixed chloroform (94%)/ methanol (6%) solvent mixture. With this optimized solvent mixture, the ZnO nanoparticle solution was stable for at least a month. (This step must be done very accurately otherwise the whole synthesis effort will be wasted).

   The concentration of the ZnO containing solution was determined gravimetrically, by adding 500µL of solution to a tared vial, and drying it in an oven at 120^{o}C for 30 minutes, then the weight difference is the net weight of the ZnO in that specific volume.

8. The ZnO dispersion/solution must be protected from light and humidity, and this was done using a paraffin seal and aluminium foil cover.

3.2 Structural characterization of ZnO nanoparticles

3.2.1 UV- Visible characterisation

A typical UV-visible absorption spectrum of the ZnO nanoparticle solution/dispersion is shown in Figure 3.1, where it can be seen that after three months storage there is a slight shift in the absorbance towards the red-end of the spectrum. The range of the wavelength on the absorbance spectrometer is 350-3500 nm.

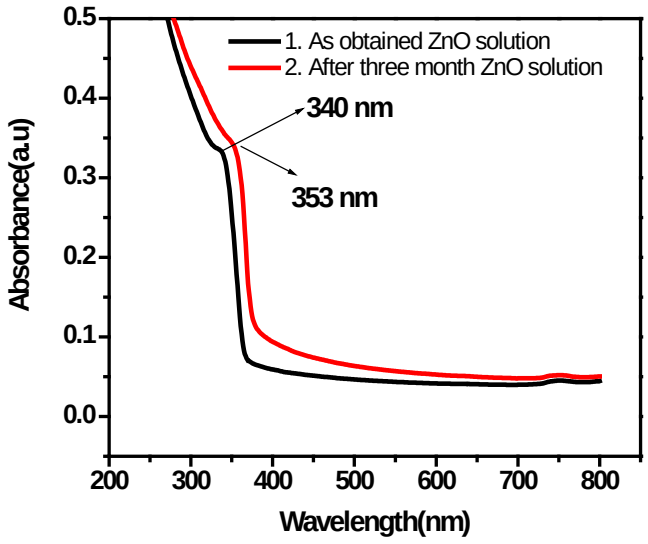

Figure 3.1 UV–Visible absorption spectrum of ZnO nanoparticles dispersed in the chloroform/methanol mixture (94-6 Volume ratio): (1) is the freshly prepared ZnO solution, and (2) is the ZnO nanoparticle solution after three months.

This change indicates that there has been a particle size growth in the solution during the three month period which resulted in decreasing the band gap energy

absorption of the ZnO nanoparticles. A very small amount of particle aggregation has occurred over this time which is quite apparent in the given graph. In figure 3.2 the UV-absorption of the highly agglomerated ZnO solution is presented. This aggregation usually have been observed between three to four month of storing the well dispersed ZnO nanoparticles in the mixture solution of 94-6 (Volume ratio) of chloroform and methanol. This agglomeration is the result of high surface charges of the ZnO nanoparticles in the comparatively dispersed in much less volume of the methanol mixed in the chloroform. ZnO nanoparticles are dispersible in the polar solution and not in the non-polar solution (chloroform) and here by decreasing the volume portion of methanol in the mixture (4% of the total volume) we increase the probability of particles to sense each (attraction) other and therefore due to the high surface changes on the surfaces of ZnO nanoparticles cause the agglomeration. It is worth noting that the reference for all the absorption spectropy measurements were air.

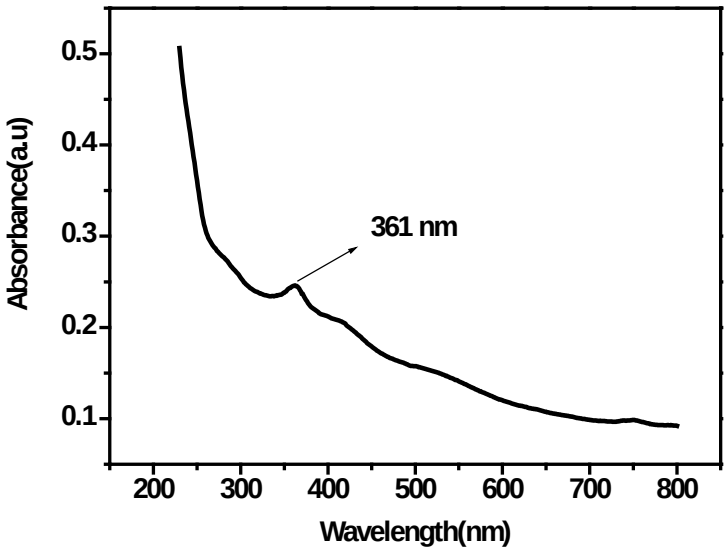

Figure 3.2 UV–Visible absorption spectrum of highly agglomerated ZnO nanoparticles dispersed in the chloroform/methanol mixture (94-6 Volume ratio) after four month.

The peak absorption wavelength has red-shifted from 340 nm in the as prepared ZnO solution to 361 nm in the agglomerated ZnO solution after four month.

Indeed, it is not only the peak position which has significantly changed but also the absorption behaviour has apparently changed. In figure 3.1 the absorption is almost negligible everywhere else except the peak absorption wavelength but in the agglomerated case in figure 3.2 there is a smooth ramp in the absorption graph versus changing the wavelength which indicates the nonuniformed sizes of agglomerated ZnO particles.

3.2.2 X-ray diffraction (XRD)

The X-ray diffraction (XRD) spectrum of the purified ZnO nanoparticles is shown in figure 3.3. The sample preparation for X-ray diffraction was done simply by drop casting the ZnO nanoparticles in the Methanol solution on the normal glass and drying the sample in room temperature. It was made sure that the thickness of the sample was enough to achieve higher intensity out of the diffracted rays. The calculated average diameter of ZnO nanoparticles was 11.7 nm diameter or 5.85 nm radius. This is perfectly matching with the obtained particle size distribution extracted from the high resolution transmission electron microscopy (see section 3.2.4). This calculation is performed using Sherrer's formula:

$$D = 0.9\lambda / B \cos\theta$$

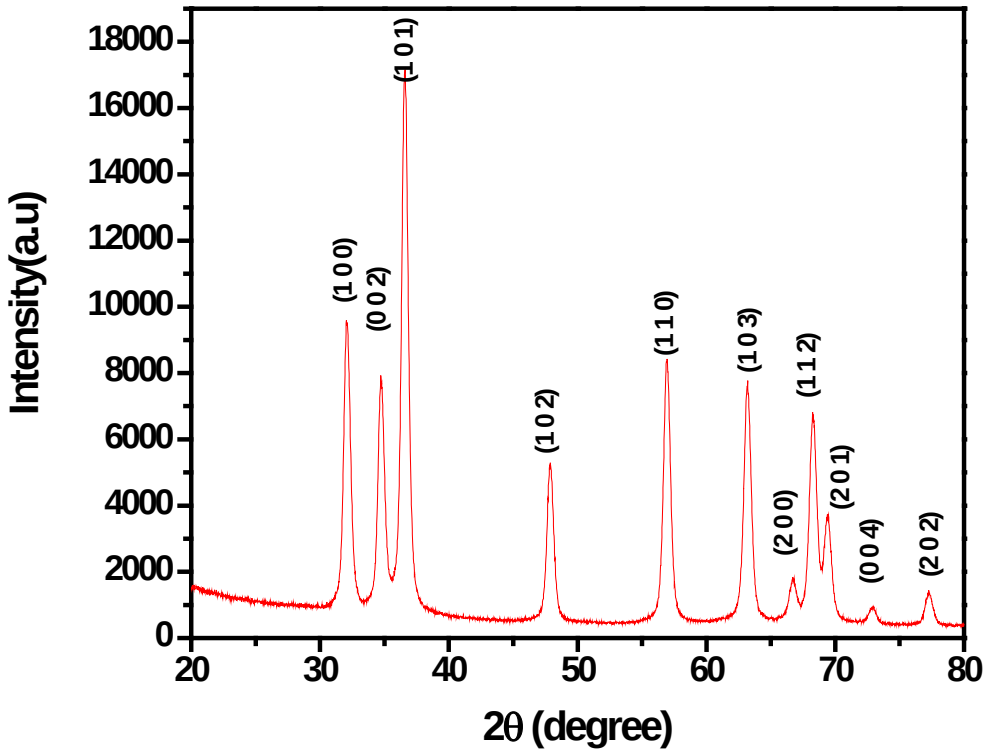

Figure 3.3 X-ray diffraction (XRD) pattern of the purified ZnO nanoparticles.

In the above Sherrer's formula λ =1.54 A^0 is the wavelength of the used X-ray, B is the full width half maximum (FWHM) in terms of radian and θ is the peak maximum angle in radian. The required values extracted from the diffraction pattern shown in figure 3.3 are placed in table 3.1. All the XRD peaks can be indexed to the hexagonal Wurtzite phase of ZnO (JCPDS Card No. 80-0075), indicating the formation of a single phase, suggesting that the nano-crystals have a preferential orientation with no significant impurities. Powder XRD patterns were recorded on a Bruker D4 ENDEAVOR X-ray diffractometer with Cu Kα radiation. The XRD pattern has beed compaired with few recent ZnO XRD patterns in order choose the correct indices. The preferred crystal orientation has found to be the c axis. Using scherrer's formula the particle sizes assigned to (100) and (002) peaks have also been calculated and the results are approximately equal to the one calculated for the (101) peak.

Miller indices and FWHM(deg)		FWHM(rad)(**B)**	Peak max 2Θ	Peak Max Θ	Max Θ (rad)	Cos Θ	dcrystal A^0**(average diameter of the nanoparticles)**	dcrystal nm
(101)	0.75	0.013083	36.54	18.27	0.318	0.9498	111.66	11.17
(002)	0.75	0.013083	34.74	17.37		0.9543	111.01	11.10
(100)	0.75	0.013083	32.09	16.05		0.9610	110.23	11.02

Table 3.1 Required information for particle size measurement using Scherrer's formula. These are extracted from the X-ray diffraction pattern depicted in figure 3.3.

In the performed experiments and characterizations only the XRD of the ZnO nanoparticles were performed in order to confirm that crystalinity is observed. Motaung et.al. has found out that the Pure region-regular P3HT film have only one peak and that is the (100) at 2Θ= 5.4˚. This peak is associated with the lamella structure of thiophene rings in P3HT. After annealing at 110˚c it shows a secondary peak (200) at 10.8˚ and at 150˚C the tertiary peak (300) appears at 15.9˚ [84].

3**.2.3 Surface area and porosity measurements**

The specific surface area (SSA-BET) of the ZnO samples was determined using the Brunauer-Emmett-Teller (BET) analysis. The average BET equivalent particle diameter (d_{BET}) was calculated using the average density of the ZnO nanoparticles. The BET specific surface areas were measured using an accelerated surface area and porosimetry system (ASAP 2010) manufactured by the Micrometrics Instrument Corporation. Samples were degassed overnight at 373 K and the surface area was measured by N_2 adsorption/desorption at 77 K. The BET surface area of the ZnO nanoparticles was found to be 29.06 m^2/g.

Using the same instrument, almost no surface porosity was found on the surface of the nanoparticles.

3.2.4 Transmission electron microscopy

A transmission electron microscopy (TEM) image of the pure ZnO nanoparticles is given in Figure 3.4.a, where it can be seen that the average particle size is about 5.1nm, which is almost half the value calculated using Sherrer's formula and the X-ray diffraction data. This may be due to agglomeration of the nanoparticles during the sample preparation for XRD.

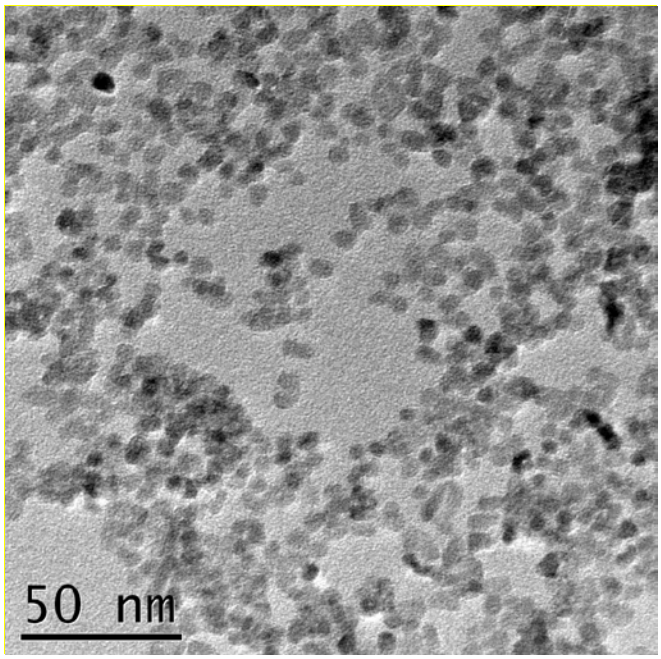

Figure 3.4 (a) Transmission electron micrograph (TEM) of ZnO nanoparticles.

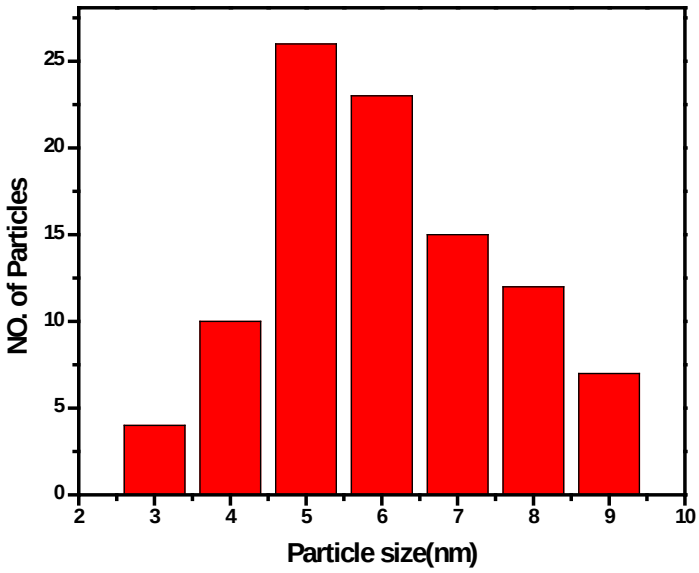

Figure 3.4 (b) Particle size distribution obtained from TEM micrograph.

Figure 3.4.b shows the particle size (diameter) distribution for the purified ZnO nanoparticles, which is in the range of 3-9 nm.

3.2.5 Energy- dispersive X-ray (EDAX) measurements

The Energy- dispersive X-ray (EDAX) spectrum of the purified ZnO nanoparticles, presented in figure 3.5, indicates the high purity of the nanoparticles. In addition to the zinc peaks, copper peaks are also detected, which arise from using a copper grid to support the particles. The TEM image and EDAX spectrum were obtained on a Jeol 2010 microscope operated at 200 kV with a Link Si(Li) X-ray detector. Sample powders were suspended in methanol and then directly deposited on a copper grid coated with a carbon film. The EDX measurements were performed to assess the purity of the ZnO nanoparticles.

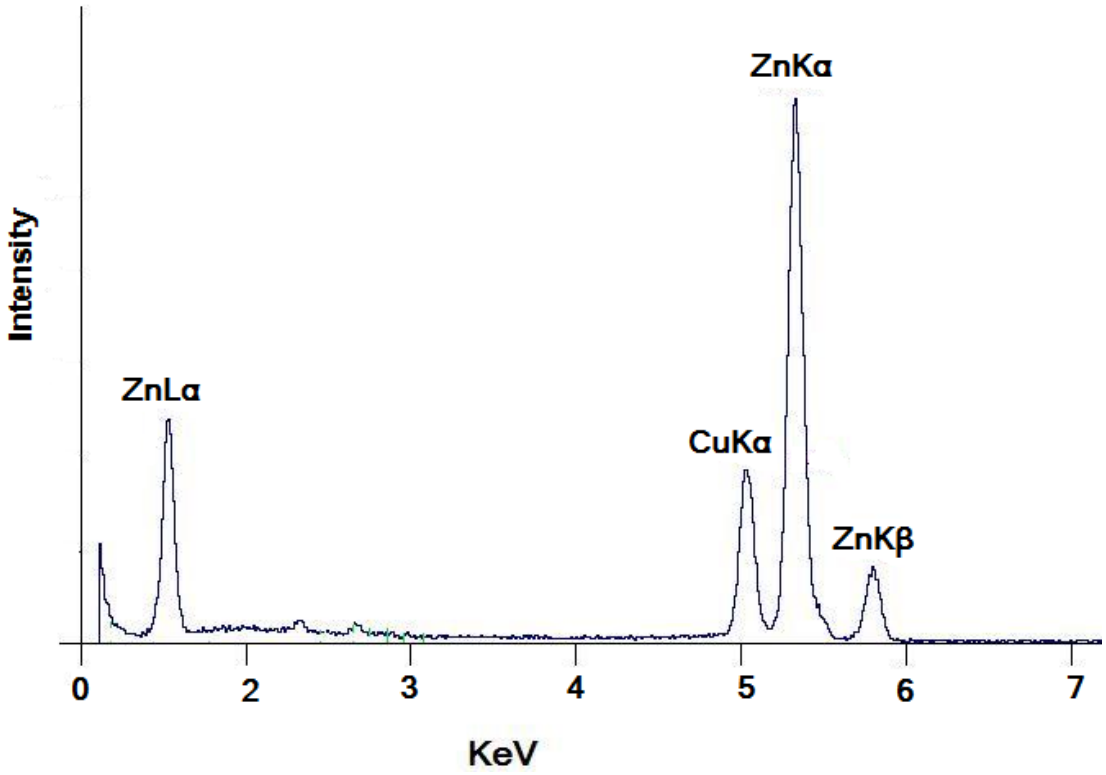

Figure 3.5 The Energy- dispersive X-ray (EDAX) spectrum of the purified ZnO nanoparticles.

3.3 Bulk hetero-junction solar Cell Fabrication

Here the preparation and cleaning steps and fabrication of bulk hetero-junction solar cell will be reviewed and discussed. The chart below shows the steps: (figure 3.6)

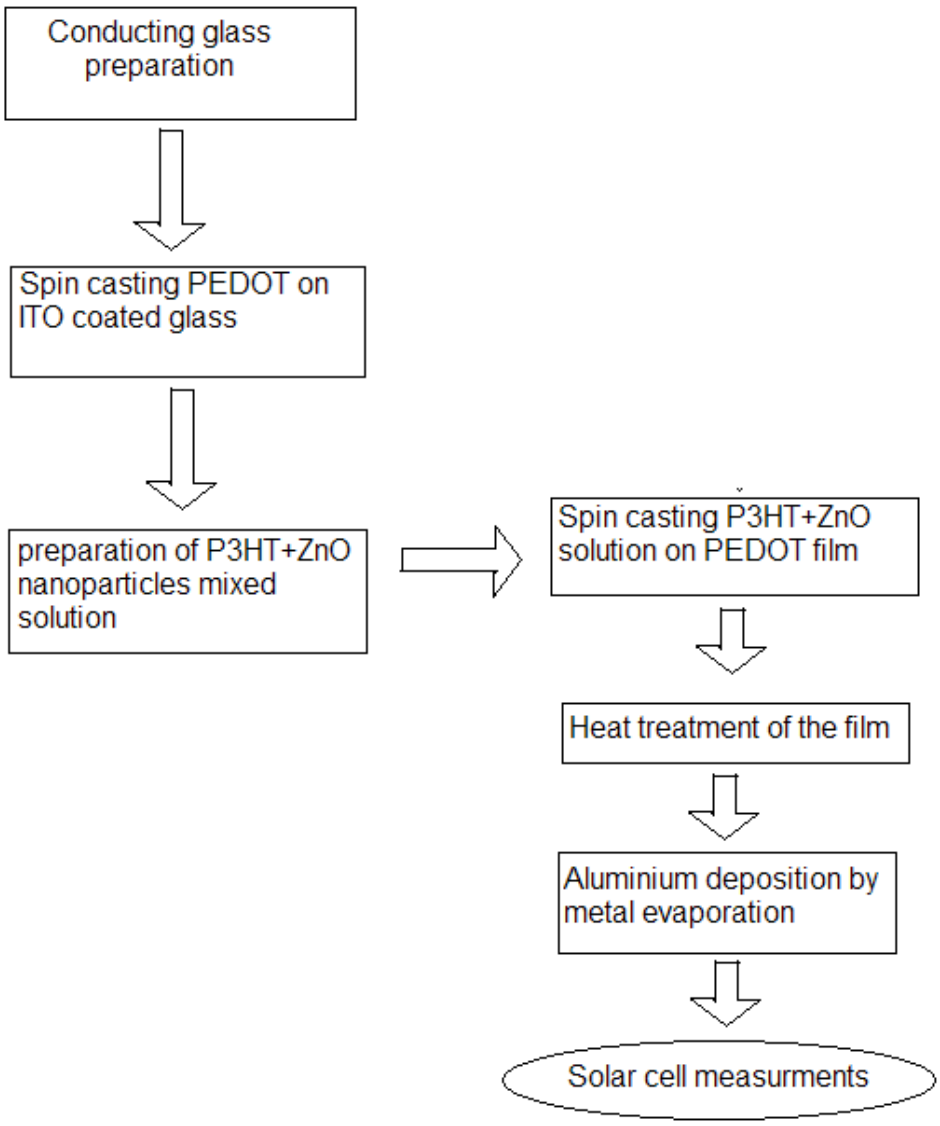

Figure 3.6 Preparation of hetero-junction solar cell.

3.3.1 Preparation of ITO substrate

Indium tin oxide (ITO) is a transparent inorganic oxide that is being used as an electrode on a substrate. There is weak absorption in the visible region of the electromagnetic spectrum therefore it makes it a very suitable electrode to be used in our designed bulk hetero-junction solar cell. The ITO coated glass was purchased from the manufacturer (Luminescence Technology Corp.). The ITO glass specification and patterning process is given in Table 3.2. Figure 3.7 shows the ITO coated glass coated with poly(3,4-ethylenedioxythiophene) poly(styrenesulfonate) (PEDOT:PSS) and active layer along with the aluminium electrode.

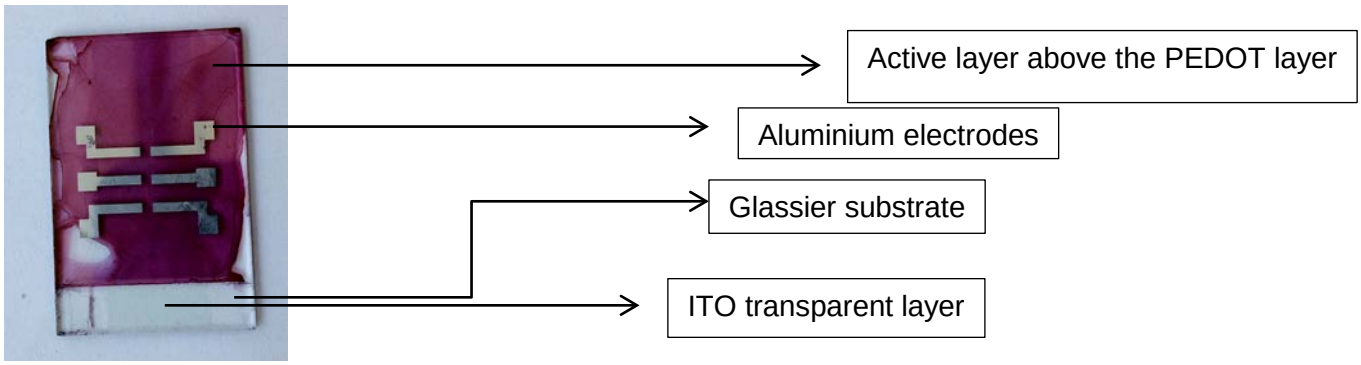

Figure 3.7 Bulk hetero-junction solar cell fabricated in laboratory. It consists of the ITO layer on the glassier substrate. The PEDOT:PSS layer spin casted on top of ITO layer and the Hybrid layer (Pink –redish color) spin casted on the PEEDOT:PSS layer and finally Aluminium electrodes deposited on the hybrid layer using metal evaporation technique (in maximum 1.8 x 10-3 pa chamber pressure)

Product No.	LT-G001
ITO Thickness	1200-1600 A^0
ITO Resistance	9-15 Ω/sq
ITO Transparency	>84% (550 nm)
Material	Polished soda lime glass
Size	370*470 nm or Customize
Glass Thickness	0.7 or 1.1 mm
SiO_2 Thickness	>200 A^0
R_a	Less than 6 nm
R_{max}	Less than 35 nm

Table 3.2 The ITO glass specification and patterning process (Luminescence Technology Corp.).

Etching the ITO layer on the glass is the first step towards the fabrication of the bulk hetero-junction solar cell. The etching has been done using 2 molar hydrochloric acid. Specific Part of the substrates was covered using a PEEDOT:PSS polymer. This was done using the spin coating technique. Since PEEDOT:PSS polymer is solved in water provides us this opportunity to have to separate sets of spinning first with 250 rpm for 30s and the second step 3000 rmp for 60s. This helps to achieve more uniform film. It case of ZnO/P3HT mixture in Chloroform solution very fast drying happens and doesn't provide enough time for spinning. The first step should be short enough. The etching process has been done very carefully since the electrode area is a very important factor later in collecting the released charges. The etching in the acidic solution was not lasting more than 10 minutes since more than the mentioned period of etching end up with over etching the ITO edges and achieving not a very soft and uniform edge. After etching the ITO layer on the glassier substrate a very proper washing and removing of the acid has been done. This was very important since the remanent acid can penetrate to the remained ITO layer and affect it. After removing the acid the next step is to wash and remove the organic contaminants on the slides. The further washing process is as follows:

1. 5 minutes wash and sonication in ethanol

2. 5 minutes wash and sonication in isopropanol
3. 5 minutes wash and sonication in the mixture of ammonium hydroxide (1 molar) and hydrogen peroxide (one molar) and water with 1,1,5 ratio
4. 30 minutes washing in the same solution (mentioned above) heated to 60 minutes.
5. 5 minutes wash and sonication in distilled water
6. 10 times rinse the slides with distilled water.
7. Drying the slides in the vacuum desiccator

3.3.2 Blending/Spin-coating of ZnO and P3HT

In this section the aim was to achieve a fairly transparent ZnO/P3HT hybrid solution. This is to be used in spin-coating stage. The ZnO nanoparticles have been dissolved in the methanol solvent and P3HT have been dissolved in the chloroform solvent. These two solvent are two different phases and miscibility is an important point to be considered in order to avoid agglomeration of ZnO nanoparticles in the ultimate solvent. Different ratios of Methanol in chloroform have been examined. The best range of the methanol percentage in chloroform has been found to be 5-5.5%. Better miscibility results in highly transparent and clear solution. Figure 3.8 is indicating the appearance difference between well dispersed ZnO in the mixed solution and the agglomerated ZnO nanoparticles.

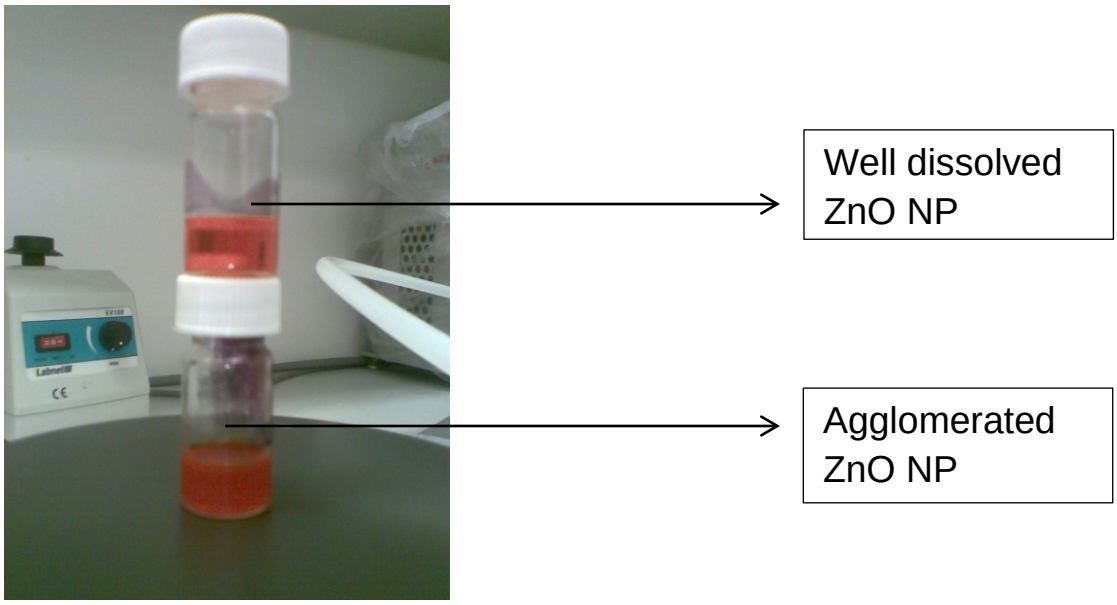

Figure 3.8 Well dispersed and agglomerated ZnO nanoparticles in solution

Of course, UV-Visible absorption spectroscopy is the best technique to investigate the dispersibility of ZnO nanoparticles in the solution which has been shown earlier in this chapter. After preparation of solution using a spin coater, we coat the PEDOT and Active layer on the ITO coated substrate. The spin coating equipment used in this experiment is depicted in figure 3.9 PEDOT films with different thicknesses and annealing temperatures were deposited on the Substrate and as the next step the ZnO/P3HT solution were drop casted on the PEDOT layer. Again, different concentrations and ratios and different annealing temperatures were tested to achieve higher solar cell performance.

3.4 Aluminium Electrodes, desighn and structure investigation of Bulk heterojunction solar

Figure 3.9 shows the structural design of the prepared bulk hetero-junction solar cell in laboratory. At first, the ITO substrate has to be etched and cleaned. The ITO substrate was etched and removed by hydrochloric acid and only an area of 0.1cm x 3.2 cm remains to act as an anode in the device. After subsequently spin coating with PEDOT:PSS and hybrid ZnO/P3HT layer six aluminium electrodes were deposited on the hybrid ZnO/P3HT layer in order to avoid the effect of the hybrid

film thickness non-uiformity. This provides six J-V and IPCE measurements for each bulk hetero-junction solar cell.Deposition of the electrodes were done in presence of a predesigned template.The active area for each electrode is exactly 0.04 cm^2.

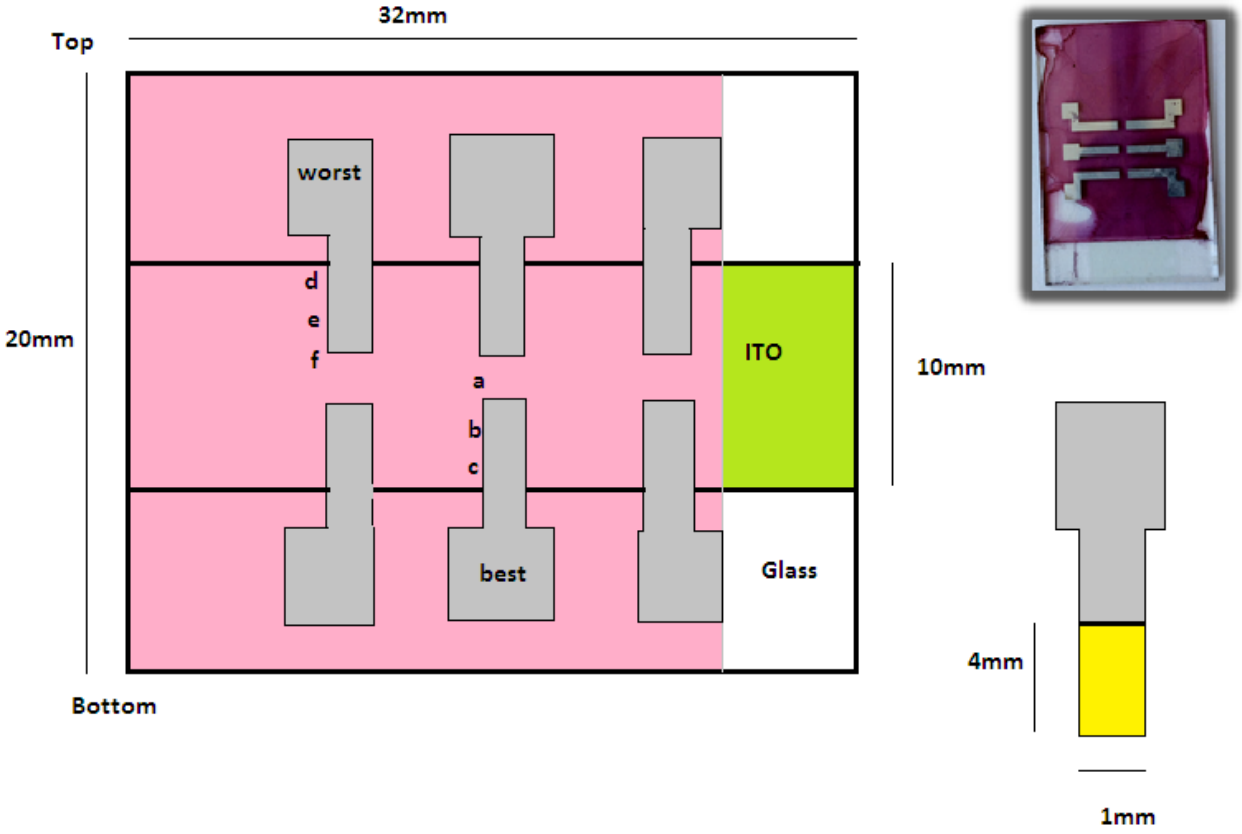

Figure 3.9 Schematic diagram of the Bulk hetero-junction solar cell structure. The best and the worst electrodes(in terms of IPCE and J-V characters) a,b,c points (Top, middle, bottom) adjacent to the best aluminum electrode and d, e, f points (Top, middle, bottom) adjacent to the worst electrode.

The last but not the least stage of fabricating the bulk heterojunction solar cell device is the deposition of aluminium metal as electrodes of the device. For this purpose, metal evaporator system has been used. As it is depicted in the figure 3.9 there are six electrodes deposited on the hybrid (P3HT and ZnO nanoparticles layer). Usually one electrode is enough to do the measurment but, here the purpose of creating six electrodes was to eliminate the effect of film nonuniformity

of the active layer (film). Aluminium wire used for evaporation was 99.99% Al, 0.5 mm diameter and.10 mm long wire was cutted and used for this metal evaporation. Since change in the thickness results in a diferent light absorption and eventually different charge carrier release. Here, the combination of metal and ITO semiconductor is required to achieve a work function difference across the device. The quality of the electrodes has been studied using Optical microscope and Scanning electron microscopy (SEM) to obtain a very close view of the electrode surface and also atomic force microscopy (AFM) studies has been performed on the surface of the electrodes in order to understand the morphology (uniformity) of the electrode surfaces. As it is depicted in figure 3.10 silver paste has been used to enhance the contact between the cell and the IPCE and solar simiulator.

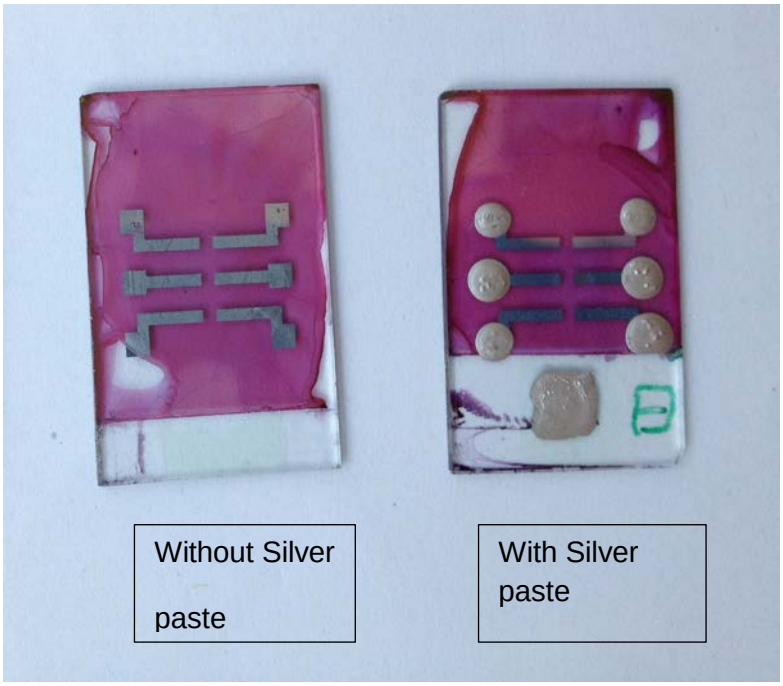

Figure 3.10 Aluminium electrodes without silver paste (at left) and with silver paste (at right)

The further studies using optical microscope has provided us a closer view in order to understand how does the hybrid film and also the deposited aluminium electrodes lay on the substrate surface. Figure 3.11 is showing the images taken using optical microscope from the hybrid layer and the electrodes. According to

profile measurment done only on the pure aluminium electrode on ITO substrate the aluminium hight is approximately 25-30 nm. Unfortunately, the resistivity of the electrodes due to contact with room vapour and gases increases. A measurement three month after fabrication resulted in a very high resistivity of aluminium electrodes which indicates that it has converted to a nonconductive element of the solar cell. There is a hight possibility that all surface have been oxidized to AlO_x.

3.4.1 Optical imaging of the highest performing lab prepared Bulk heterojunction solar cell

a) b)

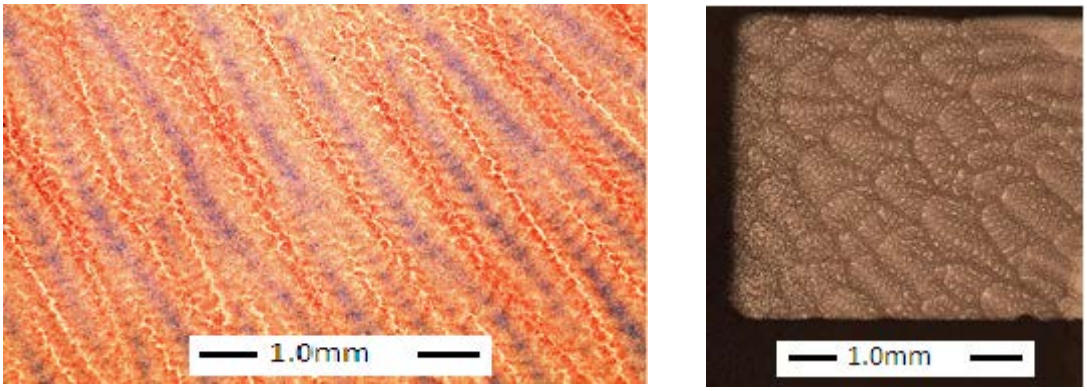

Figure 3.11 Optical imaging of **a)** hybride layer (mixture of P3HT and ZnO nanoparticles) **b)** Aluminium deposited electrode on the Hybrid

As it is depicted the quality of the hybride film and the deposited aluminium electrodes are not as uniform as we observe with an unequipt eye. The waved like and nonuniform surface of the hybrid film (figure 3.11a) is the result of the very fast evaporation of the P3HT and ZnO nanaoparticles in the mixed Chloroform and methanol solvent. The fast evaporation in addition to the high speed coating of the film results in this undesired film quality. Also it is clear from the (figure 3.11b) that the surface of the aluminium coated electrode on the hybrid film is not uniform at all and there is a tendency to form discontinous and/or domained regions (film).There are two reasons that could explain why such an undesired morphology of electrode film is being achieved. First reason is the unpolished underneath

surface (film) which is the drop casted hybrid film and the second reason can be the tendency of evaporated metals to deposit in the form of islands. The are color differences on the Al electrons because while IPCE and J-V measurments specific highly conductive carbon tapes were implied on the electrodes to properly connect Al electrods to the measurement equipments. After removing this coloration has have happened. The Thickness of the electrodes are all the same and all are uniform and the reason is that we have used same size masks to coat the Al on the Hybrid films. If there is a waviness and/or nonuniformaty it might be because of the underneath layers.The amount of Al used and the setting of the metal evaporator was set for under 20nm thickness Al electrodes. Thickness varries greatly which is studied in chapter 5.

3.4.2 SEM images of the surface of bulk hetero-junction solar cell

In addition to optical microscopy imaging of the surface of cells for sake of better understanding and having a closer view of the surface structure scanning electron microscopy (FESEM) imaging has also been performed on the surface of the devices. At this stage, the scale of our imaging is micrometre and sub-micrometre. Figure 3.13 is depicting the SEM images of the bulk hetero-junction solar cell sample prepared in the laboratory.

a)

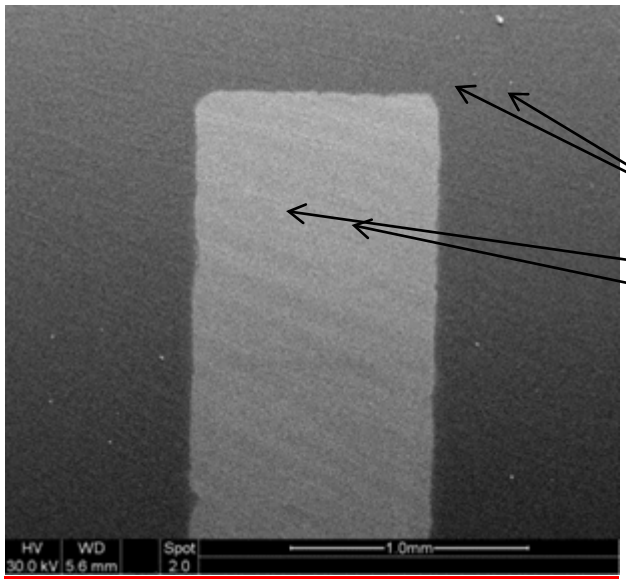

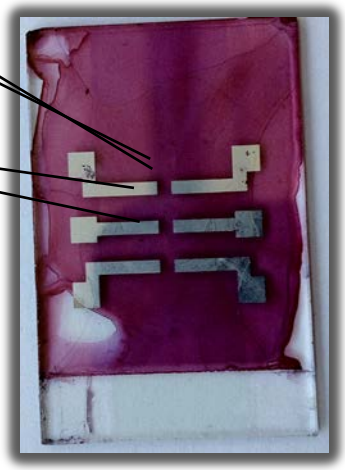

b)

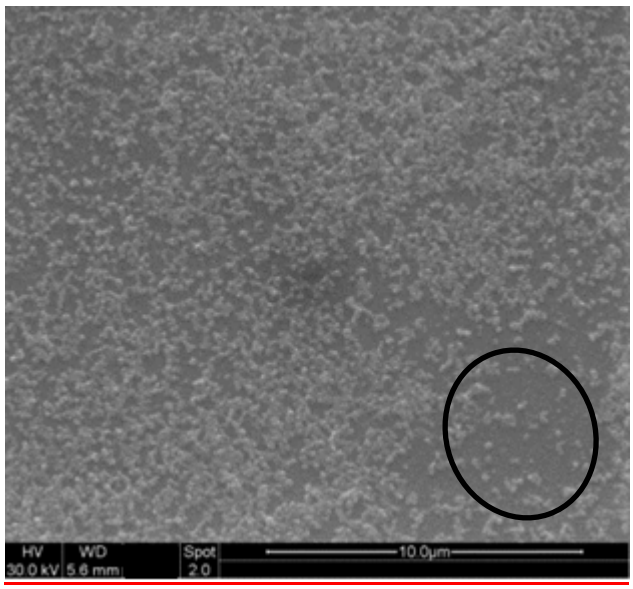

c)

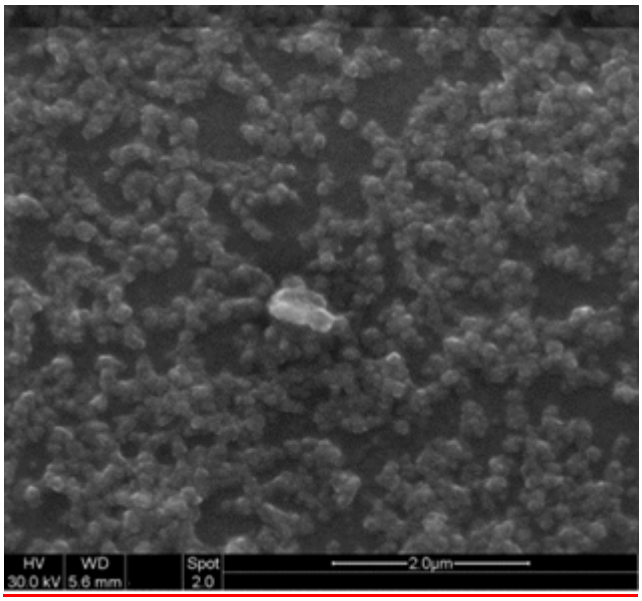

Figure 3.12 SEM images of the surface of bulk hetero-junction solar cell. a) surface of cell with small magnification b) Surface of the aluminium electrode with medium magnification. c) Surface of aluminium electrode with the highest magnification

In compare to the optical microscope images the SEM images provide us much more in detailed information related to the actual surface structure and the quality of this solar cell preparation. Of course, the optical images provided us the very important information since with the naked eyes as it is shown in figure 3.10 there was no chance to speculate the imperfection in depositing the films as well as to understand the quality of the aluminium electrode. Inferring from the optical microscope taken images in figure 3.11 it is clear that the surface of the hybrid film is not perfectly smooth and has a wavelike surface morphology. The bad surface smoothness is the result of the very fast evaporation of the chloroform solvent. This evaporation happens within a few seconds after drop casting the solution.

After the complete solvent evaporation the remaining is the pinkish colour P3HT molecular solid mixed with a specific percentage of ZnO nanoparticles. Here chloroform has been used due to it very good miscibility with methanol. This underneath layer morphology has a strong effect on the morphology of the aluminium deposited electrode. Knowing that the surface of the sample solar cell is made of organic polymer there is a probability to having electron beams (from the SEM electron gun) burn the surface and result in damaging the SEM microscope by creating gasses and contamination. Therefore, low vacuum mode was recommended to conduct the experiment safely. Because of having low vacuum and presence of the gas molecules and shielding the gun source it avoids the deposition of evaporated organic polymer on the electron gun and contaminating it. This contamination causes a severe astigmatism in the image and lowers the image quality. Later on using the high vacuum mode of the same FESEM system also was proved that the deposited organic polymer was very much stable and it didn't affect the microscope. The evaporation rates of Chloroform affect the smoothness of surface because its immediate evaporation causes rough surface. This information provides us a better future opportunity to study these types of cells more in detailed under the electron microscopes.

Chapter 4

4. Optical Study

4.1 Optical spectroscopy analysis

Optical spectroscopy has been extensively used in characterization of nanomaterials and thin layer deposited films. This spectroscopy can be mainly divided into two categories: absorption and emission spectroscopy. These two mentioned spectroscopies determine the electronic structures of atoms, ions, molecules or crystals by exciting the electrons from their ground states to excited states by absorption and relaxing from excited states to ground states which is called emission. In this section UV-Visible spectroscopy of the samples has been presented and has been used to study the optical properties of the hybrid thin films.

4.1.1 UV-Visible absorption spectroscopy study

Using UV-visible absorption spectroscopy, Jasco V-670 spectrometer, shown in the Figure 4.1 the absorption spectrum of the prepared solutions and the spin-casted films with different chemical and physical parameters has been measured. The range of the surveyed wavelength is from 200 nm to 800 nm. The samples for the measurement were prepared in the form of solutions and coloured thin films. For the liquid solution samples, high rate dilution is required in order to avoid absorption saturation and achieve reliable data. The reference sample used in the absorption measurements for all the samples were simply air and the reason was to have a unique reference since most of the solutions are composed of mixed solvents, for example the mixture of Methanol and chloroform for the ZnO and P3HT solution.

After successfully synthesis of ZnO nanoparticles, the next step was to mix it with P3HT and study the optical properties of this hybrid and understand the effect of different ratio of ZnO and P3HT in the hybrid. This examination was done after preparing the films on simple glass substrate. The very initial characterization which has been done was the UV-Visible absorption of these materials. Figure 4.1 shows the absorption of laboratory synthesized ZnO nanoparticles and pure P3HT and the hybrid film. As it is depicted there are specific absorption peak frequencies which are very important as a reference peaks. After preparing the hybrid films the reference peak can be used to monitor the peak shifts due to hybridization. This will enable us to tentatively rationalize the solar spectrum absorption of the prepared hybrid film.

Absorption spectroscopy of different mixing ratios of ZnO and P3HT has been performed and the aim was to understand the roll of different ratio and thickness of the films and understand the optical behaviour of the film. As it was explained up to some limit in the chapter one of this thesis P3HT is the important material (polymer) in absorbing the solar spectrum due to its π-π* transition. Figure 4.1 is showing the absorption spectrum of the Pure P3HT polymer used in the experiment.

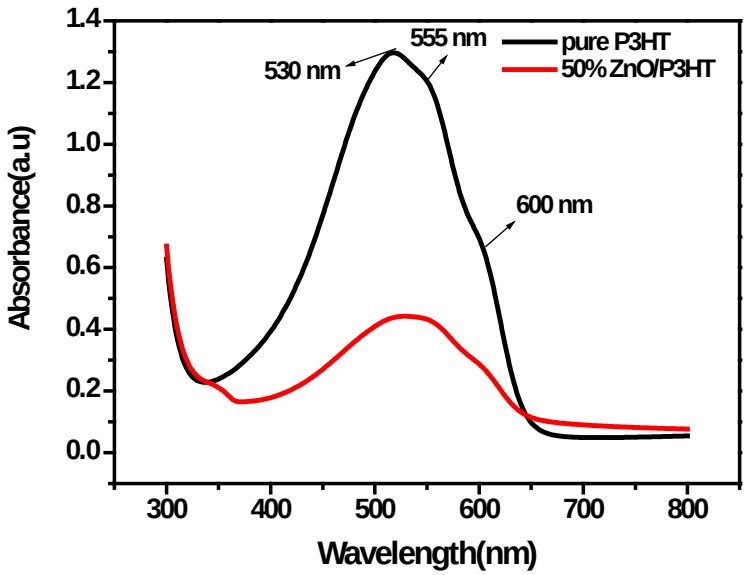

Figure 4.1 UV-Visible spectrum of the Pure P3HT and 50% -50% ZnO/P3HT hybrid films on the glass substrate after spin coating with 1500 rpm speed.

In all the absorption graphs we did not do the normalization. The only important point was to dilute the solutions in order to obtain intensity less than 1.5. This is to obtain a better resolution for the spectra. The background subtract was don using the air (no sample) spectrum. As it is apparent P3HT has three absorptions the main peak is at 530 nm and the other is 555 nm and the third one which looks like a shoulder is at 600 nm. These peaks are all attributed to the transition of electron from a bonding π orbital to an anti-bonding orbital π *. This polymer so far, has been acknowledged as an ideal conjugated polymer since has a very good absorption in the range of 450 nm to 600 nm which covers most of the solar spectrum wavelength range. In the optical studies of conductive polymers the complementary step is to investigate the emission of the polymer in pure and in conjugation with the nanoparticles. Actually, the absorption happens in the range of 600 to 800 nm. This range is the absorption of P3HT not the ZnO nanoparticles. The absorption peak for ZnO is 361nm which is way out of this range. Therefore, the only reason that adding ZnO changes the absorption is diluting the P3HT solution and decreasing the number of the wave absorbents in the mentioned wavelength range. Therefore the resultant mixed 50%-50% P3HT/ZnO has a thiner layer of P3HT and absorbs less light. Adding ZnO to the solution and

proceeding for the hybrid film changes the order of P3HT molecules this might shift the absorption peaks for a very small amount. 50% is referring to the volume ratio of ZnO solution. Indeed, a hybrid solution/mixed solution volume vise consist of half ZnO solution and half P3HT solution. Now, the concentration of Zno in its solution was 5mg/L and P3HT solution was 10 mg/L. The solvents for both ZnO Nps and P3HT powders were the same as it is mentioned before.The emission spectrum of the pure and mixed ZnO nanoparticle films is shown in the figure 4.2. The three absorption peaks have matches with the published literature with good precision. It seems that the absorption peak of P3HT changes a little bit by changing the solvent. For example the spectrum of the P3HT solved in Chloroform, 1,2 dichlorobenzene and toluene are not exactly the same but the absorption peaks occurs at the same wavelength for all three[85].

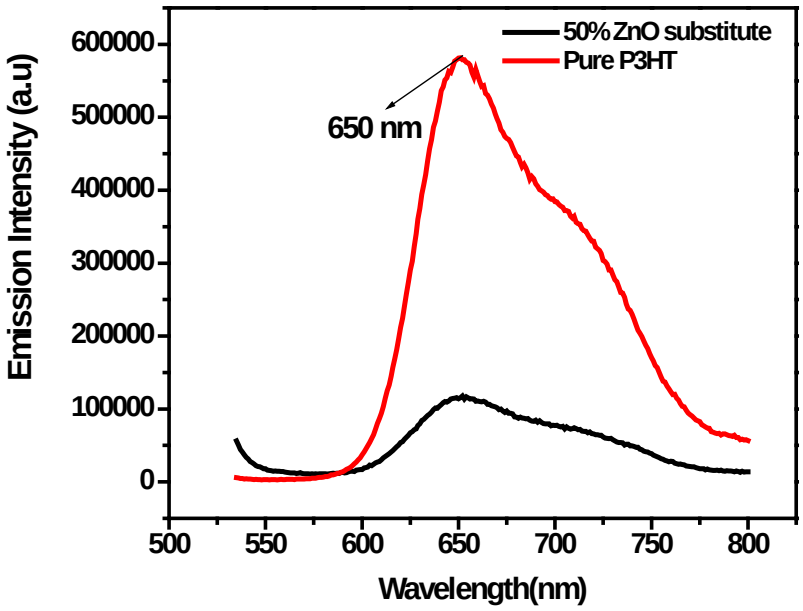

Figure 4.2 Emission spectrum of the Pure P3HT and 50% -50% ZnO/P3HT hybrid films on the glass substrate after spin coating with 1500 rpm speed.

In figure 4.1 the absorption comparison between a pure P3HT and 50% substitute ZnO nanoparticles is depicted. As it is apparent, there is a very obvious reduction

in the absorption by the film after substituting 50% of P3HT with ZnO. This initial measurement was to achieve preliminary information of how the ZnO will affect the light absorption of the film. UV-Visible absorption spectroscopy of the pure ZnO nanoparticles were performed as it is shown in figure 3.1, the peak of absorption of the ZnO nanoparticles is at 340 nm which in occurring in the UV region of spectrum. This shows that ZnO nanoparticles do not contribute in the visible –Infra red absorption. In figure 4.1 the severe reduction in the absorption is due to reduction in the P3HT portion in the film and effectively a thinner P3HT layer.

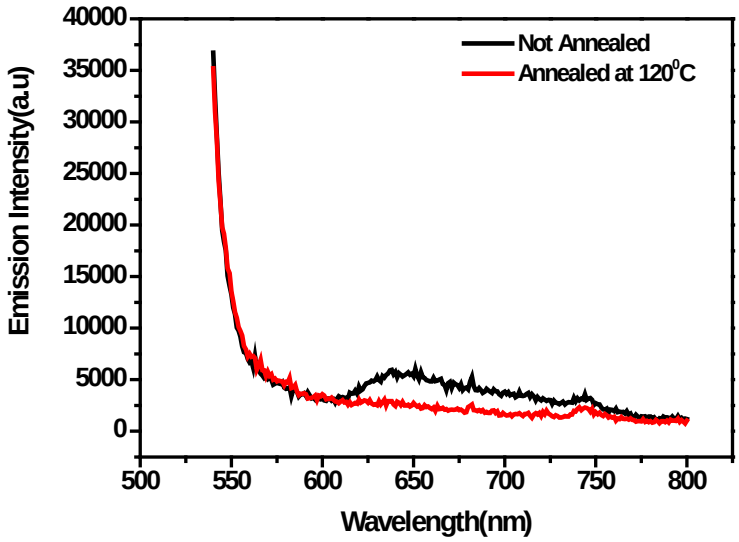

Figure 4.3 Emission spectra of the annealed and not annealed hybrid films on the glass

In figure 4.3 the emission spectra of annealed and as it obtained hybrid film on glass substrate has been shown. This measurement proves that annealing the hybrid film is quite effective in the emission quenching and results in electron transferring from the P3HT polymer to the acceptor compounds, ZnO nanoparticles. Several papers have discussed the reason of this phenomenon in the hybrid film and tested the annealing effect on the performance of the solar device [35], [16], [18]. One of the main reasons proposed for the further emission quenching after the annealing procedure is the enhancement in the chain order and/or the morphology of the film surface and increasing the crystalinity of the solid polymer. As it depicted in chapter three, images 3.11a and 3.11b, the

morphology of the surface are quite not uniform and rough on the surface which is a negative factor in the solar device function.

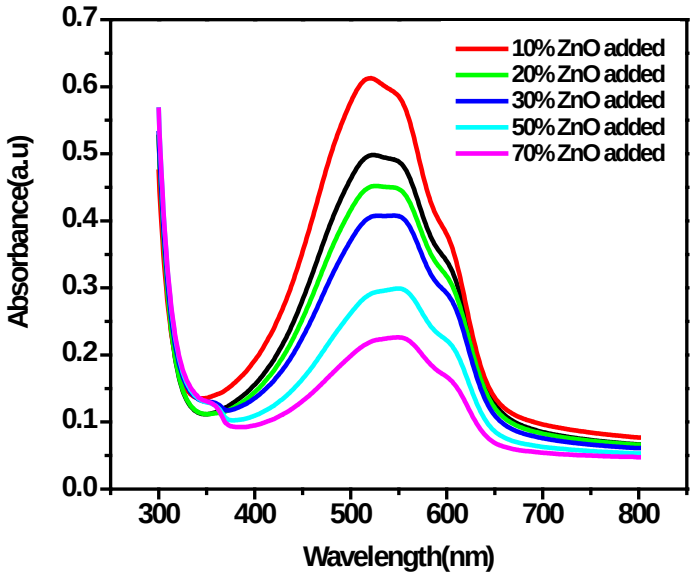

Figure 4.4 Absorption spectra of the hybrid film with different ZnO and P3HT ratio

In figure 4.4 the UV-Visible spectra of different ratio of ZnO nanoparticles and P3HT solution have been measured. As it can be inferred from the spectra by increasing the concentration of ZnO nanoparticles and finally decreasing the concentration of P3HT in the hybrid layer the absorption decreases subsequently. In this device the enhancement of photoluminescence quenching by increasing the concentration of ZnO nanoparticles should be compensate with the reduction of absorption which is an unwanted incident. There should be a proper compromise between these two parameters in the hybrid film. It is worthy to point out that by increasing the ZnO nanoparticle concentration in the hybrid film the small hump at 607 nm which is due to the ZnO nanoparticle absorption in the UV region starts to appear and it is quite predominant in the higher ZnO conc entrations. The photoluminescence property of different ratios of the ZnO and P3HT in hybrid films also have been studied using photoluminescence spectroscopy and the result matched with the reported peer reviewed papers [16]. Figure 4.5 is indicating the emission spectra of the laboratory prepared film samples. As it is depicted in figure

4.5 the emission spectra of different ratios of ZnO and P3HT are very well matching with the reported published papers [35].

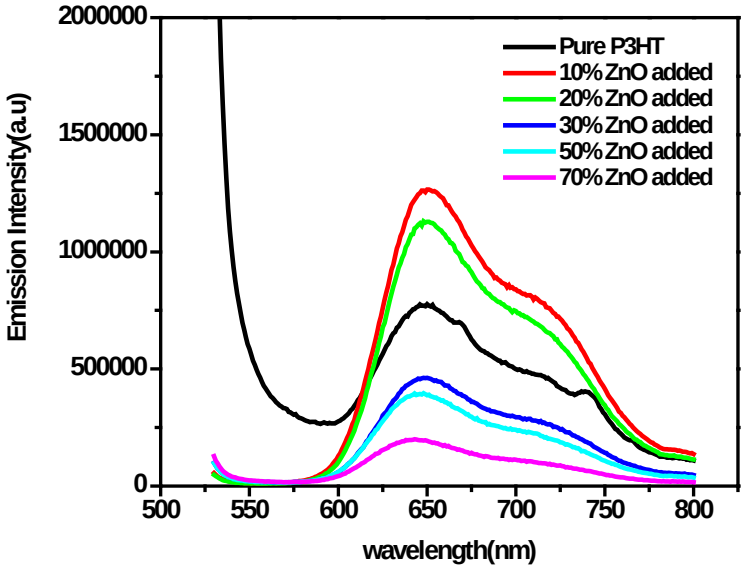

Figure 4.5 Emission spectra of different ratios of Hybrid film drop-casted on glass

After accomplishing the absorption spectroscopy of the hybrid film, using fluorescence spectroscopy (PTI Quantum Master Fluorometer), emission spectra of the films have been measured. Figure 4.5 shows the emission spectra of different ratios of ZnO and P3HT in the hybrid film. In these graphs the subsequent changes in the emittance of the films is directly proportional to the ration of the compounds in the hybrid film. As it is being expected by increasing the amount of the ZnO nanoparticles there should be a gradual decrease in the emittance and photoluminescence of the films. Since, the ZnO nanoparticles act as acceptors by increasing the ZnO ratio there will be a greater probability for the created excitons in the P3HT polymer to get separated and give up the electron to the acceptor material (ZnO). As it is apparent these prediction appears true except in the 10% and 20% added ZnO nanoparticles. These unexpected results have been observed before, in that for the small portion of ZnO concentration up to 20% (Weight percentage) the emission intensity increases even more than the Pure P3HT. The proposed reason for this result is that the photoluminescence of P3HT

is up to a very high level sensitive to the degree of chain order initially by adding small amount of ZnO nanoparticles we are helping to increase the chain disorder [35]. Of course, by increasing the concentration of ZnO the competition between an intensity increases resulted of more disordered chains of P3HT and the decrease in the emission intensity because of photo induced electron transfer to ZnO will result in decreasing in the intensity of the emission spectra. The Quoted concentration of ZnO nanoparticles in Volume percentage [Vol%] were 8,15,26,35,42. In our experiment also we tried to understand the effect of volume increasing of ZnO on the photoluminancy of the hybrid film which the observed results were matching with the reference[35].

4.2 Aging effect study on the prepared Hybrid film

Durability of the hybrid films which are being used in Organic solar cells is one of the interesting and of course important factors that should be investigated. Industry is investing to clearly understand the effect of aging and the influence of environmental factors on the degradation process of P3HT film and ultimately the performance of the hybrid solar cell devices. In this respect, here we have compared basic characteristics of the in-lab prepared hybrid films immediately after spin coating and also after a period of 9 month. UV-Visible and Emission spectroscopy of the prepared hybrid films have been monitored immediately after film preparation and after a period of 9 month. The stability of P3HT semiconductor is a main challenge that has to be solved out in order to allow industry to invest on fabricating devices like organic solar cells and organic field-effect transistors. P3HT is still the most popular organic semiconductor. Understanding the degradation mechanisms and durability of the polymer helps synthesis a broad variety higher quality polymers. Light and oxygen lead to destruction of the π-conjugated system in both, solution and solid phases [51]. This has inversely effect on the absorption of the light by the polymer.After 9 month storing the film in the room temperature and laboratory environment (out of desiccator), UV-Visible and emission spectroscopy measurement were performed on the same set of hybrid films to compare the absorption and emission properties

and understand the environment imposed changes in the quality of the films. Figure 4.6 shows the UV-Visible of one set of the films nine months after preparation.

Figure 4.7 Shows the emission spectra of the same set nine months after preparation. It is obvious that there is a notable change in the absorption spectra for all the ZnO/P3HT ratios. Indeed, this change is towards reduction of the absorption of the film. The reduction in the absorption of light by the hybrid films has an immediate impact on the number of the created excitons and in the solar cell device this definitely reduces the efficiency. This change is mainly due to the exposure of the films to the oxygen and UV light which causes irreversible degradation of P3HT which is a radical – based degradation mechanism. UV light in the presence of oxygen and humidity and temperature can cause this damage to polymer. Using nanodentor, in chapter 5, for thickness measurements of the hybrid films it was observed that the thickness of the films on each film is not uniform at all. It varies between 55.4 and 840 nm. The same thickness variation has been observed for the other hybrid films as well. This wide range is mainly due to manual drop casting the hybrid solution on the substrate.

Also humidity is one of the main reasons that inversely effect on the quality of the hybrid material and apparently will decrease the efficiency of the solar cell device [46-48]. The reduction in the device performance under long period exposure or relatively high humidity can be attributed to charge trapping at the grain boundaries because of the polar water molecules which cause in reducing the rate of the charge transport [48,50]. In figure 4.6 the UV-Visible spectrum peak after nine month has a blue-shifted from 525 nm to 510 nm. This shift indicates the reduction in the order of P3HT polymer [50,51]. In overall formation of grain boundaries by humidity and photo degradation of polymer are the main reasons for the absorption change in the P3HT as the main absorbent in the hybrid film. In figure 4.7 It is apparent that there is a significant change in the emission spectrum after 9 month. The significant spectrum change is mainly because of the polymer

degradation due to exposure to light and environment humidity [51]. Indeed one of the main reasons of losing performance can be the formation of $P3HT^{+}:O_2^{-}$ complex at the Polymer and ZnO interface. This complex reduces the concentration of pure P3HT present in the film in accordance with the absorption and emission spectroscopies [83].

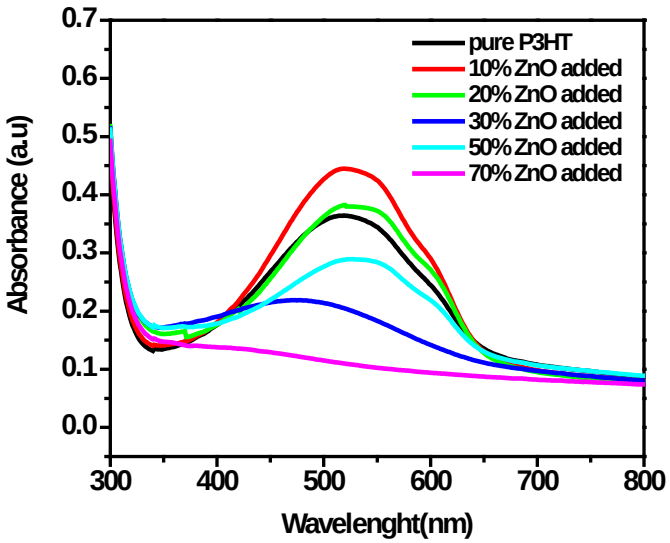

Figure 4.6 Absorption spectrum of a set of different ZnO/P3HT ratio hybrid films on glass substrates after nine month.

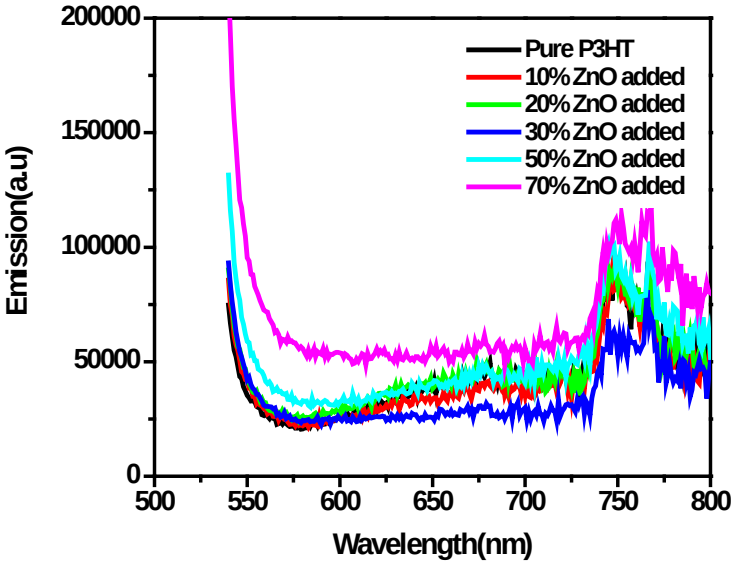

Figure 4.7 Emission spectrum of a set of different ZnO/P3HT ratio hybrid films on glass substrates after nine month.

Chapter 5

5. Electrical measurements

After preparing the bulk hetero-junction solar cell devices in the laboratory and optically studying the hybrid solution and film, we perform the electrical measurements of the devices. This is do understand the performance of the prepared solar cells and mainly observe the role of the prepared hybrid layer and also underneath layer (PEDOT:PSS) in the performance of the devices.

5.1 photovoltaic characterization

The photovoltaic characterization is to study and understand the interaction of light with the material. Here depending on the frequency range and intensity of light, material might show deferent reactions. The aim in photovoltaic mainly is to understand what is the best way to extract electricity out of this interaction.

5.2 Solar cell characterization

In order to study the interaction of sun light and the prepared solar cell devices, two main measuring equipment are used with simulating the solar light in terms of 7rage of frequency and the intensity. These two widely manipulated techniques for photovoltaic characterizations are current-voltage measurements under simulated sunlight and monochromatic light generated current measurements; IPCE.

Solar simulator equipment used in laboratory to study the I-V characterization of the bulk hetero-junction solar cells. Integration of the spectral response with the solar spectrum having the condition of AM 1.5, normalized 100 mW cm^{-2}, provides information on J_{sc}, the short circuit current. The J-V curve is being measured under white light illumination using tungsten-halogen lamp.

Incident photon to electron conversion efficiency (IPCE) which has been used to measure the IPCE value of the bulk hetero-junction solar cells in the photovoltaic laboratory. IPCE value specifies the ratio of charge carriers collected at the electrodes to the number of incident photon. Here the reference spectrum used was silicon based solar cell.

Here in this chapter the aim is to investigate the functionality of the organic conjugated polymer/ ZnO nano-particle hybrid films prepared, characterized and optimized for solar cell applications. The IPCE and J-V characterizations of three selected prepared solar cells will be measured and studied. First, the highest performing solar cell and the lowest performing will be compared and then the one with different ZnO/P3HT ratio will be presented. At the end the effect of PEDOT:PSS concentration parameter will be tested in the highest performing solar cell. Table 5.1 shows the parameters which have been studied through this research and it is worthy to know that the collection of the bold written parameters result in the highest solar cell performance.

5.2.1 Solar cell measurements of the highest performing solar cell

Figure 5.1 depicts the solar Cell characterization of the of 50%-50% lab- made bulk hetero-junction device. In figure 5.1a we can compare the incident photon to collected electron which is wavelength dependent. The best and worse electrodes are showing the same behaviour by varying the wavelength and they have only 5% difference at the peak point. The IPCE values at 537 nm wavelength are 19% and 14% for the best and worse electrodes. In figure 5.1b using Asahi solar simulator we could do the J-V characteristics. We can compare the Current densities extracted from both the electrodes. The V_{oc} are 0.23 V and 0.05 V and the I_{sc} are 1.13 mA.Cm^{-2} and 0.63 mA.Cm^{-2} for best and worse electrodes.

a) b)

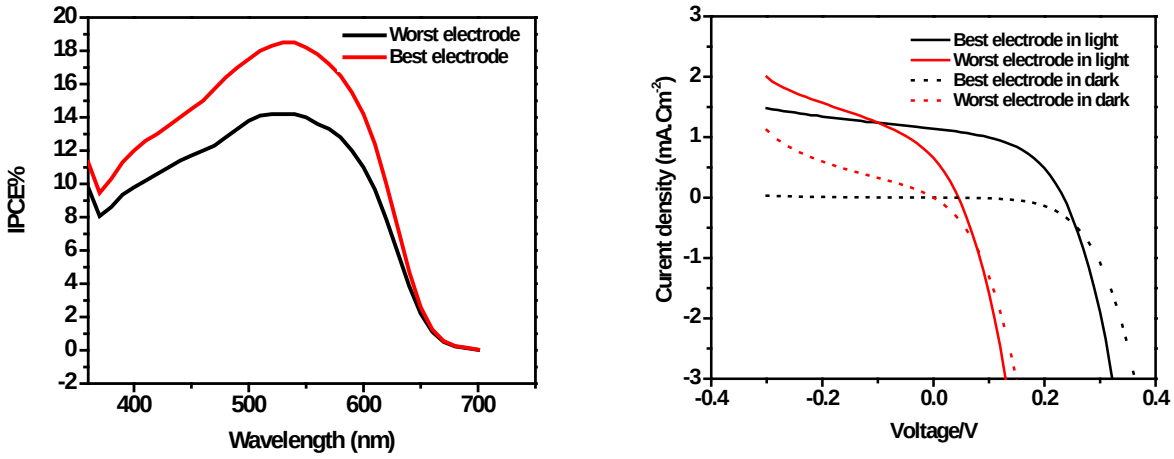

Figure 5.1 Solar cell measurements of best performing solar cell **a)** IPCE measurement **b)** J-V measurements

5.2.2 Solar cell characteristics of lowest performing solar cell

Figure 5.2 depicts the solar Cell characterization of the of 50%-50% lab- made bulk hetero-junction device. In figure 5.2a we can compare the incident photon to current conversion which is wavelength dependent. The best and worse electrodes are showing the same behaviour by varying the wavelength and they have more than 1% difference at the peak point. The IPCE values at 508 nm wavelength are 2.3% and 1.2% for the best and worse electrodes. In figure 5.2b also we can compare the Current densities extracted from both the electrodes. The V_{oc} are 0.27 V and 0.09 V and the I_{sc} are 0.32 mA.Cm^{-2} and 0.29 mA.Cm^{-2} for best and worse electrodes.

a) b)

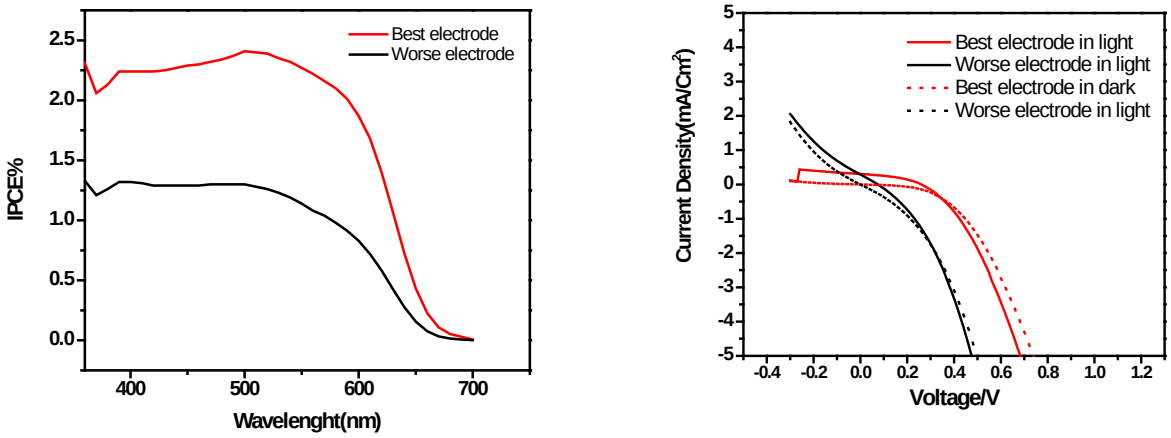

Figure 5.2 Solar cell measurements of lowest performing solar cell a) IPCE measurement b) J-V measurements

The IPCE measurements shows that what is the rate of conversion of photons in the unit of wavelength to electrons but due to the quality of the file/electron pathway all the electrons might not reach to the cathodes. There is a high probability of electron leakage which results in reducing the open circuit voltage. This electron leakage decreases the Shunt resistivity as well.

5.2.3 Electrical characteristics of lowest performing solar cell

Figure 5.3 depicts the solar Cell characterization of the of 30%-70% lab- made bulk hetero-junction device. In figure 5.3a we can compare the incident photon to electron conversion efficiency which is wavelength dependent. The best and worse electrodes are showing the same behaviour by varying the wavelength and they have only have less than 1% difference at the peak point. The IPCE values at 535 nm wavelength are 3.5% and 2.8% for the best and worse electrodes. In figure 5.3b also we can compare the Current densities extracted from both the

electrodes. The V_{oc} are 0.32 V and 0.22 V and the I_{SC} are 0.43 mA.Cm^{-2} and 0.23 mA.Cm^{-2} for best and worse electrodes.

a) b)

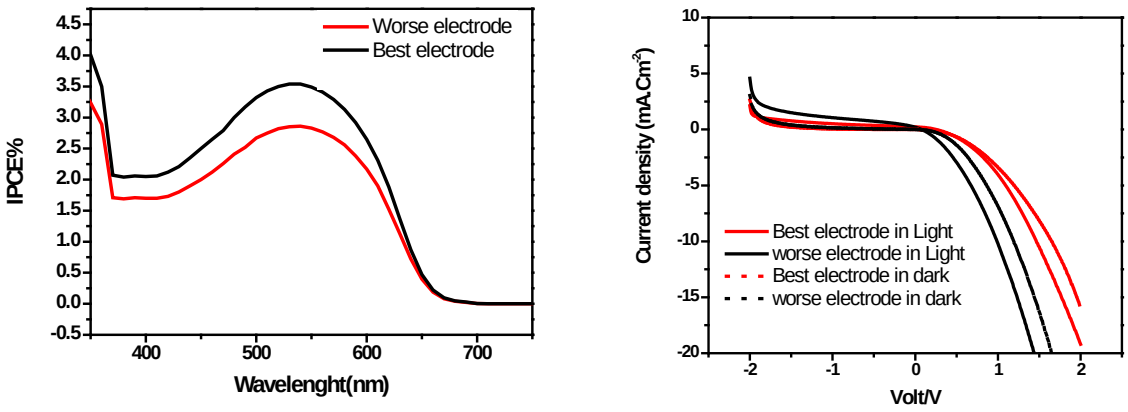

Figure 5.3 Solar cell measurements of 30-70% lab- made bulk hetero-junction solar sell a) IPCE measurement b) J-V measurements

5.3 Studying the effect of few important parameters in the Solar cell performance

5.3.1 ZnO and P3HT ratios (mass ratio)

Using the absorption spectra and the emissions and comparing them enabled us to choose two different ratios among the vast range of the mass ratios of ZnO and P3HT in hybrid layer . These parameters were used in assembling the bulk hetero-junction solar cells. We chose 30-70% and 50-50% of ZnO nanoparticles blended in P3HT polymer solution. This means that out of 100% solution which was drop casted and spin coated on the PEDOT:PSS layer 30% was ZnO nanoparticles

solution and 70% P3HT solution (30-70%).and in the second one 50% ZnO nanoparticles solution and 50% P3HT solution were mixed (The mass measured the pure solid ZnO and solid P3HT). The ratios were chosen because of two main reasons. First of all by considering the emission spectra in figure 5.3 is was apparent that these two ratios comparatively show higher emission and the second reason is that, experimentally, we observed much more stable mixture solution and no ZnO agglomeration were observed even in a highly organic phase of 95.5% chloroform and 4.5% methanol. Figure 5.5a and 5.3b are showing the highest measured IPCE and J-V of the 30-70% ZnO:P3HT blend of course, this is show very low performance in compare to maximum IPCE and J-V data obtained from the 50-50% ratio results shown in figure 5.1

As it can be inferred from figures 5.3 and 5.1 by increasing the ratio of ZnO from 30% to 50% a significant improve in the IPCE and J-V is observed. This improvement can be explained in this way that by increasing the weight percentage of ZnO nanoparticle more p-n junction are being created and also more paths in order to transport the separated electrons from the conductive polymers to the Aluminium made cathode. It is worthy to have this point in mind that by increasing the ZnO nanoparticles ratio, the probability of agglomeration of nanoparticles will also increase. This will bring a limitation in busting the efficiency. By calculation It is known that the 50%-50% mass ratio of ZnO and P3HT is equivalent to 18%-82% volume ratio.

5.3.2 PEDOT:PSS layer

Poly (3,4-ethylenedioxythiophene) (PEDOT:PSS),is a polymer used as a hole-collecting/ electron blocking layer. This polymer is spin coated on the ITO layer. High conductivity (up to 1000 S/Cm) and light transparency has made this polymer a good material to be used in the solar cell body and variety of other photonic devices. Here, prior to applying this polymer in the bulk hetero-junction solar cell we have measured the conductivity of the available PEDOT:PSS (Heraeus). Figure 5.4 shows the J-V characteristic of the spin coated PEDOT:PSS on the ITO

layer. The electrodes are ITO as anode and deposited Aluminium using metal evaporator, as cathode. The measured conductivity calculated from the J-V characteristic was 310 S/cm. The main reason of having lower conductivity in the spin coated PEDOT:PSS film in compare with the manufacturer reported PEDOT:PSS conductivity (approximately 1000 S/Cm) is the external resistivity raising from the deposited aluminium electrode and of course quality and uniformity of the PEDOT:PSS film on the ITO substrate. In order to understand the effect of PEDOT:PSS thickness and concentration, several experiments have been performed, in which only the thickness of PEDOT:PSS have been varied. Through the whole experiments it understood that the best speed in order to achieve a reasonable thickness which does not create disrupted film was 3000 rpm. This speed also was suggested by other well recognized research groups as well [35]. It is worthy to know that a disrupted film causes pin-holes and ends up with leaking the electrons and lowering the efficiency. Figure 5.4 demonstrates the effect of PEDOT:PSS concentration change in the J-V and IPCE characterization of the completed device. In this measurement four different concentrations were tested, not diluted and as purchased from the PEDOT:PSS producer compony (Heraes) and two and three times diluted by double ionised water. Three times and four time dilutions resulted in PEDOT:PSS film disruption and no result was obtained. Disruption was due to the viscosity decrease of diluted PEDOT:PSS solution. In all these sets we stock to the thickness resulted from 250 rpm for 30 s in the first step and 3000 rpm for 60 s in the second step. The Concentration of the used PEDOT in the solution was 0.5 Wt% and the ratio of the PEDOT to PSS was 1:2.5 (W/W). This is the as obtained PEDO:PSS concentration from the chemical company (Heraeus). One of the main issues with bulk heterojunction solar cells is the non-uniformity of active layer surface. This non-uniformity and active layer causes leakage of electrons/pinholes. With the comparatively low open circuit voltage which we have got in our measurements there is a high probability of having pinholes [35]

It was understood from the results, that the two times dilution of the PEDOT:PSS significantly improves the IPCE of the solar cell. Figure 5.4 depicts the effect of diluting the PEDOT:PSS to half.

5.3.3 Active layer Thickness

The thickness of active layer is one of the most important parameters to optimize. Indeed, this parameter directly effects on the IPCE and J-V character and in overall on the efficiency of the solar cell. In the performed experiments this parameter was altered by changing the speed of the spin coater. Very high speed results in disrupted films and creates pin-holes and of course low speeds creates thick and inhomogeneous films which increases the probability of electron and hole recombination and it is an unwanted phenomenon in solar cells. The optimum speed was recorded 500rpm for 4 seconds in the first step and continuing with the speed of 1500 rpm in the second step for 60 seconds.

5.3.4 Annealing process

In general, annealing the active layer and PEDOT:PSS separately has resulted in a higher IPCE. It has been reported that annealing increases the crystalinity and decreases the grain size in the hybrid film. This results in improvement in charge carrier mobility and finally improving the performance of the solar cell device[84]. It is also recommended to anneal the films in order to remove the humidity and solidify the film. This will improve charge transportation. Thermal annealing was done in two steps. The first step was annealing the PEDOT:PSS layer at 120 C for 10 minutes and the second step was annealing the active layer deposited on PEDOT:PSS. The second step was performed at 80 C for 30 minutes in the low vacuum (provided by rotary vacuum pump). It is worthy to add this that In general high temperature is not suitable working condition for the bulk heterojunction solar cell since if increases the series resistance and reduces the short circuit current

which affects negatively on the solar cell efficiency. It is proved that decreasing temperature results in decreasing the overall solar cell efficiency. Of course by decreasing the temperature we can reduce the ohmic effect which helps to increases the series resistance in the device. By increasing temperature the short circuit current will be thermally activated. The dominant contribution of shallow defects to the Jsc overcomes the ohmic affect [82]. The variation in performance with temperature was not studied in this thesis.

5.3.5 Concentrations

Starting from the equal concentration of each ZnO and P3HT (5 mg/L) in the solution and modifying the concentration the optimum obtained concentrations were 5 mg/L ZnO and 10 mg/L P3HT in solution. Increasing the concentration of ZnO often ended with agglomeration of ZnO nanoparticles which is an undesired quality of solution.

5.3.6 Optimum performance achieved

By varying of few certain parameters (as above) such as concentrations, active layer thickness, mass ratio of the ZnO nanoparticles and P3HT conductive polymers and PEDOT:PSS concentration and annealing temperature. We could optimise the IPCE and hardly rectify the J-V character of the in-laboratory prepared bulk hetero-junction solar cells. Figures 5.5 indicate the progress made from the start to the end of experiments. As it is showed in the figure 5.4 A and 5.4 B in the device b all the optimised parameters (shown in the table 5.1) has been applied except the PEDOT:PSS concentration. Here by optimizing the concentration there is a significant improvement in the IPCE and up to some extend in J-V characterizations which resulted in the best performing device a. Indeed, over fifty sets of experiments have been performed and nearly150 bulk hetero-junction cells have been assembled. In these figure only three different data from beginning (low cell performance) to the finally optimized (highest

performance) has been shown. The parameters that have been experimentally tested in the assembly of bulk hetero-junction solar cells are listed in the Table 5.1. The bold parameters are the optimised parameters and all together result in a higher device performance. The PEDOT:PSS was one of the parameters that is changed and optimization results in the very significant change in the performance of device. Figure 5.4 we shows the effect of dilution of as purchased PEDOT:PSS. In a) we have diluted the concentration of PEDOT:PSS two times and obtimised the active layer as well . In c) PETOD is diluted two times but the active layer is not optimized. In b) nither the PEDOT:PSS is diluted nor active layer is optimized.

A) B)

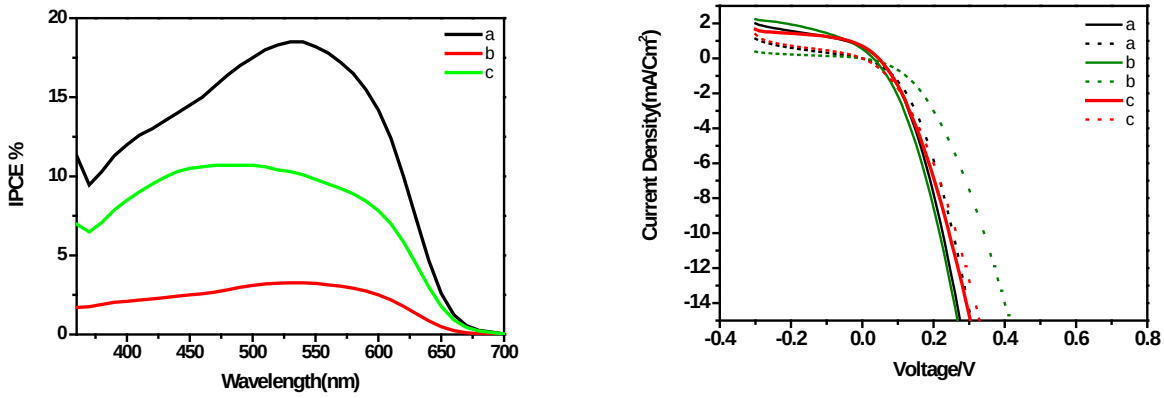

Figure 5.4 A) IPCE characteristics of the devices for 3 devices a, b, c.. B) J-V characteristics of the three devices a, b, c. **(a)** PEDOT:PSS concentration of 0.65 Wt% and blend layer thickness reduction and the obtimized active layer. **(b)** PEDOT:PSS concentration of 1.3 Wt% (as perchased PEDOT:PSS) with obtimizing the active layer. **(c)** PEDOT:PSS concentration of 0.65 Wt% (diluted to half concentration). In all a, b, c the ZnO/P3HT mass ratio is 50%-50%.

Blend concentration (ZnO,P3HT)	(5,5)/ **(5,10)/** (10,10)
Ratio (ZnO,P3HT)	30%-70% / **50%-50%**
Active layer thickness in terms of the spinning speed (rpm)	1000 / 1200/ **1500**
PEDOT:PSS dilution	No diluted /**two times**, tree times
Thermal annealing (PEDOT:PSS, blended layer)	(0,0) / **(120,80)** / (0,80)

Table 5.1 The tested cell parameters. The bold numbers are the optimum obtained parameters for the highest cell performance.

Chapter 6

6. Surface morphology of Hybrid film investigation using AFM

In order to further understand the effect of the morphology of the films on the electrical properties and the condition of aluminium electrode which deposited on the hybrid film by metal evaporation technique, atomic force microscopy of the film (AFM) and the electrodes especially at the border/edge of the electrode and hybrid film has been performed. AFM measurements were performed using digital instruments D3100 scanning probe microscope operating in tapping mode. Here the effort was made to understand the morphology of the film surrounding the electrodes. Three bulk hetero-junction solar cells with different performance were chosen for this study. The first solar cell was the best performing one with the highest J-V and IPCE characteristics with the 50-50%(mass ration) ZnO/P3HT ratio. The second solar cell was the one with 30-70% (mass ratio) ZnO/P3HT ratio and the third one was with 50-50%(mass ration) ZnO/P3HT ratio bulk hetero-junction prepared before optimizing the ZnO solubility in P3HT solution with large agglomeration of ZnO nanoparticles in P3HT solution (figure 3.8). This is to understand film morphologies especially near the aluminium electrodes and the relation between the film morphologies and their solar cell performance. In order to have a better understanding of the surface morphology of the hybrid films six different points have been selected on the solar cell surface to be investigated using AFM microscopy. These six points are three points of a, b and c near the best electrode and the next three positions are near the worst solar cell performing electrodes. Here we chose three points, up, middle and bottom of each electrode. This was to have a better statistical data. Figure 3.9 is schematically showing the structure of the bulk hetero-junction solar cell and the position of the chosen points for the AFM studies. The whole AFM studies can be categorized to three main aspects of study; Surface 3D imaging, Roughness measurement and Grain size measurement. As it explained before three different in-laboratory prepared bulk hetero-junction solar cells were chosen for the AFM study. The first bulk hetero-

junction solar cell which has the best performance provided us the following information:

6.1 Highest performing solar cell

6.1.1 Three dimension (3D) imagining of the surface

3D imaging of the surface of the best performing bulk hetero-junction solar cell has been obtained which is shown in figure 6.1. These 3D images are the result of surface scanning of 3 µm x3 µm 50%-50% ZnO/P3HT top hybrid layer surfaces surrounding the best and the worst electrodes out of the total six electrodes on the lab-made device. The best electrode is the electrode with the highest IPCE and J-V characteristics and the worst is the one with lowest mentioned measured characters (see chapter 5).

a **d**

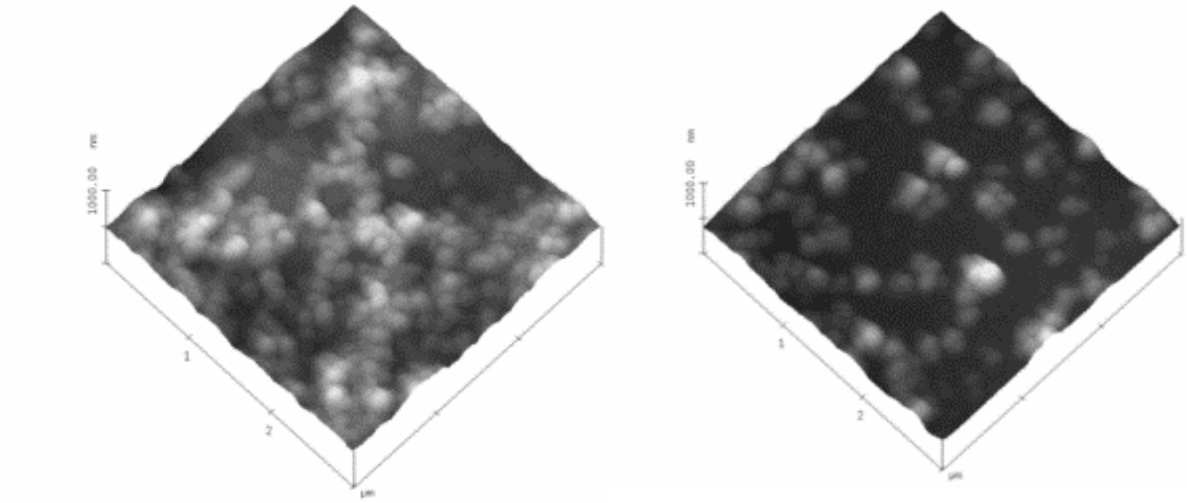

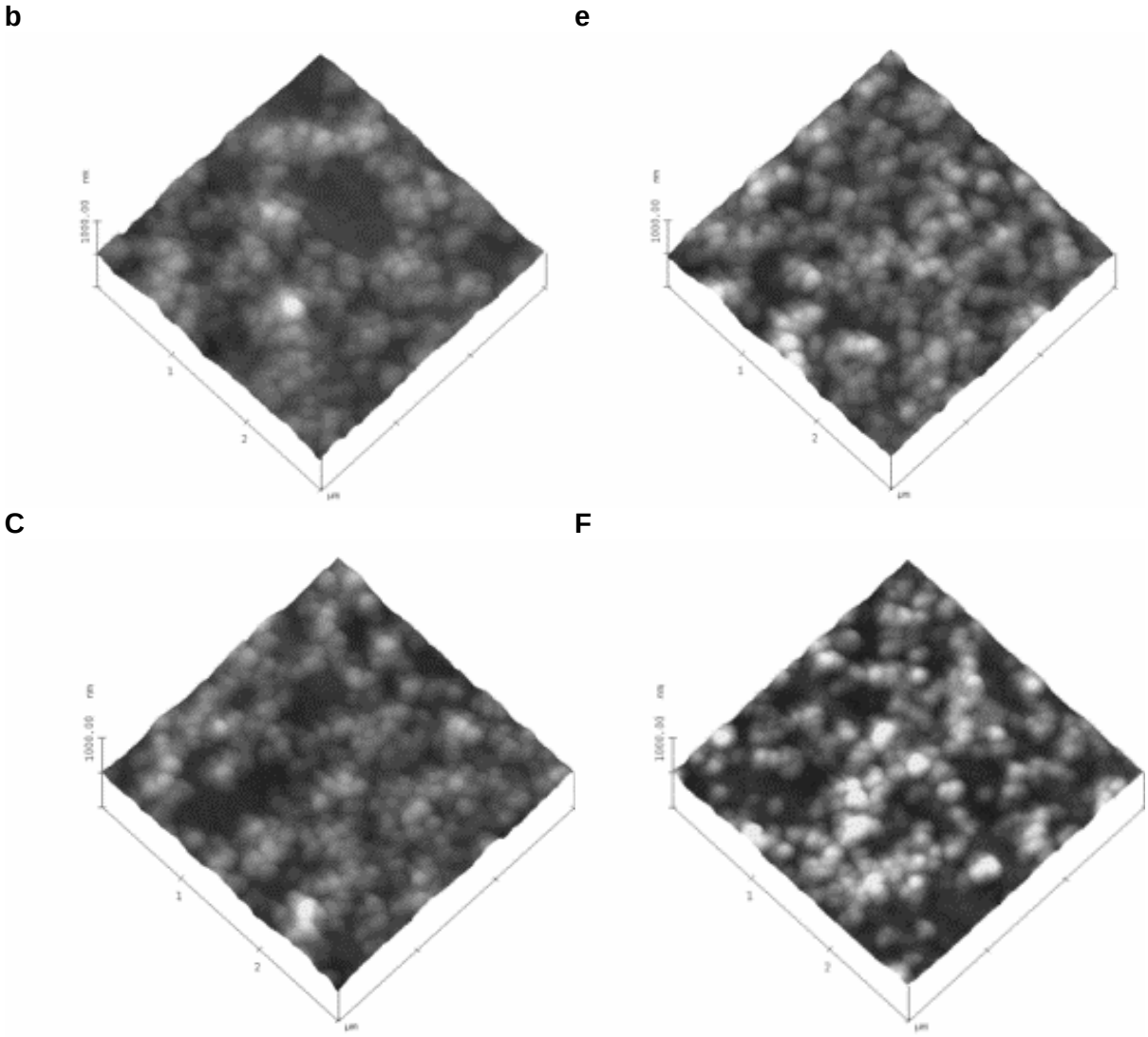

Figure 6.1 3D AFM images of the Best sample. The best and the worst electrodes (in terms of IPCE and J-V characters) a,b,c points (Top, middle, bottom) adjacent to the best aluminium electrode and d, e, f points (Top, middle, bottom) adjacent to the worst electrode. The scanned area is 3µm x 3µm.

In figure 6.1 it is quite clear that the obtained surface morphologies comparatively and also individually are not uniform. Of course there is not a high expectation of achieving a uniform surface since these films are deposited using the spin coating technique. Also comparatively high vapour pressure of the manipulated solvent (Chloroform) and very fast drying process of the film are the main reasons.

6.1.2 Roughness measurements of the highest performing solar cell

Further surface analysis has been done using the obtained raw AFM morphology images to understand and measure the roughness of the selected areas near to the electrodes. Table 6.1 shows the measured surface roughness for each area (point) very close to the chosen electrodes. As it is clear from this table that the surface roughness variation is very small and the average surface roughness of the device is 23.1 nm. In terms of the areas around the best electrode, points a,b and c the average roughness is 24 nm and for the worst electrode the average roughness is 23 nm.

a

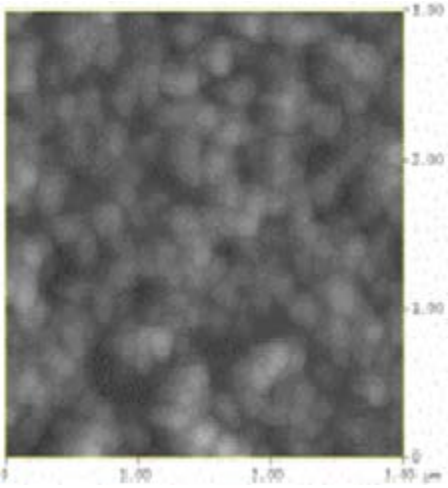

d

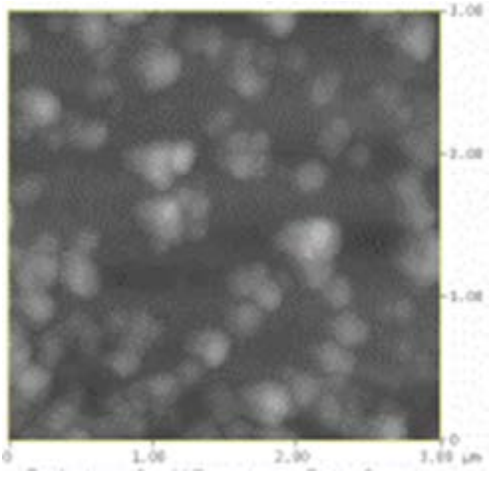

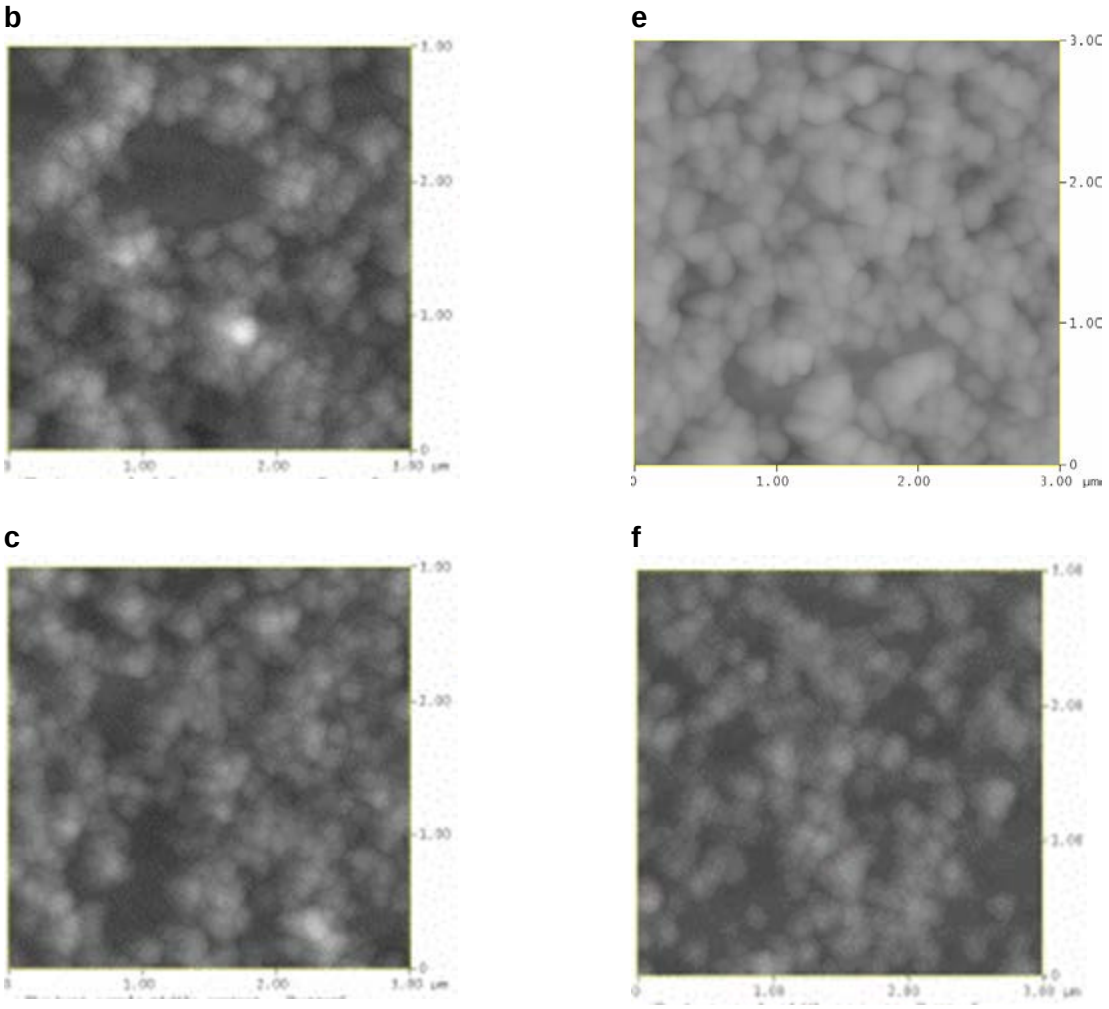

Figure 6.2 Plane AFM images and roughness measurements The best and the worst electrodes (in terms of IPCE and J-V characters) a,b,c points (Top, middle, bottom) adjacent to the best aluminium electrode and d, e, f points (Top, middle, bottom) adjacent to the worst electrode.

6.1.3 Granular size of the highest performing solar cell

Figure 6.3 shows the mean grain size measurement using the Gwyddion AFM analysis software. This data provide us the granular sizes on the surface of the hybrid layer in the actual bulk hetero-junction device. The measured values are presented in the table 6.1.

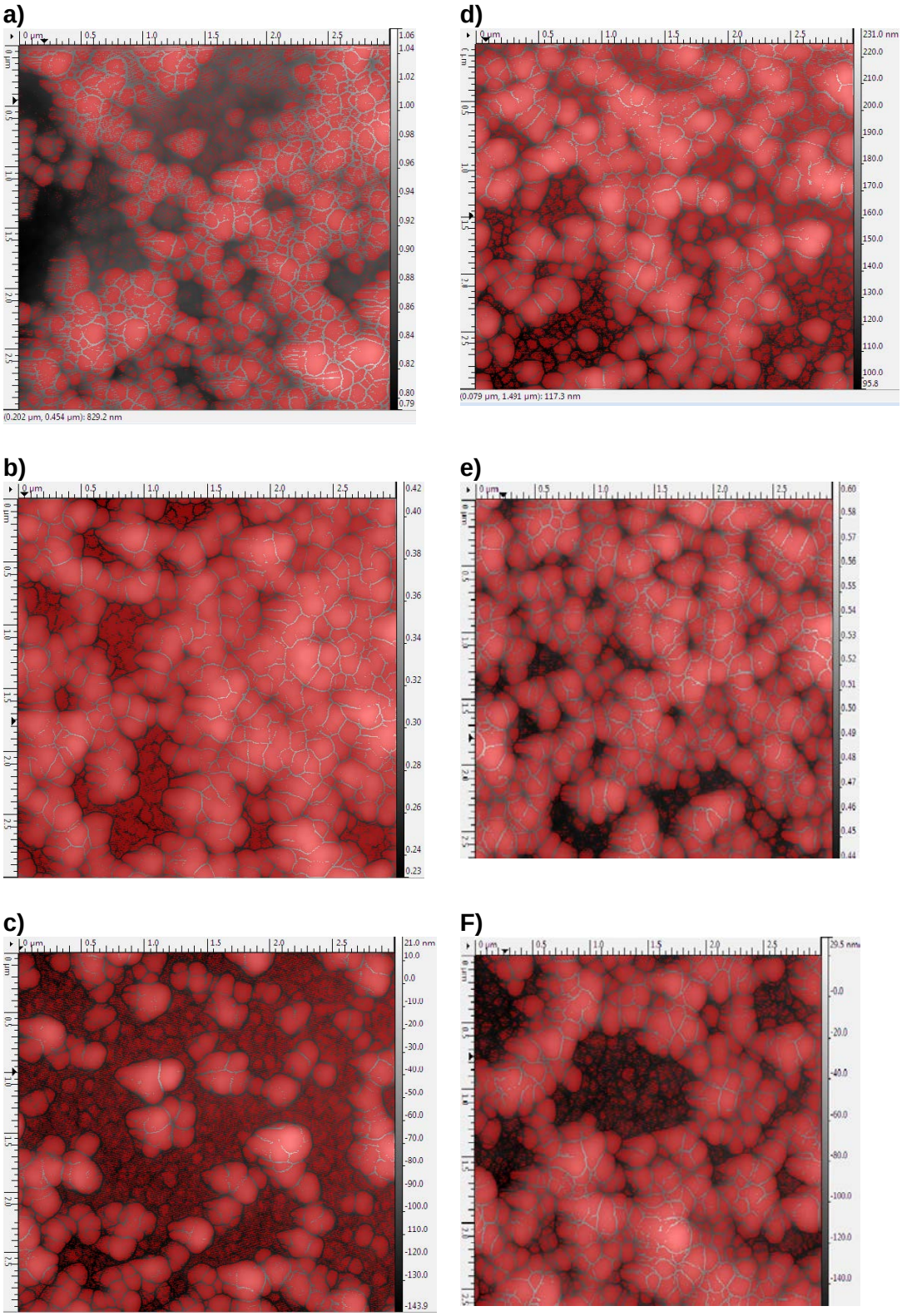

Figure 6.3 Mean grian size measurements. The best and the worst electrodes (in terms of IPCE and J-V characters) a,b,c points (Top, middle, bottom) adjacent to the best aluminium electrode and d, e, f points (Top, middle, bottom) adjacent to the worst electrode.

As it can be inferred from the given data in table 6.1, the average mean grain size on the hybrid surface is 18.65 nm. Also the average grain size near to the best electrode in this device was 17.6 nm and near the worst electrode 19.7 nm. This data helps us to understand whether there has been formation of lumps on the surface after fabrication of the hybrid layer on the top most layer or not.

Electrodes	points	Roughness(nm)	Granular size(nm)
Best electrode	**a**	**25**	**13.7**
	b	**25**	**18.6**
	c	**22**	**20.4**
Worst electrode	**d**	**23**	**10.6**
	e	**25**	**32**
	f	**21**	**16.6**

Table 6.1 The Best performing lab- made bulk hetero-junction solar sell. Roughness and granular size of the points a,b,c,d,e,f.

6.2 The lowest performing solar cell (made of agglomerated solution)

6.2.1 Three dimension (3D) imagining of the surface

3D imaging of the surface of the lowest performing bulk hetero-junction solar cell has been obtained which is shown in figure 6.4. These 3D images are the result of surface scanning of 3 µm x3 µm 50%-50%, agglomerated ZnO/P3HT hybrid layer surfaces surrounding the best and the worst electrodes out of the total six electrodes on the lab-made device. The best electrode is the electrode with the highest IPCE and J-V characteristics and the worst is the one with lowest mentioned measured characters.

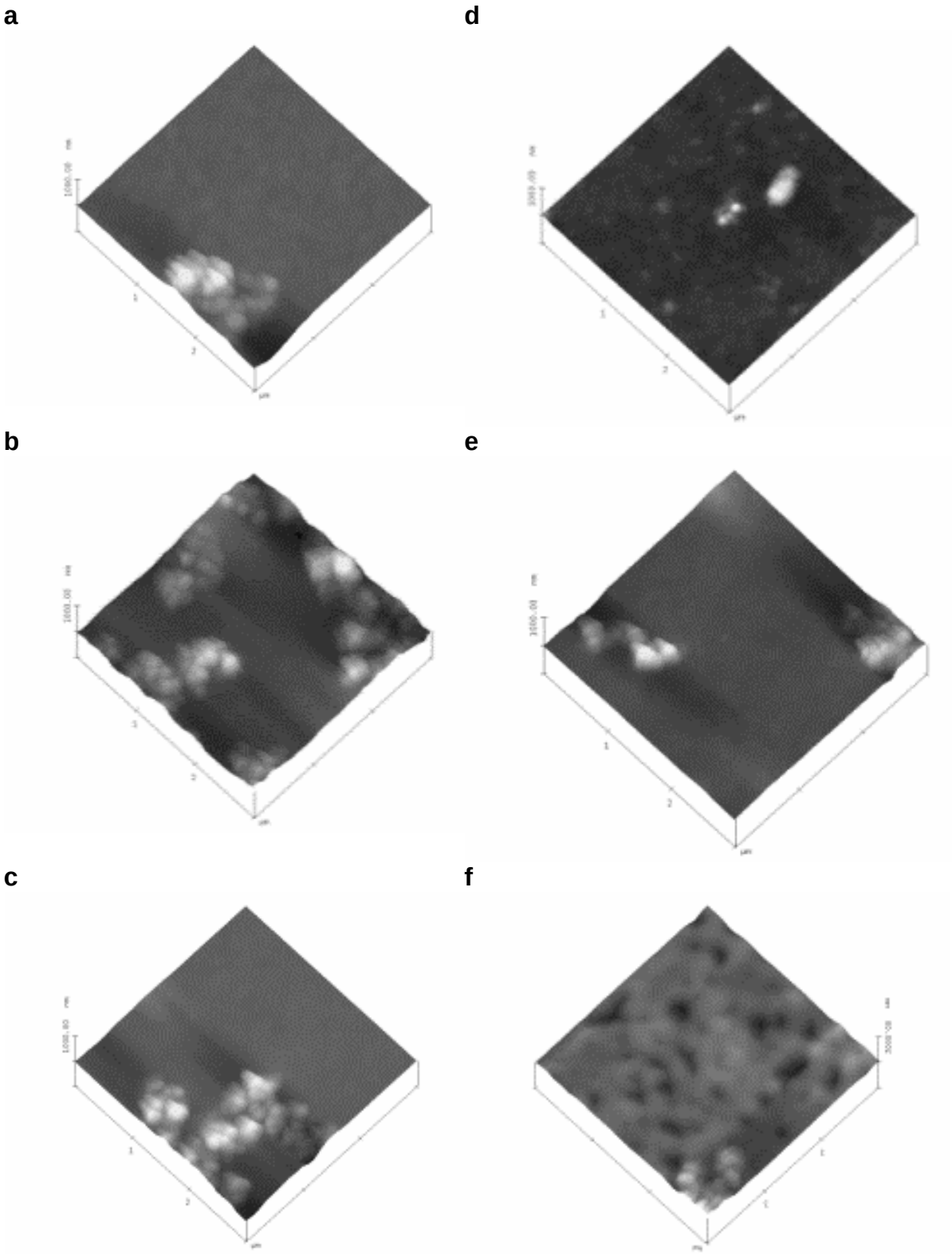

Figure 6.4 3D AFM images of the lowest performing solar cell. The best and the worst electrodes (in terms of IPCE and J-V characters) a,b,c points (Top, middle, bottom) adjacent to the best aluminium electrode and d, e, f points (Top, middle, bottom) adjacent to the worst electrode. The scanned area is 3µm x 3µm.

In figure 6.4 it is quite clear that the obtained surface morphologies are significantly different than those of the ideal (highest performing) device. There is no uniform distribution of the surface roughness. Of course there is not a high expectation of achieving a uniform surface in this sample because there was a clear agglomeration in the ZnO/P3HT hybrid solution layer deposition using the spin coating technique and high vapour pressure of the manipulated solvent (Chloroform) and very fast drying process of the film common reasons for surface morphology quality reduction in the prepared films.

6.2.2 Roughness measurements

Further surface analysis has been done using the obtained raw 3D morphology images to understand and measure the roughness of the selected areas near to the electrodes. Table 6.2 shows the measured surface roughness for each area (point) which are very close to the chosen electrodes. As it is clear from this table the surface roughness variation is very not small and the average surface roughness of the device is 22.4 nm. In terms of the areas around the best electrode, points a, b and c the average roughness is 29.5 and for the worst electrode the average roughness is 15.2 nm. From the Table 6.2 it is clear that the average roughness near to the best electrode is bigger than the average roughness near to the worst electrode. Also it is important to point out that the film is more uniform near the best electrode and all the point have almost the same roughness.

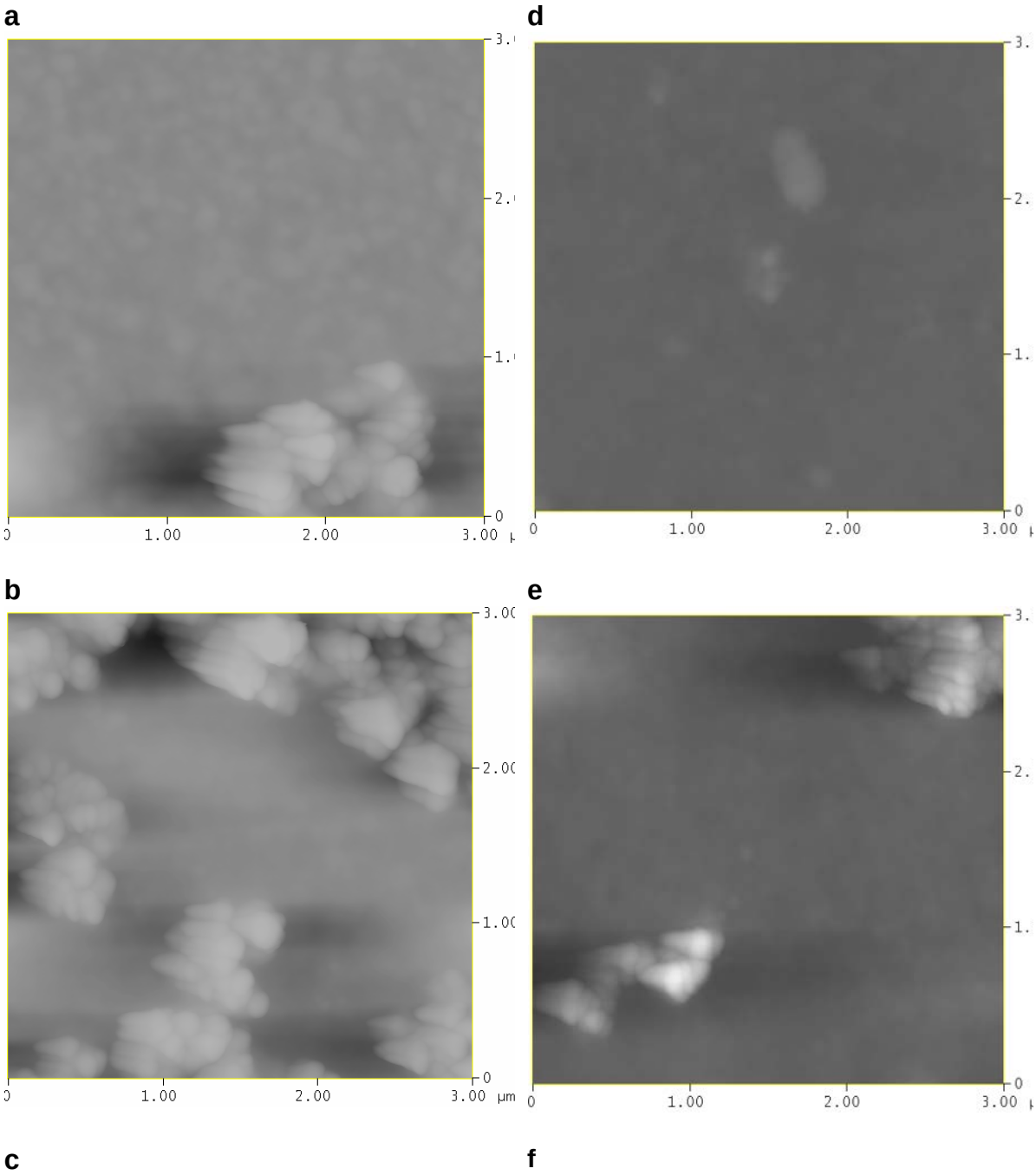
a
d
b
e
c
f
1.00
2.00
3.00
µm

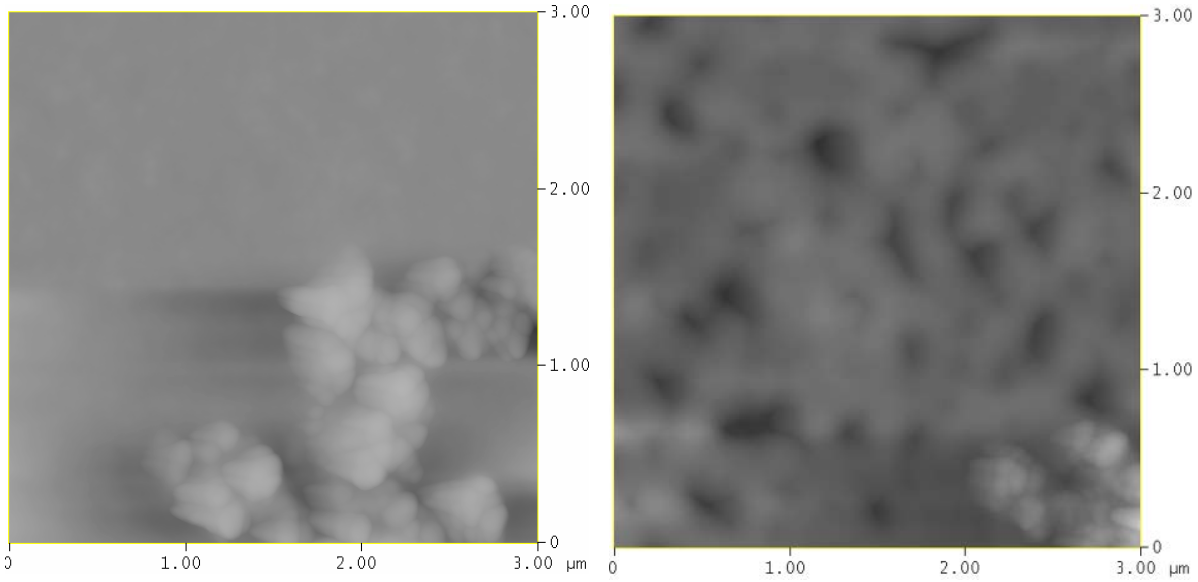

Figure 6.5 Plane AFM images and roughness measurements of the lowest performing solar cell. The best and the worst electrodes (in terms of IPCE and J-V characters) a,b,c points (Top, middle, bottom) adjacent to the best aluminium electrode and d, e, f points (Top, middle, bottom) adjacent to the worst electrode.

6.2.3 Granular size of the lowest performing solar cell

In figure 6.6 as above shows the granular measurement using the Gwyddion AFM analysis software. This data provide us the granular sizes on the surface of the hybrid layer in the actual bulk hetero-junction device. The measured values are presented in the table 6.2

a)

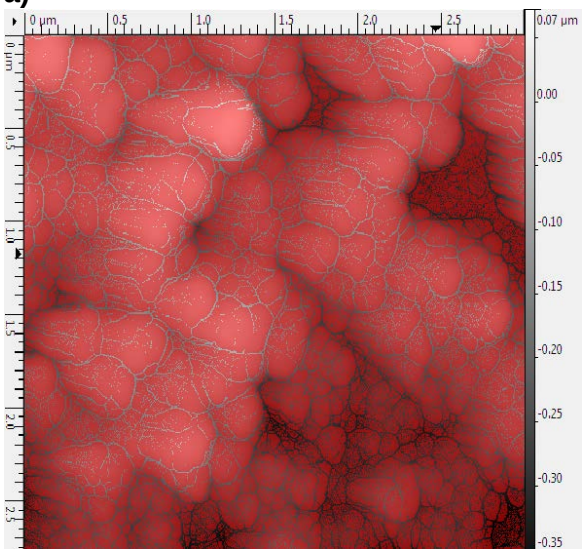
0 µm
0.5
1.0
1.5
2.0
2.5
0.07 µm
0.00
-0.05
-0.10
-0.15
-0.20
-0.25
-0.30
-0.35

d)

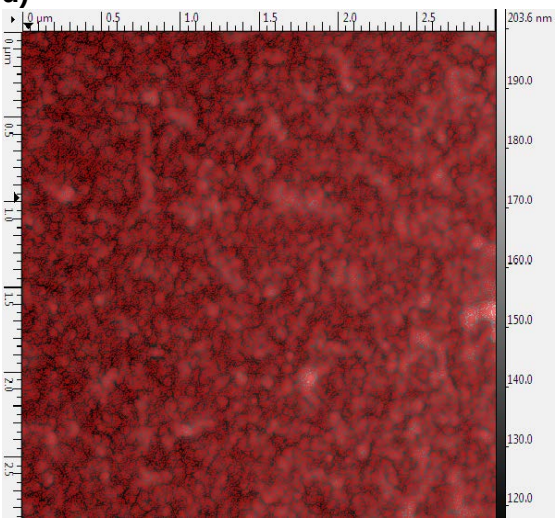
0 µm
0.5
1.0
1.5
2.0
2.5
203.6 nm
190.0
180.0
170.0
160.0
150.0
140.0
130.0
120.0

b)

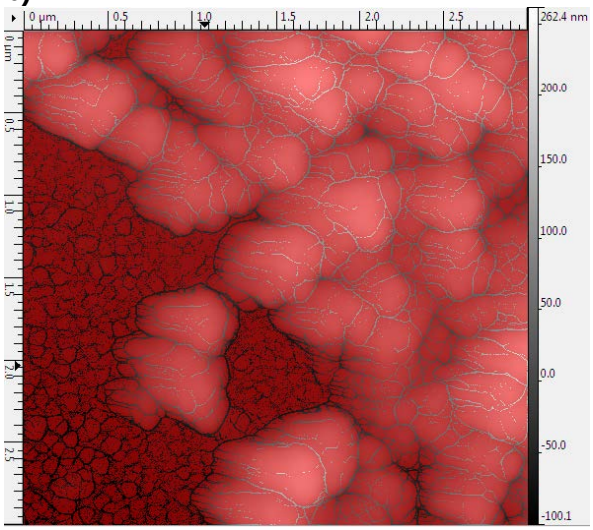
0 µm
0.5
1.0
1.5
2.0
2.5
262.4 nm
200.0
150.0
100.0
50.0
0.0
-50.0
-100.1

e)

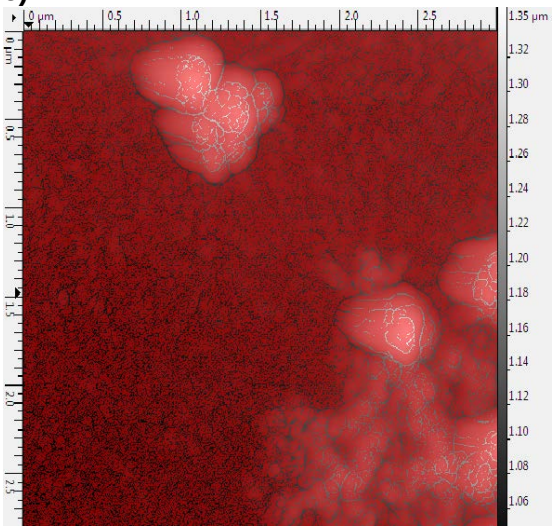
0 µm
0.5
1.0
1.5
2.0
2.5
1.35 µm
1.32
1.30
1.28
1.26
1.24
1.22
1.20
1.18
1.16
1.14
1.12
1.10
1.08
1.06

c)

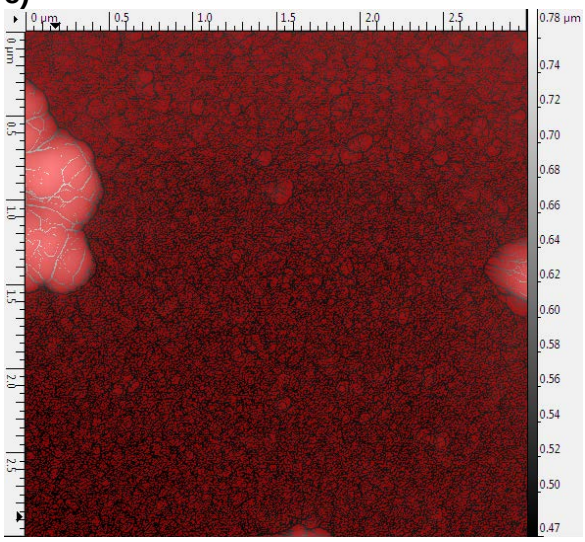
0 µm
0.5
1.0
1.5
2.0
2.5
0.78 µm
0.74
0.72
0.70
0.68
0.66
0.64
0.62
0.60
0.58
0.56
0.54
0.52
0.50
0.47

f)

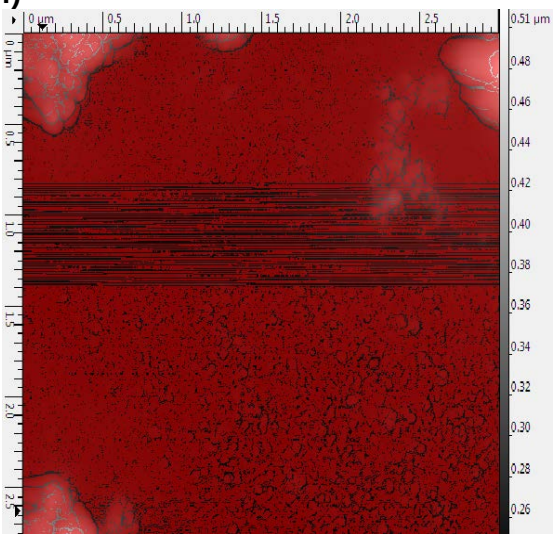
0 µm
0.5
1.0
1.5
2.0
2.5
0.51 µm
0.48
0.46
0.44
0.42
0.40
0.38
0.36
0.34
0.32
0.30
0.28
0.26

Figure 6.6 Mean grain size measurement of the lowest performing solar cell. The best and the worst electrodes (in terms of IPCE and J-V characters) a,b,c points (Top, middle, bottom) adjacent to the best aluminium electrode and d, e, f points (Top, middle, bottom) adjacent to the worst electrode.

As it can be inferred from the given data in table 6.2, the average mean grain size on the hybrid surface is 7.7 nm. Also the average grain size near to the best electrode in this device was 7.4 nm and near the worst electrode 8 nm. This data shows that there are mostly disrupted hybrid layers since the very small grain sizes measured around the electrodes can be mainly of the grains formed by underneath layer which is the PEEDOT:PSS layer. This layer is much softer than the hybrid layer because of lower rate of drying. As it is depicted in the figure 6.6 which is showing the mean grain sizes near the best and worst electrodes the film as a whole is not very uniform and even if we look at the actual device we can understand that during spin coating of hybrid layer, the hybrid layer was not uniformly distributed over the PEEDOT:PSS. The color contrast on the films where there is more pinkish is where we mostly have got hybrid layer and if there is only red which is more smooth is the film of mainly PEEDOT:PSS.

Electrodes	Points	Roughness(nm)	Granular size(nm)
Best electrode	**a**	**27.5**	**7.1**
	b	**38.8**	**7.3**
	c	**22.2**	**7.8**
Worst electrode	**d**	**3.9**	**7.9**
	e	**22.7**	**8.2**
	f	**19.1**	**7.8**

Table 6.2 The lowest performing lab- made bulk hetero-junction solar sell. Roughness and granular size of the points a,b,c,d,e,f.

6.3 30%-70% (mass ratio) ZnO/P3HT solar cell

6.3.1 Three dimension (3D) imagining of the surface

3D imaging of the surface of the 30%-70% bulk hetero-junction solar cell has been obtained which is shown in figure 6.7. These 3D images are the result of surface scanning of 3 µm x3 µm 30%-70% ZnO/P3HT top hybrid layer surfaces surrounding the best and the worst electrodes out of the total six electrodes on the lab-made device. The best electrode is the electrode with the highest IPCE and J-V characteristics and the worst is the one with lowest mentioned measured characters.

a

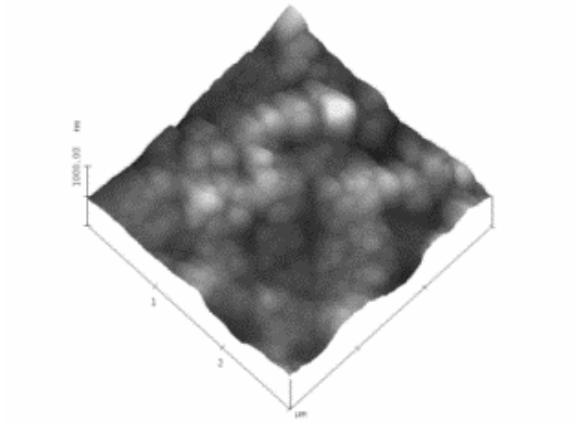

d

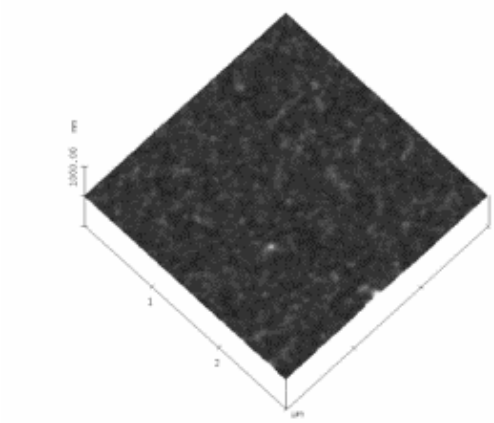

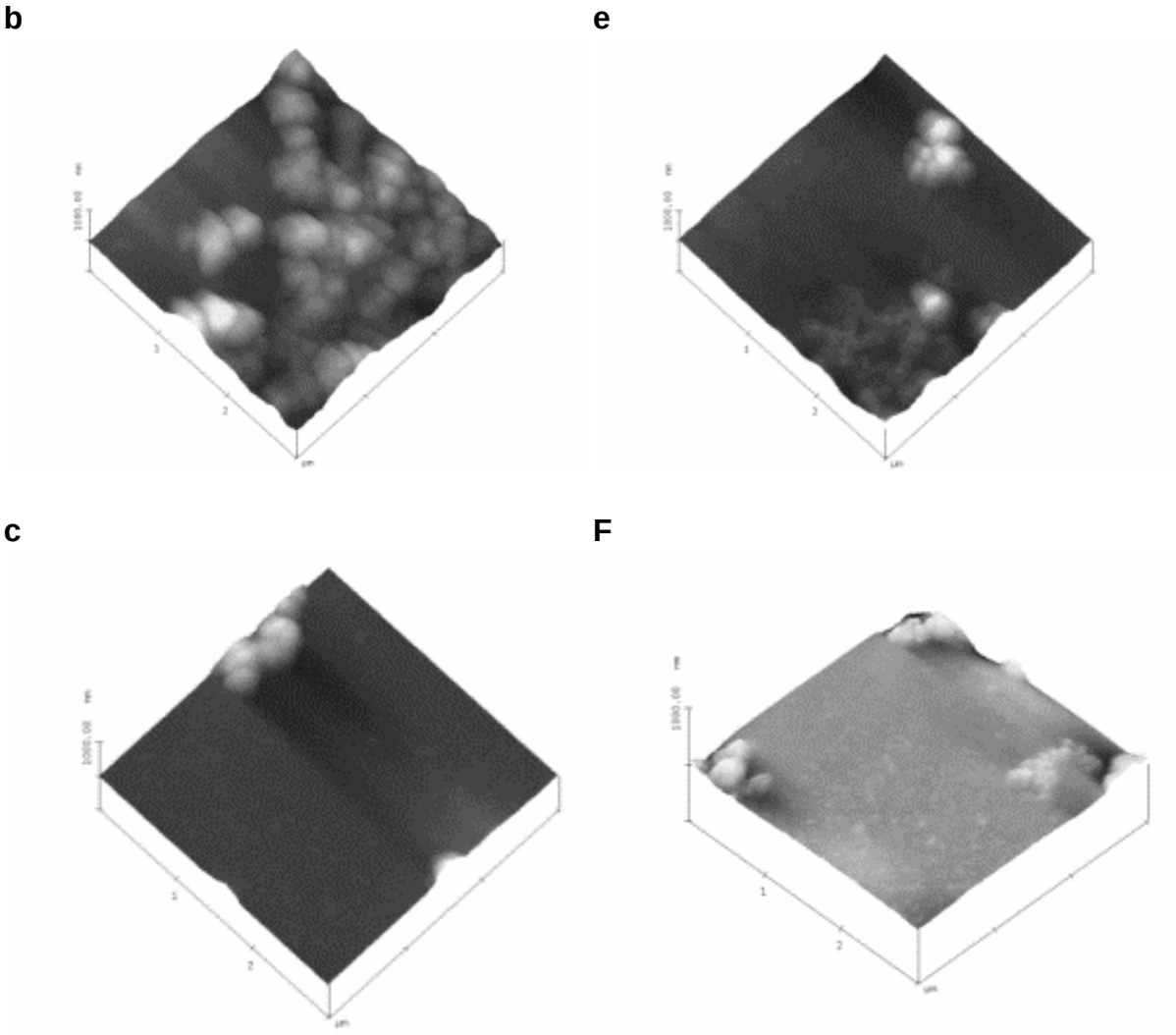

Figure 6.7 3D AFM images of 30-70% (mass ratio) ZnO/P3HT solar cell. The best and the worst electrodes (in terms of IPCE and J-V characters) a,b,c points (Top, middle, bottom) adjacent to the best aluminium electrode and d, e, f points (Top, middle, bottom) adjacent to the worst electrode. The scanned area is 3µm x 3µm.

In figure 6.7 it is quite clear that the obtained surface morphologies comparatively and also individually are not uniform. As mentioned before there is not a high expectation of achieving a uniform surface since these films are deposited using the spin coating technique. Also comparatively high vapour pressure of the manipulated solvent (Chloroform) and very fast drying process of the film are the main reasons.

6.3.2 Roughness measurement of 30-70% (mass ratio) ZnO/P3HT solar cell hybrid Film

Further surface analysis has been done using the obtained raw 3D morphology images to understand and measure the roughness of the selected areas near to the electrodes. Table 6.3 shows the measured surface roughness for each area (point) very close to the chosen electrodes. As it is clear from this table the surface roughness variation is very small and the average surface roughness of the device is 33.8 nm. In terms of the areas around the best electrode, points a,b and c the average roughness is 48.5 nm and for the worst electrode the average roughness is 19.1 nm.

a

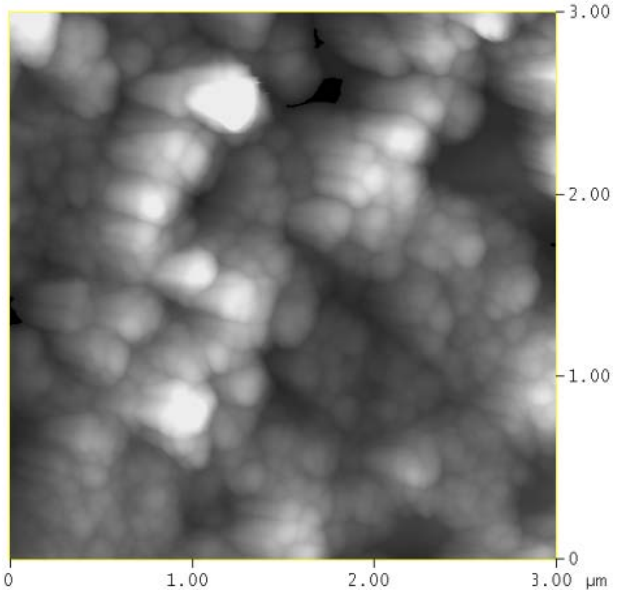

d

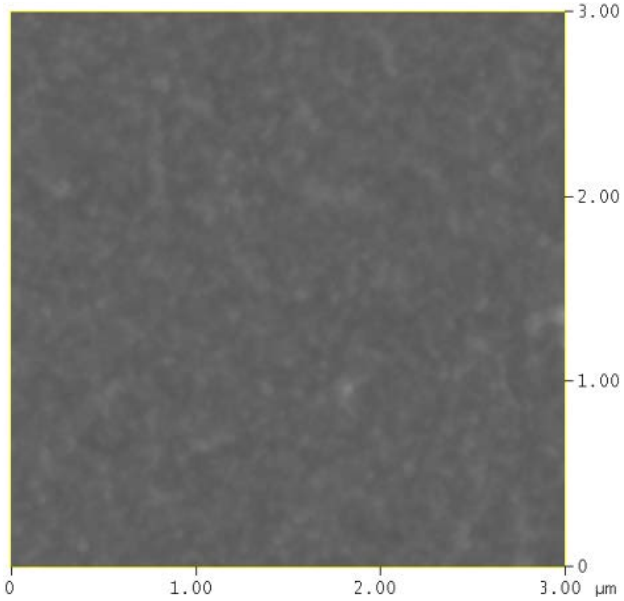

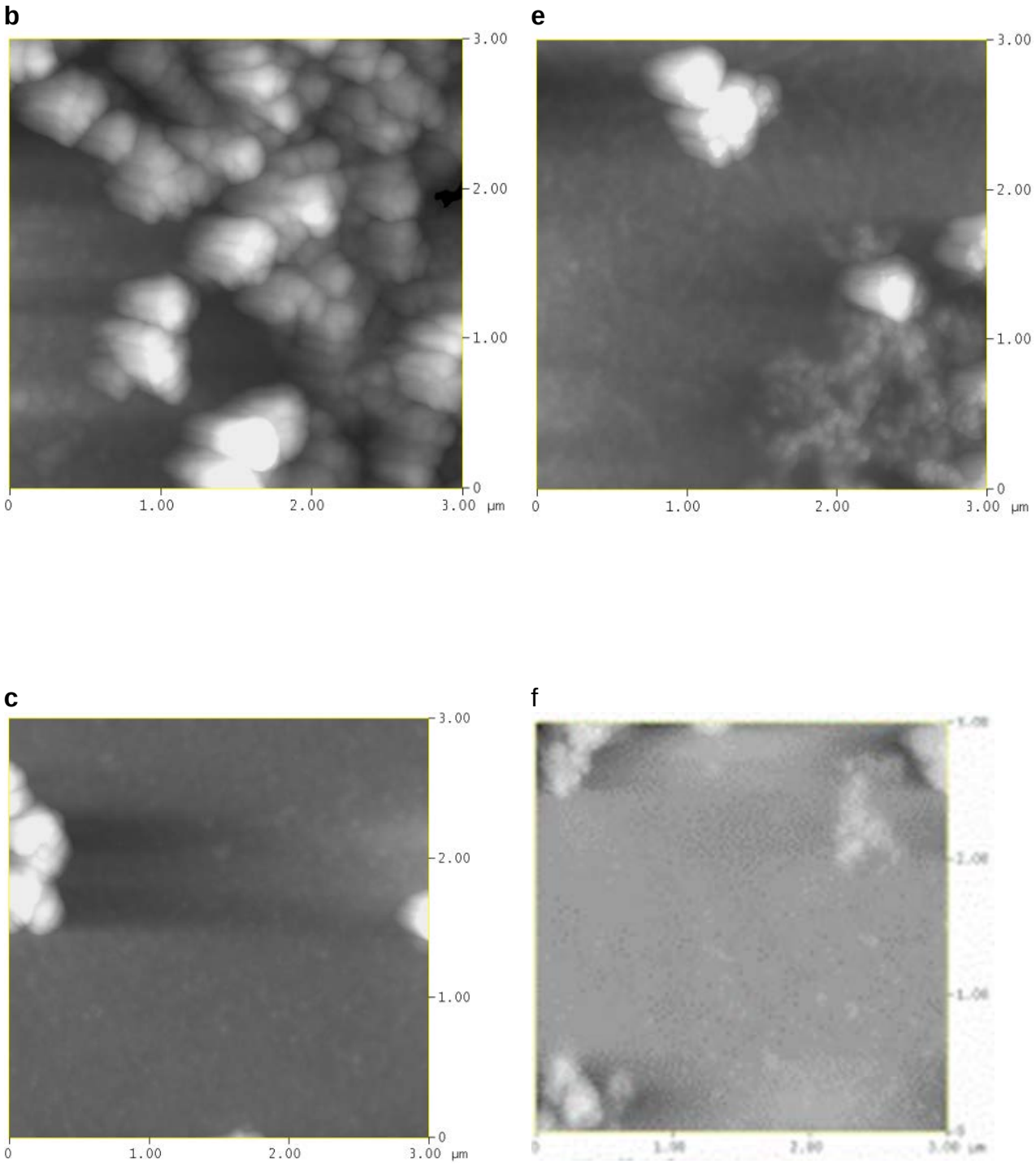

Figure 6.8 Plane AFM images and roughness measurements of 30-70% (mass ratio) ZnO/P3HT solar cell. The best and the worst electrodes (in terms of IPCE and J-V characters) a,b,c points (Top, middle, bottom) adjacent to the best aluminium electrode and d, e, f points (Top, middle, bottom) adjacent to the worst electrode.

6.3.3 Granular size of the lowest performing solar cell

Figure 6.9 shows the granular measurement using the Gwyddion AFM analysis software. This data provide us the granular sizes on the surface of the hybrid layer in the 30%-70% bulk hetero-junction device. The measured values are presented in the table 6.3

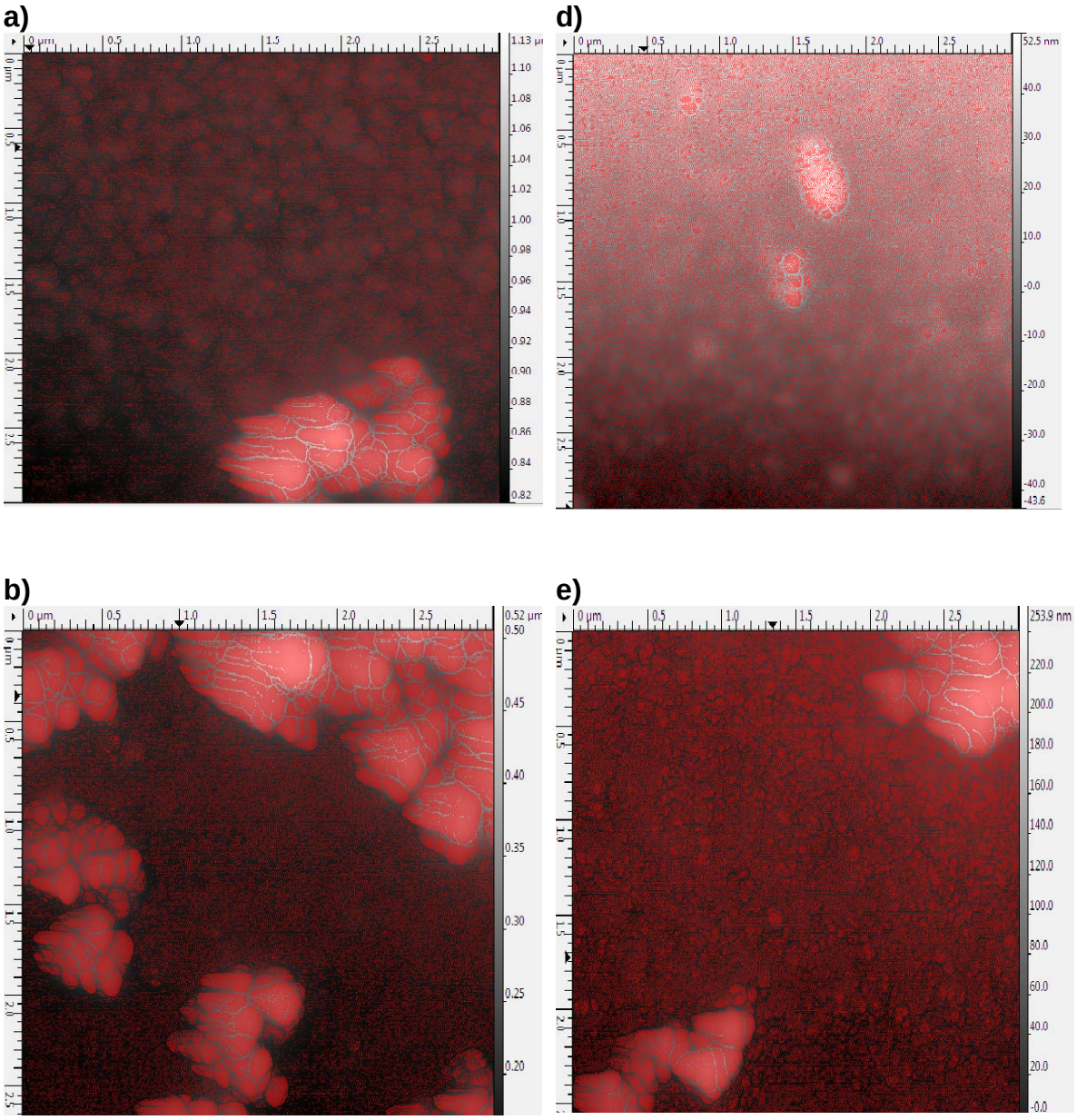

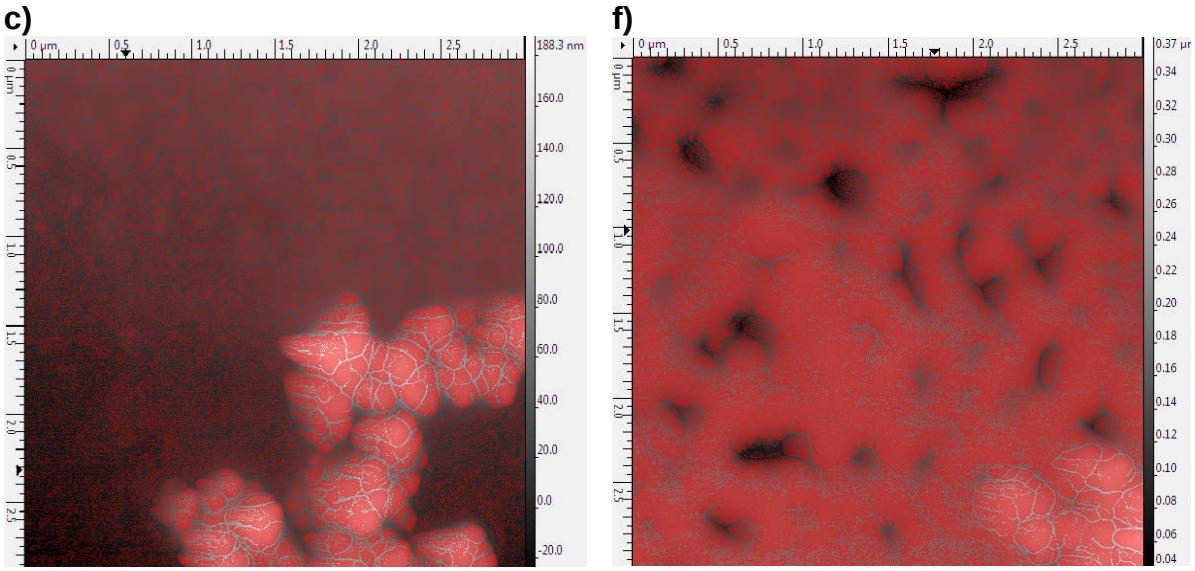

Figure 6.9 Mean grain size measurement of 30-70% (mass ratio) ZnO/P3HT solar cell. The best and the worst electrodes (in terms of IPCE and J-V characters) a,b,c points (Top, middle, bottom) adjacent to the best aluminium electrode and d, e, f points (Top, middle, bottom) adjacent to the worst electrode.

As it can be inferred from the given data in table 6.3, the average mean grain size on the hybrid surface is 18.6 nm. Also the average grain size near to the best electrode in this device was 22.13 nm and near the worst electrode 15 nm. In compare to the highest performing solar cell the grain size and roughness are both quite ununiformed. The main deference is the roughness of the hybrid layer.

Electrodes	points	Roughness(nm)	Granular size(nm)
Best electrode	**a**	**58.2**	**19.6**
	b	**56.9**	**32.2**
	c	**30.4**	**14.6**
Worst electrode	**d**	**5.4**	**10.2**
	e	**37.2**	**12.5**
	f	**14.6**	**22.3**

Table 6.3 The 30-70% lab- made bulk hetero-junction solar sell. Roughness and granular size of the points a,b,c,d,e,f.

6.4 Step height of the aluminium electrode and the thickness study of the best performing solar cell films

Figure 6.10 depicts the two dimensional profiles of the surface. Using Surface profiler (Tencor Surface Profiler) we have measured the thickness of the hybrid film and the deposited aluminium electrodes. The same parameters of ZnO/P3HT ratio and thickness were chosen as it was used in the best performing prepared bulk hetero-junction solar cell. The film was only composed of 50% ZnO and 50% P3HT (mass ratio) and it was spin coated on the glass substrate with the speed of 1500 rms. The measured thickness (step height) which is shown in Figure 6.10a is 40 nm. The same measurement has been performed to measure the thickness of deposited aluminium electrode on the glass and on the hybrid film in the prepared bulk hetro-junction solar cell. Also in order to understand the whole film thickness differences in the actual solar cell device three points along the length of the solar cell device were chosen and by making scratches on these points and across the width of the device we could measure the thickness of the film from the underneath which is the ITO layer. Figure 6.10a is showing the thickness of the only 50%-50% ZnO/P3HT hybrid film on a glass slide, this is done by creating a scratch line across the film. In figure 6.10b the only aluminium electrode thickness after deposition on the ITO layer was measured. As it is clear in this figure the

height of the aluminium electrode varies between 20 to 40 nm. Figure 6.10 c shows the deposited aluminium thickness on the hybrid film in the actual bulk hetero-junction solar cell. It is clear that there is an approximately 40-50 nm step height for the aluminium electrode on the film which is almost the height of the bare aluminium electrode. Figures 6.10 d to 6.10 f shows three subsequent thickness measurements across the length of the best performing bulk hetero-junction solar cell. This was made to understand the thickness variation along the Bulk hetero-junction solar cell surface. Subsequently, along the length three different thicknesses of 55.4 nm, 132.8 nm and 840 nm were measured. This indicates that there is an obvious thickness variation along the bulk hetero-junction solar cell and also shows that this thickness is maximum at the centre of the device.

a)

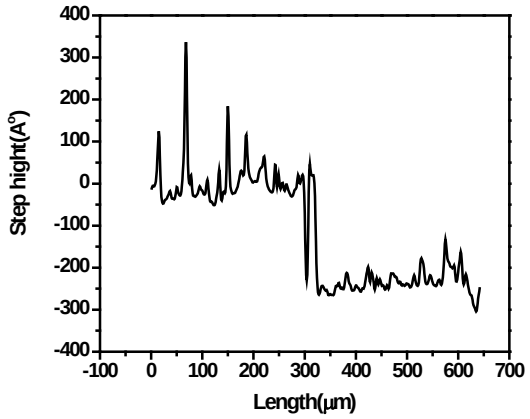

b)

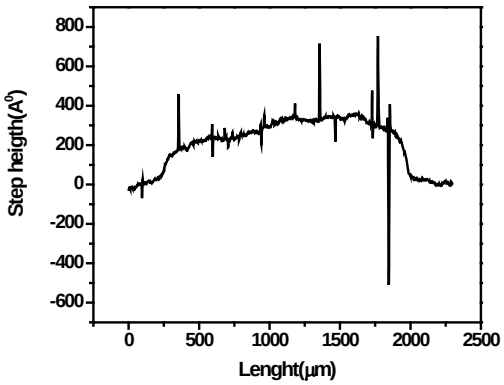

c)

d)

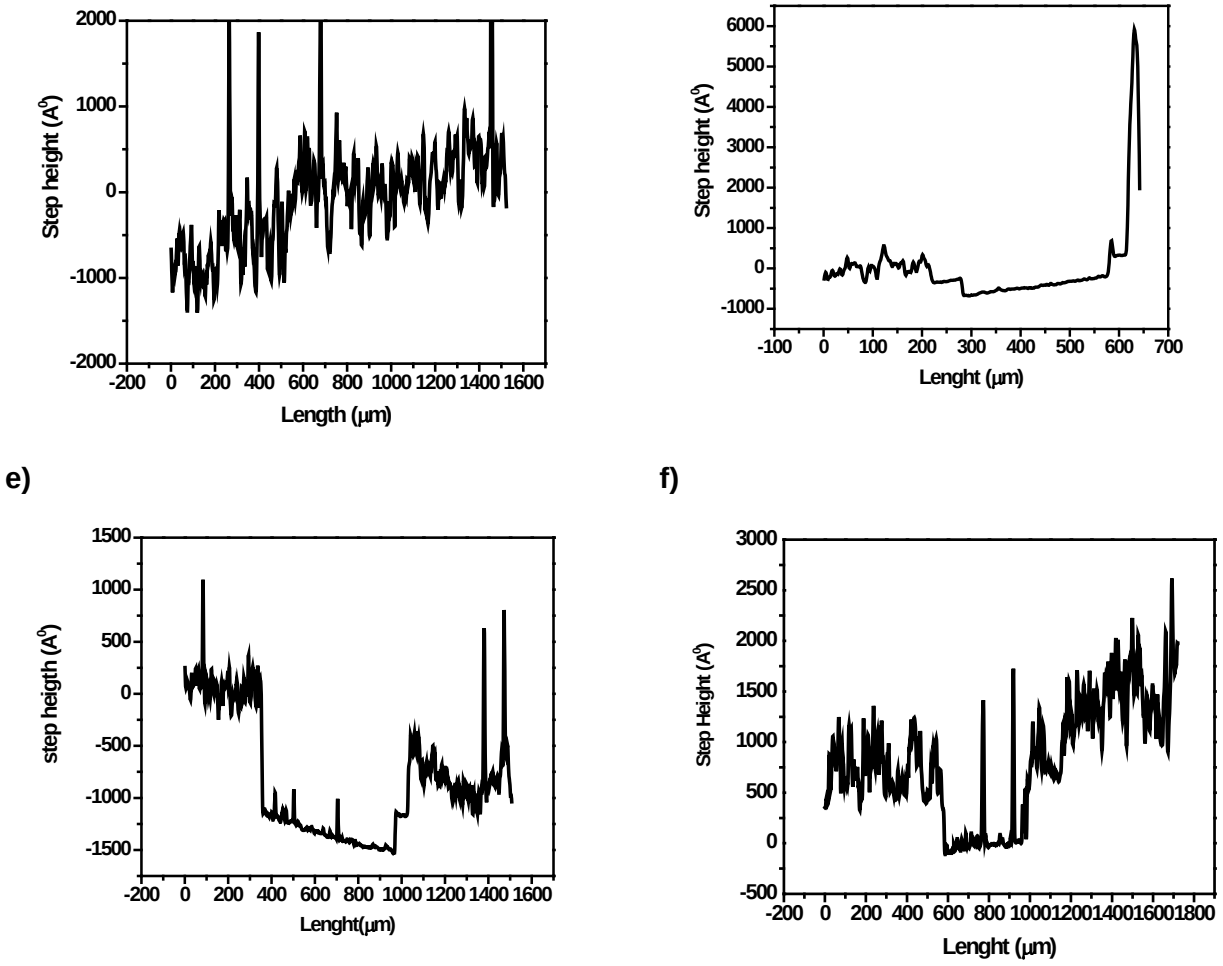

Figure 6.10 Thickness measurements of Hybrid layer and aluminium electrode using surface profiler. **a)** Thickness of the only 50-50% (mass ratio) ZnO/P3HT hybrid film on the glass. **b)** Step height of the only aluminium electrode on the ITO coated glass. **c)** Step height of aluminium electrode deposited on the hybrid layer in the bulk hetero-junction solar cell **d), e) and f)** are three subsequent thicknesses along the best performing Bulk hetero-junction solar cell.

The collected data from the three selected types of lab-made Bulk hetero-junction solar cells brings us to this conclusion that the best performing solar cell has few distinguished characteristics. Comparatively good surface uniformity is there in every scanned area. The roughness of the surfaces for all the selected areas, near to the electrodes, are approximately equal. There is no agglomeration resulting in big lumps. The average mean grain size is18.65 and there is not a wide mean grain size distribution for all the AFM scanned positions. Opposite to the best

performing solar cell in the lowest performing solar cell, the roughness of the surfaces for all the selected areas, near to the electrodes, are very much different in scanned each area. There is no uniformity, which was expectable because of the initial agglomeration of ZnO nanoparticles in the prepared solution. It is worthy to mention that the very small and approximately equal grain sizes are because of the high agglomeration in the hybrid layer and very low uniformity and the resulted disruption in the hybrid film. This causes the analysis software to bring into account the mean grain size of the underneath and softer layer of PEDOT:PSS. In the 30%-70% ZnO/P3HT hybrid layer made bulk hero-junction solar cell the hybrid film roughness is still much higher than the best performing solar cell. The grain sizes can be more related to the hybrid layer than the underneath layer and their distributions are closer to the best performing solar cell. Still the hybrid film has a very low uniformity. The variation in electrode thickness is relatively large and could have contributed strongly to the large variation between good and bad electrodes. From the set of the experiments performed on the lab made bulk heterojunction solar cells we could understand that the cells with smooth and uniform surface under and near to the aluminum contact result in a better J-V and IPCE values. We should bear in mind that a uniform morphology provides a better unrestricted connection pathways for charge carriers towards their respective electrodes.

Chapter 7

Conclusions and Future work

Because the fabrication of organic/inorganic bulk hetero-junction solar cells is relatively straightforward and cost effective, they are becoming a popular research field in comparison to alternative solar cells. In the last 15 years, significant improvements have been achieved in the efficiency of bulk hetero-junction solar cells, and if the light-to-electricity conversion efficiency improves further, this type of solar cell will provide an excellent alternative to the expensive silicon solar cells currently in use.

Hence, it becomes important to understand the effect of the parameters involved in producing a hybrid organic/inorganic solar cell, and to identify the key parameter(s) which need(s) to be optimised to increase the solar cell efficiency. The results of different sets of experiments conducted in this project focused on the optical characterization of the bulk hetero-junction solar cell, and the relevant light-to-electron charge conversion. This provided evidence of how the combination of different parameters resulted in improved performance.

This investigation began with the optimisation of the chemical synthesis of the ZnO nanoparticles and their physical and spectroscopic characterization. The synthesised ZnO nanoparticles were found to have an average diameter of 5.1 nm, and the TEM images indicated the particles were well distributed with almost no agglomeration.

Stable, clear dispersions / solutions of the ZnO nanoparticles in a mixed solvent containing 5% v/v methanol (the minimum amount required) and 95%v/v chloroform were found to be most suitable, since they avoided any undesirable agglomeration of the ZnO nanparticles.

The organic components (P3HT and PEDOT:PSS) were studied individually, and in combination, using spectroscopic and electrical measurements. The long-term stability of the hybrid films to humidity, elevated temperature and oxygen (in the air) was evaluated, with each factor detrimental to the film's performance, essentially because of chemical degradation of the unsaturated polymer chains. Here also, the aging effect after a period of nine month on the prepared bulk hetero-junction solar cells was investigated. There was a significant change in the quality of the hybrid layer since both the absorption and emission spectrum have clearly changed. It was not possible to perform the solar cell characterization (IPCE and J-V characterization) since the aluminium electrodes were oxidized and they were no more conductors.

Bulk, hybrid ZnO/P3HT photoactive films coated on a PEDOT:PSS surface were then incorporated into a solar cell device. The effect of annealing on the performance of the cells was determined, with the annealed samples exhibiting improved efficiency. Films containing different percentages of ZnO/P3HT, and at different thicknesses, were examined. It was found that a 50%:50% film was the best performing, with a thickness of 40 nm , and exhibiting 19% IPCE and 1.13 $mA.Cm^{-2}$ saturated current density and 0.23 V open circuit voltage. The P3HT used in the experiment has been optically characterized using absorption and emission spectroscopies. The peak absorption occurs at the wavelength of 650 nm which matches with the literature. Also it has been observed that after mixing with the ZnO nanoparticles the absorption intensity decreases significantly. With the 50%-50% ZnO/P3HT volume ratio it drops by a factor of 1/6. Two more absorption peaks also has been observed at the wavelengths of 555 and 600 nm. Also, from the emission spectroscopy we understood that the annealing of the hybrid film can be very helpful in improving the films quality this has resulted in a very clear emission quenching in the annealed film in compare to the not-annealed. The peak of the films were excited with the frequency of 650 nm but only in the not-annealed hybrid film the emission is observed at the wavelength of 640 and 740 nm. Few Sets of hybrid films with different ratios of ZnO from 10% to 70% were optically tested and the results were very close to the related research

references. These results were used as benchmark for fabricating bulk heterojunction solar cells. With the concentration of ZnO it is found out that 5 mg/L ZnO is the optimum because by increasing the concentration ZnO agglomeration will likely happen.

Surface morphology studies on the organic polymer film and the aluminium electrodes were conducted using atomic force microscopy. Three different bulk hetero-junction solar cell devices, with different hybrid layer films, were investigated for their roughness and granular (particle) size distributions. It was found that the roughness and uniformity of the hybrid layer on the surface of the bulk hetero-junction solar cell can be considered as two important characters to be improved in order to achieve a higher IPCE and J-V characteristics. Putting together the results from the scanning electron microscopy, atomic force microscopy and thickness measurements using surface profiler we can understand that roughness of the best performing solar cell which was approximately 25 nm and the thickness of the aluminium electrode are almost equal this might result in a non-uniform electrode surface and even we might having the aluminium grains buried in the rough hybrid surface. In the Scanning electron microscopy we have indicated some point with very less amount of aluminium. It is apparent that the deposited aluminium grains have not created a uniform and continues aluminium electrode. For the future work it is strongly suggested to change the amount (mass) of the deposited aluminium and investigate the effect of aluminium electrode on the functionality of this device. Here it is suggested to increase the thickness of the aluminium at least to two times to increase the uniformity and solidity of the electrode. This will result in better pathway for the electrons to eject out from the Cell.

In every case an uneven surface morphology was observed which suggests the photo-generated charge carriers would not contribute efficiently to the resultant net current, and so this random arrangement would have a detrimental effect on the

final solar cell efficiency. Therefore, future attempts to improve the quality of the cell electrode contacts in terms of the uniformity of the metal coating, and the smoothness of the surface of the underlying hybrid layer, can be considered one of the most critical steps in achieving a higher solar cell efficiency.

References

[1] P. Gomez-Romero, *Hybrid organic-Inorganic materials-In search of synergic activity*, *Adv. Mater.* 2001, *13*, 163.

[2] Fritts, C.E., *On a New Form of Selenium Photocell*, American J. of Science, 1883, 26, 465.

[3] Shaheen, S.E., Ginley, D.S., and Jabbour, G.E., Guest Editors, *Organic-Based Photovoltaic: Toward Low-Cost Power Generation.* MRS BULLETIN, January 2005, 30, 10-19.

[4] M.A. Green, *Third generation photovoltaics: solar cells for 2020 and beyond,* Physica, 2002, 14 , 65-70.

[5] Kittel*, C., Introduction to Solid State Physics*, Wiley, 5th Edition, 1976.

[6] Lin, Y.Y., Lee, YY, Chang, L. Wu, J.J, Chen, C.W., *The influence of interface modifier on the performance of nanostructured ZnO/Polymer hybrid solar cells*, Appl. Phys. Lett. 2009, 94, 063308-1 to 3.

[7] McConnell, R.D. *Assessment of the dye-sensitized solar cell*. Renew. Sust. Energy. Rev., 2002, 6, 273-295.

[8] (6) Moller, H., *Semiconductors for solar Cells*: Artech House: Norwood, MA, 1993:65.

[9] Cervantes, D.M., 2008, '*Silicon heterojunction solar cells obtained by Hot-Wire CVD*, PhD thesis', Universitat politecnica de catalunya, viewed 5 november2012, <www.lib.uts.edu.au>.

[10] Blom, P.W.M., Mihailetchi, V.D., Koster, L.J.A., and Markov, D.E., *Device Ds of Polymer: Fullerene Bulk Heterojunction Solar Cells*. Adv.Mater, 2007, 19, 1551-1566.

[11] Chapin, D. M., Fuller, C. S., Pearson, G. L., *A New Silicon p-n Junction Photocell for Converting Solar Radiation into Electrical Power*, J. Appl. Phys. 1954,25,676.

[12] Shaheen, S.E., Radspinner, R., Peyghambarian, N., Jabbour, G.E., *Fabrication of bulk hetero-junction plastic solar cells by screen printing*. Appl. Phys. Lett. 2001,79, 2996.

[13] Halls, J.J.M., Walsh, C.A., Greenham, N.C., Mareseglia, E.A., Friend, R.H., Moratti, S.C., Holmes, A.B., *Efficient photodiodes from interpenetrating polymer networks*, Nature 1995, 376, 498-500.

[14] Yu, G., Gao, J., Hummelen,J.C., Wudl, F., Heeger, A.J., *Polymer Photovoltaic Cells: Enhanced Efficiencies via a Network of Internal Donor-Acceptor Heterojunctions*, Science.1995. 270, 1789-1791.

[15] Brabec, C.J., Sariciftci, N.S., Hummelen, J.C., *Plastic Solar Cells*, Adv. Funct. Mater. 2001, 11, 15.

[16] Beek, W.J.E., Wienk, M.M., and Janssen, R.A.J., *Hybrid polymer solar cells based on zinc Oxide*, J. Mat. Chem, 2005, 15, 2985-2988.

[17] Liao, H.C., Chantarat, N., Chen, S.Y., Peng, S.H., *Annealing Effect on photovoltaic performance of Hybrid P3HT/In-situ Grown CdS Nanocrystal Solar Cells*. J. Electrochem. Soc. 2011, 158, 7, E67-E72.

[18] Sirrnghaus, H., Brown, P.A., Friend, R.H., Nielsen, M.M., Bechgaard, K., Langeveld-Voss, B.M.W., Spiering, A.J.H., Janssen, R.A.J., Meijer, E.W., Herwing, P. and de Leeuw, D., *T-dimensional charge transport in self-organized, high-mobility conjugated polymers*, Nature, 401, 1999, 685-687.

[19] Lin,Y.Y, Lee, Y.Y., Chang, L., Wu, J.J., and Chen, C. W., *The influence of interface modifier on the performance of nanostructured ZnO/polymer hybrid solar cells*. Appl. Phys. Lett., 2009, 94, 063309-063312.

[20] Li, G., Shrotriya, V., Yao, Y., and Yang, Y. *Investigation of annealing effects and film thickness dependence of polymer solar cells based on poly (3-hexylthiophene)*, J. Appl. Phys. 2005, 98, 043704-043709.

[21] Oosterhout, S.D., Wienk, M.M, Banvel, S.V., Thiedmann, R., Koster, L.J.A., Gilot, J.,Loos, J. Schmidt, V. and Janssen, R. A. J., *The effect of three-dimensional morphology on the efficiency of hybrid polymer solar cells. Nature materials*, 8, Oct 2009, 818-824.

[22] Fox, M. (2001). *Optical properties of solids. Great Clarendon street, Oxford.: Oxford University Press.*

[23] Pacholski, C., Koronowski, A., and Weller. H., *Self-Assembly of ZnO: From nanodots to nanorods.* Angew. Chem. Int.Ed.2002, 41(7), 1188-1191.

[24] Seow, Z. L. S., Wong, A.S. W., Thavasi, V., jose, R., Ramakrishna, S., and Ho. G. W., *Controlled synthesis and application of ZnO nanoparticles, nanorods and nanospheres in dye-sensitized solar cells*. Nanotechnology 20 (2009) 045604 (6pp).

[25] Shrotriya, V., Li, G., Yao, Y., Moriarty, T., Emery, K., and Yang, Y. *Accurate measurement and characterization of organic solar cells*. Adv. Funct. Mater, 16, 2016-2023.

[26] Lin, Y., Chu, T., Li, S., Chuang, C., Chang, C., Su, W., Chang, C., Chu, M., Chen, C., *Interfacial Nanostructuring on the Performance of Polymer/TiO_2 Nanorod Bulk Heterojunction Solar Cells.* J. Am. Chem. Soc. 2009, 131, 3644-3649.

[27] Otsuka, Y., Okamoto, Y., Akiyama, H. Y., Umekita, K., Tachibana, Y., Kuwabata, S*., Photoinduced Formation of Polythiophene/TiO_2 Nanohybrid Heterojunction Films for Solar Cell Applications*, J. Phys. Chem. C 2008, 112, 4767-4775.

[28] S. Barth,H. Bassler, *Intrinsic Photoconduction in PPV-Type Conjugated Polymers*, Phs. Rev. Lett. 1997, 79, 4445.

[29] R.N. Marks, J.J.M. Halls, D.D.C. Bradley, R. H. Friend, A. B. Holmes, *The Photovoltaic Response in Poly(p-phenylene vinylene) thin- film devices,* J. Phys. Condens. Matter 1994, 6, 1379.

[30] Oleksandr V. Mikhnenko, Azimi, H., Scharber, M., Moronic, M. Blomad, P.W.M., *Exciton diffusion length in narrow bandgap polymers*. Energy Environ. Sci., 2012,5, 6960-6965.

[31] Sun, D., Wong, M., sun, L., Li, Y., Miyatake, N., Sue, H. J., *Purification and Stabilization of colloidal ZnO nanoparticles in Methanol*, J. Sol-Gel Sci Technol, 2007,43, 237-243.

[32] Burns, G., *Solid State Physics*, Academics Pr, 1985.

[33] Tang, C.W., *Twolayer organic photovoltaic cell.* Appl.Phys. Lett 1986,48,183.

[34] Gratzel, M., *Photoelectrochemical cells*, Nature 2001, 414, 338-344.

[35] Beek, W.J.E., Wienk, M.M., and Janssen, R. A. J., *Hybrid Solar Cell from Regioregular Polythiophene and ZnO Nanoparticles.* Adv. Funct. Mater. 2006, 16, 1112-1116.

[36] Gordon, I., Carnel, L., Gestel, V.D., Beaucarne, G., Poortmans, J., *Fabrication and characterization of highly efficient thin-film polycrystalline-silicon solar cells based on aluminium-induced crystallization*, Thin solid films, 2008, 516, 6984-6988.

[37] Kastner, C., Susarova, D. K.,Jadhav, R., Ulbricht, C., Egbe, D.A.M., Rathgeber, S., Troshin, P.A., and Hoppe, H., *Morphology evaluation of a polmer-fullerene bulk heterojunction ensemble generated by the fullerene derivatization,* J. Mater. Chem. 2012,22, 15987-15997

[38] Halls J.J.M., Friend R.H., Organic photovoltaic devices. In: Archer MD, Hill RD, editors, *Clean electricity from photovoltaics*, London: Imperial College Press, 2001, PP. 377-445, Adetailed review of the science and development of organic photovoltaic devices.

[39] Gregg, B.A., *The photoconversion mechanism of excitonic solar cells*. Mrs Bulletin, 2005. 30(1): p.20-22.

[40] Gregg, B.A., *Excitonic solar cells*. B J. Phys. Chem. B, 2003. 107(20): P.4688-4698.

[41] Hoppe,H. and N,S. Sariciftci, *Organic solar cells: An overview*. J.M.R., 2004. 19(7): P. 1924-1945.

[42] Haugeneder, A., Neges, M., Kallinger, C., Spirkl, W., Lemmer, U., Feldman, J., Scherf, U., Harth, E., Gugel, A. and Mullen, K., *Exciton diffusion and dissociation in conjugated polymer/fullerene blends and heterostructures*, Phys,Rev.B: Condens. Matter,1999,59,15346-15351.

[43] Shaw, P. E., Ruseckas, A., and Samuel, I. D. W.,*Exciton diffusion measurements in poly (3-hexylthiophene)*, Adv. Mater., 2008, 20, 3516-3520.

[44] Murthy, D. H. K., Gao, M., Vermeulen, M. J. W., Siebbeles, L. D. A., Savenije, T. J., *Mechanism of Mobile Charge Carrier Generation in Blends of Conjugated Polymers and Fullerenes: Significance of Charge Delocalization and Excess Free Energy*, J. Phys. Chem. C 2012, 116, 9214-9220.

[45] Jailaubekov, A.E., Willard, A.P., Tristsch, J.R., Chan, W., Sai, N., Gearba, R., Kaake, L.G., Williams, K.J., Leung, K., Rossky, P.J., Zhu, X*., Hot charge-transfer excitons set the time limit for charge separation at donor/acceptor interfaces in organic photovoltaic.*, Nature Materials, Vol 12, January 2013, 66-73

[46] Punkka, E., Isotalo, H., Ahlskog, M. and Stubb, H., *Effect of Humidity and Heat on the conductivity of poly (3-Alkylthiophenes)*, MRS Proceeding, 1992,247,753.

[47] Backlund, T.G., Osterbacka, R., and Stubb, H., *Operation principle of polymer insulator organic thin-film transistors exposed to moisture*, J. Appl. Phys. 2005, 98, 074504

[48] Dawen, L., Borkent, E., Nortrup, R., Moon, H., Katz, H. and Bao, Z*., Humidity effect on electrical performance of organic thin-film transistors*, , Appl. Phys. Lett. 2005, 86, 042105

[49] Beek, W.J.E., Wienk, M.M.& Janssen, R.A.J. (2004). *Efficient hybrid solar cells from znic oxide nanoparticles and a conjugated polymer*., Adv. Mater. 16(12), 1009-1013.

[50] Kymissis, C. D. Dimitrakopoulos, and S. Purushothaman, *High-Performance Bottom Electrode Organic thin-Film Transistors*. IEEE Trans. Electron Devices, 2001, 48,1060 s2001d.

[51] Hintz, H., Peisert, H., Egelhaaf, H. J., Chasse, T. *Photodegradation of P3HT-A Systematic Study of Environmental Factors*, J. Phys. Chem.C 2011, 115, 13373 −13376.

[52] Kwong, C. Y., Djurisic, A. B., Chui, P. C., Cheng, K. W. & Chan, W. K. *Influence of solvent on film morphology and device performance of poly(3-hexylthiophene): TiO2 nanocomposite solar cells.* Chem. Phys. Lett., 2004,384, 372-375.

[53] Duren, V., J. K. J. et al. *Relating the morphology of poly(p-phenylene vinylene) / methanofullerene blends to solar-cell performance*. Adv. Funct. Mater., 2004,14, 425-434.

[54] Yang, X., van Duren, J. K. J., Janssen, R. A. J., Michels, M. A. J. & Loos, J. *Morphology and thermal stability of the active layer in poly(p-phenylenevinylene)/ methanofullerene plastic photovoltaic devices*. Macromolecules, 2004, 37, 2151-2158.

[55] Yoo, H.G., Fauchet, P.M., *Experimental verification of dielectric constant decrease in silicon nanostructures*, proc .of SPIE, 2008, 6902,690203-8

[56] Liu, Y., Scully, S.R., McGehee, M.D., Liu, J., Luscombe, C.K., Frechet, J. M. J., Shaheen, S..E., and Ginley, D.S., *Dependence of band offset and open-curicuit*

voltage on the interfacial interaction between TiO2 and carboxylated polythiophenes, J.Phys. Chem. B, 2006, 110, 3257-3261.

[57] K. Coakley, Y. Liu, M. D. McGehee, K. L. Frindell and G. D. Stucky, *Infiltrating semiconducting polymers into self-assembled mesoporous titania films for photovoltaic applications*, Adv. Funct. Mater., 2003, 13, 301.

[58] K. Coakley and M. D. McGehee, *Photovoltaic cells made from conjugated polymers infiltrated into mesoporous titania*, Appl.Phys., Lett., 2003, 83, 3380.

[59] Mayer, A.C., Scully, S.R. Hardin, Rowell, M.W, McGehee, M. D., *Polymer based solar cells*, Materials today, 2007, 10, 11, 28-33

[60] Riordan, M.,Hoddeson, L., ' *Crystal fire'* , Amazon, 1998.

[61] H.L. Yip, S.K. Hau, N.S. Baek, A.K.Y. Jen, *Self-assembled monolayer modified ZnO/metal bilayer cathodes for polymer/fullerene bulk-heterojunction solar cells*, Appl. Phys. Lett. 92 (2008) 193313–193315.

[62] A.L. Roest, J.J. Kelly, D. Vanmaekelbergh, E.A. Meulenkamp, *Staircase in the electron mobility of a ZnO quantum dot assembly due to shell filling*, Phys. Rev. Lett. 89 (2002) 036801–036804.

[63] National reneable energy laboratory, "*Best Reserch –Cell Efficiency*", (5 December 2012), Retrived from: http://nrl.gov/ncpv/images/efficiency_chart.jp Last accessed: March 2013.

[64] L.Travi, B. Venkataraman, D. Venkataraman,. *Organic solar cells: An overview focusing on active layer morphology*, Photosynthesis Research, 2006, 87, 73-81

[65] O'Regan, B.,Gratzel, M., *A low-cost, high- efficiency solar cell based on dye-sensitized colloidal TiO_2 films*, Nature, 1991, 353, 737-740.

[66] Uninted state census burea., "World POPClock Projection" Retrived from: http://www.census.gov/, last accessed: March 2013.

[67] U.S. Photovoltaic Industry Roadmap, U.S.Dept. of Energy, http://www.nrel.gov, last accessed: March 2013.

[68] L. E. Greene, M. Law, B. D. Yuhas, and P. Yang., ZnO-TiO2 Core-Shell Nanorod/P3HT Solar Cells, J. Phys. Chem. C,2007, 111, 18451-18456.

[69] S. D. Oosterhout, L. J. A. Koster, S. S. V. Bavel, J. Loos, O. Stenzel, R. Thiedmann, V. Schmidt, B. Campo, T. J. Cleij, L. Lutzen, D. Vanderzande, M. M.

Wienk, and R. A. J. Janssen, Controlling the Morphology and Efficiency of Hybrid ZnO:Polythiophene Solar Cells Via Side Chain Functionalization, Adv. Energy Mater. 2011, 1, 90–96.

[70] T. Hu, F. Li, K. Yuan,Y. Chen, Efficiency and Air-Stability Improvement of Flexible Inverted Polymer Solar Cells Using ZnO/Poly(ethylene glycol) Hybrids as Cathode Buffer Layers, ACS Appl. Mater. Interfaces 2013, 5, 5763−5770

[71] B. Park, J. H. Lee, M. Chang, E. Reichmanis, Exciton Dissociation and Charge Transport Properties at a Modified Donor/Acceptor Interface: Poly(3-hexylthiophene)/Thiol-ZnO Bulk Heterojunction Interfaces, J. Phys. Chem. C, 2012, 116, 4252−4258.

[72] S. AbdulAlmohsin, J. B. Cui, Graphene-Enriched P3HT and Porphyrin-Modified ZnO Nanowire Arrays for Hybrid Solar Cell Applications
S. AbdulAlmohsin and J. B. Cui, J. Phys. Chem. C 2012, 116, 9433−9438
[73] A. J. Said, G. Poize, C. Martini, D. Ferry, W. Marine, S. Giorgio, F. Fages, J. Hocq, J. Boucle´, J. Nelson, J. R. Durrant, J. Ackermann, Hybrid Bulk Heterojunction Solar Cells Based on P3HT and Porphyrin-Modified ZnO Nanorods, J. Phys. Chem. C, 2010, 114, 11273–11278.
[73] S. Wu, Q. Tai, F. Yan, Hybrid Photovoltaic Devices Based on Poly (3-hexylthiophene) and Ordered Electrospun
ZnO Nanofibers, J. Phys. Chem. C 2010, 114, 6197–6200.
[74] Y. Shi, F. Li, Y. Chen, Controlling morphology and improving the photovoltaic performances of P3HT/ZnO hybrid solarcells via P3HT-b-PEO as an interfacial compatibilizer, New J. Chem., 2013, 37, 236—244.
[75] Y. Vaynzof, D. Kabra, L. Zhao, P. K. H. Ho, A. T.-S. Wee, R. H. Friend, Improved photoinduced charge carriers separation in organic-inorganic hybrid photovoltaic devices, Appl. Phys. Lett. 2010, 97, 033309.

[76] G. Chen , H. Sasabe , Z. Wang , X. F. Wang , Z. Hong , Y. Yang , J. Kido, Co-Evaporated Bulk Heterojunction Solar Cells with > 6.0% Effi ciency, Adv. Mater. 2012, 24, 2768–2773.

[77] D. W. Chen, T.C. Wang, W.P. Liao, J. J. Wu, Synergistic Effect of Dual Interfacial Modifications with Room-Temperature-Grown Epitaxial ZnO and Adsorbed Indoline Dye for ZnO Nanorod Array/P3HT Hybrid Solar Cell, ACS Appl. Mater. Interfaces 2013, 5, 8359−8365.

[78] Ideal Energy-Level Alignment at the ZnO/P3HT Photovoltaic Interface, K. Noori, F. Giustino, Adv. Funct. Mater. 2012, 22, 5089–5095.

[79] Q. Shen, Y. Ogomi, S. K. Das, S. S. Pandey, K.Yoshino, K. Katayama, H. Momose, T. Toyodaab, S. Hayase., Huge suppression of charge recombination in P3HT–ZnO organic–inorganic hybrid solar cells by locating dyes at the ZnO/P3HT interfaces., Phys. Chem. Chem. Phys., 2013, 15, 14370--14376

[80] S. Nowak. Global PV markets and policies. Proceedings of EU-PVSEC 2011, 2011.

[81] S Mehta. GMT research, Press release June 17,2013, Sited on the March 7,2014. WWW.greentechmedia.com/research/report/pv-technology-and-cost-outlook-2013-2017.

[82] I. Riedel, J. Parisi, V. Dyakonov, L. Lutsen, D. Vanderzande and J. C. Hummelen. Effect of temperature and illumination on the electrical characteristics of plolymer-fullerene bulk-heterojunction solar cell, Advanced Functional Material, 2004, 14, No. 1, January

[83] A. Guerreo, P. P. Boix, L. F. Marchesi, T. Ripolles-Sanchis, E. C. Pereira, G. Garcia-Belmonte, Oxigen doping-induced photogeneration loss in P3HT:PCBM solar cells, Solar Energy Materials & Solar Cell, 2012, doi: 10.1016.

[84] D. E. Motaung, G. F. Malgas, C. J. Arendse, S. E. Mavundla, C. J. Oliphant and D. Knoesen, The influence of thermal annealing on the morphology and structural properties of a conjucated polymer in blends with an organic acceptor material. J Mater Sci (2009) 44:3192-3197.

[85] B. M. Omer, Optical properties of Poly (3-hexylthiophene-2,5-diyl) and poly (3-hexylthiophene-2,5-diyl)/ [6,6]-Phenyl C61-butyric Acid 3-ethylthiophene Ester Thin Films, J. Nano-Electron. Phys. (2013) 5, 03010,